Available online at www.sciencedirect.com
SCIENCE DIRECT®
PERGAMON
Progress in Aerospace Sciences 39 (2003) 249–315
PROGRESS IN AEROSPACE SCIENCES
www.elsevier.com/locate/paerosci

Advances in global linear instability analysis of nonparallel and three-dimensional flows

Vassilios Theofilis*

DLR Institute of Aerodynamics and Flow Technology, Bunsenstraße 10, D-37073 Göttingen, Germany

Abstract

A summary is presented of physical insights gained into three-dimensional linear instability through solution of the two-dimensional partial-differential-equation-based nonsymmetric real or complex generalised eigenvalue problem. The latter governs linear development of small-amplitude disturbances upon two-dimensional steady or time-periodic *essentially nonparallel* basic states; on account of this property the term BiGlobal instability analysis has been introduced to discern the present from earlier global instability methodologies which are concerned with the analysis of *mildly inhomogeneous* two-dimensional basic flows. Alternative forms of the two-dimensional eigenvalue problem are reviewed, alongside a discussion of appropriate boundary conditions and numerical methods for the accurate and efficient recovery of the most interesting window of the global eigenspectrum. A number of paradigms of open and closed flow systems of relevance to aeronautics are then discussed in some detail. Besides demonstrating the strengths and limitations of the theory, these examples serve to demarcate the current state-of-the-art in applications of the theory to aeronautics and thus underline the steps necessary to be taken for further progress to be achieved.

Contents

*Fax: +49-551-709-2830.
E-mail address: vassilios.theofilis@dir.de (V. Theofilis).

0376-0421/03/$ - see front matter © 2003 Published by Elsevier Science Ltd.
doi:10.1016/S0376-0421(02)00030-1

Nomenclature

Abbreviations

EVD	eigenvalue decomposition
EVP	eigenvalue problem
DNS	direct numerical simulation
OSE	Orr–Sommerfeld equation
PSE	parabolised stability equations
LHS	left-hand side
LNSE	linearised Navier–Stokes equations
TS	Tollmien–Schlichting
WKB	Wentzel/Kramers/Brillouin

Latin symbols

A	aspect ratio
$\mathbf{A}$, $\mathbf{B}$, $\mathbf{C}$	matrices describing a discrete EVP
b_1, b_2	distances between vortex centres/centroids
c	chord length
c_{ph}	phase velocity
C_μ	momentum coefficient
D	cylinder diameter/base-height
$\mathbf{e}_z$	unit vector in the z-direction
f	frequency
f_{e}	excitation frequency
F^+	reduced frequency
i	imaginary unit
L_z	periodicity length in the z-direction
m	leading dimension of Hessenberg matrix in the Arnoldi algorithm
M	Mach number
$\bar{p}$	basic flow pressure
$\tilde{p}$	disturbance flow pressure
$\hat{p}$	amplitude function of disturbance flow pressure
r	radial distance
Re	Reynolds number
$\bar{T}$	basic flow temperature
$\tilde{T}$	disturbance flow temperature
$\hat{T}$	amplitude function of disturbance flow temperature
T	time period
t	time
tr	trailing-edge
U_∞	free-stream velocity value
$(\bar{u}, \bar{v}, \bar{w})^{\mathrm{T}}$	basic flow velocity vector
$(\tilde{u}, \tilde{v}, \tilde{w})^{\mathrm{T}}$	disturbance flow velocity vector
$(\hat{u}, \hat{v}, \hat{w})^{\mathrm{T}}$	amplitude functions of disturbance flow velocity vector
W_z	peak corrugation height
(x, y, z)	cartesian coordinates

Calligraphic symbols

$\mathscr{D}_x$	$\partial/\partial x$
$\mathscr{D}_y$	$\partial/\partial y$
$\mathscr{B}, \mathscr{D}, \mathscr{E}, \mathscr{L}, \mathscr{M}, \mathscr{N}, \mathscr{O}, \mathscr{P}, \mathscr{R}, \mathscr{S}$	linear operators

Greek symbols

α, δ	real wavenumbers in the x-direction
β	real wavenumber in the z-direction
β_0, β_1	velocity and deceleration scales
ε	infinitesimal quantity
Γ, γ	circulation values
δ^*	boundary layer displacement thickness
ζ	vorticity in 2D
Θ	phase function
ϑ	azimuth
θ	boundary layer momentum thickness
κ	ratio of specific heats
λ	shift parameter
ν	kinematic viscosity
ξ	scaled x-direction
ρ	density
$\bar{\rho}$	basic flow density
$\tilde{\rho}$	disturbance flow density
$\hat{\rho}$	amplitude function of disturbance flow density
σ	complex eigenvalue
τ	wall-shear stress
ϕ	angle
ψ	stream function in 2D
Ω	complex eigenvalue

Superscripts

$'$	time-dependent disturbance

Subscripts

1D,2D, 3D	one-, two-, three-dimensional
i	imaginary part
r	real part
s	$\dfrac{\partial}{\partial s}$, s measured along a tangential spatial direction
x, y, t	$\dfrac{\partial}{\partial x}$, $\dfrac{\partial}{\partial y}$, $\dfrac{\partial}{\partial t}$

1. Introduction

Flow instability research plays a central role in the quest for identification of deterministic routes leading a laminar flow through transition into turbulence. Understanding the physics of laminar-turbulent flow transition has been originally motivated by aerodynamic applications and actively pursued by means of the classic linear instability theory due to Tollmien [1] for the best part of the last century. Tollmien's theory deals with instability of basic states that develop in two homogeneous and one resolved spatial direction and may mathematically be formulated by the eigenvalue problem (EVP) expressed by the system of the Orr–Sommerfeld and Squire equations [2]. Numerous attempts to incorporate non-parallel and nonlinear phenomena into the Orr–Sommerfeld equation (OSE) culminated in the successful applications of spatial and temporal direct numerical simulation (DNS) to flows in aerodynamics [3,4] and the relaxation of the assumption of homogeneity in one

spatial coordinate into one of weak dependence of flow by the parabolised stability equations (PSE; Herbert [5]). The distinction between convective and absolute instability, which originated in a different field [6], was put forward in the context of fluid flows in the seminal work of Huerre and Monkewitz [7]. This work remains essential reading in this respect, especially since confusion can be generated regarding the use of the term 'global' in the sense of these authors and that employed herein, as will be discussed in what follows.

Irrespective of whether the instability problem has been addressed by the OSE, the PSE, DNS or with respect to its absolute/convective instability, most attention in aeronautics to-date has been paid to flows in which the underlying basic state is taken to be an one-dimensional solution of the equations of motion, or one which varies mildly in the downstream direction. The flat-plate boundary layer monitored in the context of OSE or temporal DNS at specific locations/Reynolds number values on a flat plate or the same problem studied by PSE or spatial DNS is the archetypal example in external aerodynamics. One can arrive at useful predictions using the aforementioned methodologies also when the basic state is two-dimensional by performing the analysis at successive downstream locations in isolation from upstream effects or downstream propagation phenomena. Instability of a laminar separation bubble [8] or that in an open cavity [9] are two well-known examples in this class of flows. However, the scope of aerodynamically relevant basic flows in which two spatial directions are homogeneous or mildly developing is rather limited. Most basic states of industrial significance are inhomogeneous in either two or all three spatial directions. Examples in aerodynamics include flows in ducts, cavities, corners, forward- or backward facing steps as well as flows on cylinders/lifting surfaces, delta-wings and the wake vortex system. In most of these flows classic OSE/PSE analyses have been attempted with various degrees of success while it is always possible, though not necessarily practicable in such flows, to employ DNS in order to gain understanding of flow instability. On the other hand, an appropriate linear instability theory, in which the inhomogeneous spatial directions are resolved numerically without any assumptions on the form of the basic state, has a prominent role to play in furthering current understanding of flow instability physics. It is the objective of the present review to discuss details of this theory.

Specifically, recent advances in algorithms for the numerical solution of large nonsymmetric real/complex generalised EVPs alongside continuous computing hardware improvements have resulted in the ability to extend both Tollmien's local theory and the PSE into a new theory which is concerned with the instability of flows developing in two inhomogeneous and one homogeneous spatial direction. The scope of applications of linear theory is thereby dramatically broadened compared with that of older instability analysis methodologies. A natural extension of the Orr–Sommerfeld/Squire system, the tool utilised in the context of this extended linear theory is solution of the partial-differential-equation-based two-dimensional EVP describing linear growth/damping of small-amplitude three-dimensional disturbances which are inhomogeneous in two and periodic in the third spatial direction. This defines the term 'global' linear instability analysis in the present context.

Results obtained using global linear instability analysis are slowly emerging in all areas of fluid mechanics, following the pace of hardware and algorithmic developments. In the first analysis of its kind, Pierrehumbert [10] reported the discovery of short-wavelength elliptic instability in inviscid vortex flows, a problem of relevance to both transition and turbulence research. Viscous global analysis were reported by Jackson [11] and Zebib [12], who studied global instability of flow around a cylinder, Lee et al. [13] who addressed stability of fluid in a rectangular container and Tatsumi and Yoshimura [14] who presented the first application with relevance to internal aerodynamics, namely flow in a rectangular duct driven by a constant pressure gradient. Several works in this vein followed, a representative sample of which (in the context of aeronautics) is reviewed herein. The penalty of the ability to resolve two spatial dimensions is that the size of the real or complex nonsymmetric generalised EVPs in which the linearised Navier–Stokes and continuity equations are recast can be challenging even on present-day hardware. Several early global instability analyses have circumvented this challenge by addressing the computationally much less demanding inviscid global linear instability problem, by solving problems the viscous global linear instability of which is manifested at low Reynolds numbers, by addressing reduced systems in which the same viscous instability problem may be recast, by imposing symmetries in the expected solutions, or by combination of the last three approaches. An additional hurdle for successful analysis of aeronautical-engineering relevant high-Reynolds number viscous instability problems has been the use of the classic QZ algorithm [15], which returns the full eigenvalue spectrum. The QZ algorithm requires the storage of four matrices the leading dimension of which is the product of the number of nodes used to resolve the two spatial directions. The size required to address interesting applications can be of $O(Gb)$ for each matrix; worse, the CPU time necessary for the solution of the eigenproblem scales with the cube of the leading dimension of the matrices involved; both reasons make use of this algorithm entirely inappropriate for global instability analysis of all but the most academic flows. A breakthrough was achieved in the mid-1990s

independently by several investigators [16–18] who combined viscous global linear instability analysis with efficient Krylov subspace iteration [19–21] to recover the part of the eigenspectrum which contains the most interesting, from a physical point of view, most unstable/least stable global linear eigenmodes. A single LU-factorisation followed by a small number of matrix–vector multiplications and storage of a single matrix is required by this approach. Methodologies also exist [22–24] which circumvent storage of the matrix altogether. Subspace iteration methods permit investment of the freed memory compared with the QZ to improve resolution and thus attain substantially higher Reynolds numbers and it is only consequent that this has been reflected in the accuracy of most of the currently available results in the literature.

This review is bound to be limited by the low degree of exposure of the author to global instability problems beyond aeronautics. The reader should be aware that a growing body of results of two-dimensional EVPs is being generated in magnetohydrodynamics, theoretical physics, electrical engineering, with the list of applications of the concept being continuously enlarged. Without any pretense of being exhaustive, but merely as an indication of the potential areas of application to aeronautics, a small sample of the basic flows that have been analysed by solution of two-dimensional EVPs is presented schematically in Fig. 1. Areas of critical importance in this context, the instability of which has traditionally been performed using local analysis and in which recent global linear analyses have shed new light in the physical mechanisms at play, are highlighted. Inevitably, some comments are made on the issue of flow control; readers interested in this topic are referred to the comprehensive recent reviews of Greenblatt and Wygnanski [25] and Stanewsky [26]. Even within the limited scope of the present review, the interpretation of results could be unwillingly partial and/or reference to recent/current work could be missing. It is hoped that this will not hamper the objective of the paper to provide an outline of the capabilities of the emerging global linear instability theory in a self-contained source and to highlight validated numerical approaches so as to stimulate further research into this topic.

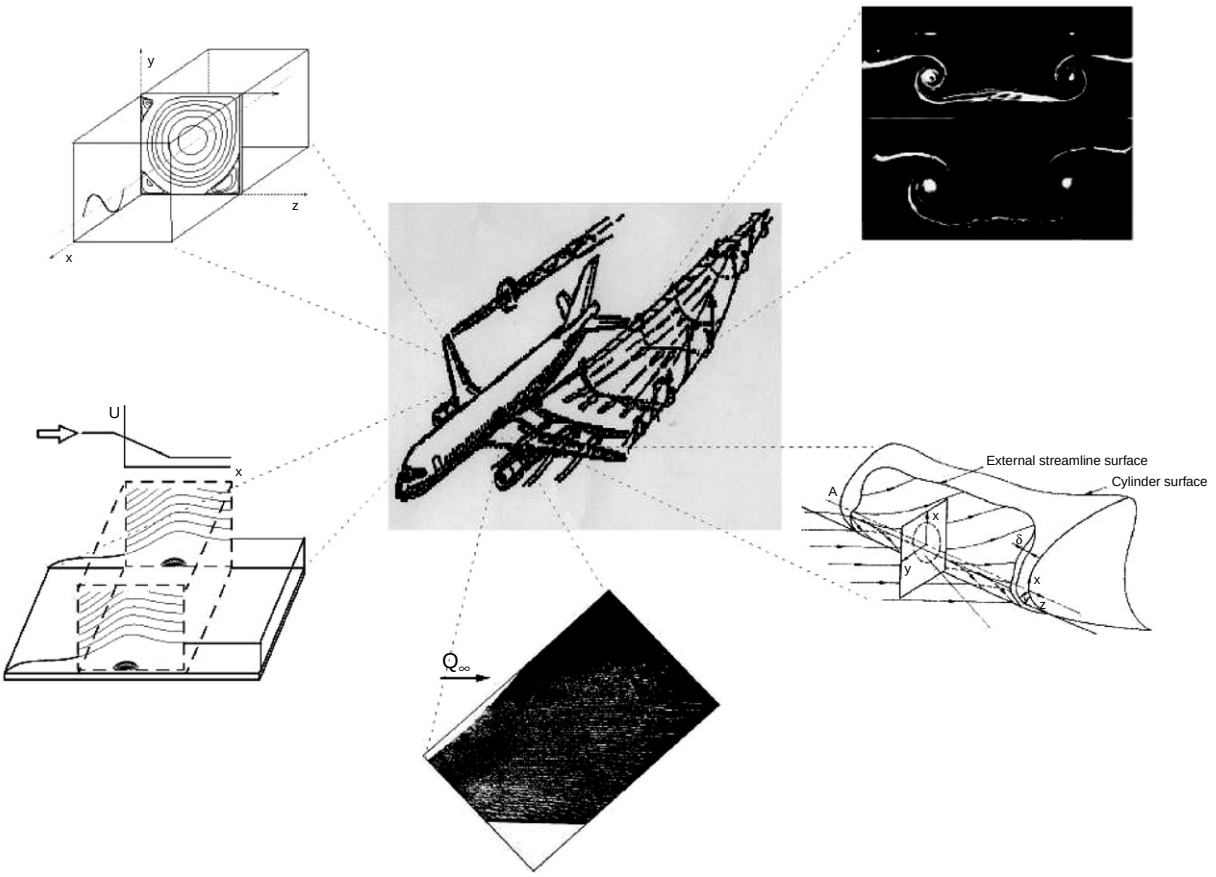

Fig. 1. Representative areas of application of global instability analysis in aeronautics.

In an attempt to elucidate the differences in 'global' theory as discussed in the literature and as proposed herein, we return to and elaborate somewhat on the issue of terminology. Huerre and Monkewitz [7] have used the term 'absolute' instability to discern between flow behaviour after the introduction of an infinitesimal disturbance; given a predominant downstream flow direction, *convectively unstable* flows are characterised by propagation of a disturbance introduced at a location in the flow in the downstream direction (albeit amplifying/decaying in the process) while a flow in which the disturbance remains at or propagates upstream from its point of introduction is characterised as being *absolutely unstable*. In either case, the key assumption underlying this distinction is that *the basic state is a truly parallel flow*. Consequently, homogeneity of space in two out of three directions permits *wave-like* solutions of the disturbance equations, schematically depicted in Fig. 2. On the other hand, the term 'global' instability has been introduced in the literature as the analogon of 'absolute' instability, when the assumption of independence of the basic state on the downstream spatial direction is relaxed and a basic state which is *weakly dependent* on the downstream direction is considered. In this case progress can be made by combined analysis based on a WKB approximation and computation. Model differential equations have been used in this respect, which mimic the essential properties of the equations of motion, while being amenable to analysis (e.g. [27–29]). An overlapping area of application of this concept of global instability and that used herein exists when the basic state is weakly dependent on the predominant flow direction. The results of the former approach may be related with those of the two-dimensional limit (i.e. the limit of infinitely long wavelength in the third/homogeneous spatial direction) of the global analysis in the present sense. Boundary-layer flow encompassing a closed recirculation region, discussed herein, illustrates this point. In case the two aforementioned directions are different, it is presently unclear whether/how the two concepts of global instability can be related. Indeed, work is necessary in this area in order for the concept of global flow instability (in the present sense) to benefit from the wealth of knowledge which has been generated in the last decade by analysis of weakly nonparallel flows. In the author's view, on account of its capacity to analyse both weakly nonparallel and *essentially nonparallel* (as well as three-dimensional) flows, the concept of global instability analysis based on the solution of multidimensional EVPs is broader than that based on the assumption of weakly varying basic state. As such the present review will only be concerned with presentation of results arising from numerical solution of linear eigenvalue problems; for clarity 'global' will be refined herein by the introduction of the terms *BiGlobal* and *TriGlobal* to describe instability analyses of two- and three-dimensional basic states, respectively. This also clarifies the present use of the term 'global' instability in comparison with that of Manneville [30], the latter author using this term to describe nonlinear instability or global bifurcations.

The article is organised as follows. In Section 2 the concept of decomposition into basic flow and small-amplitude perturbations is utilised to arrive at a systematic presentation of the alternative forms of the two-dimensional eigenvalue problem. This is followed by discussion of appropriate boundary conditions to close the related elliptic problems. Numerical aspects

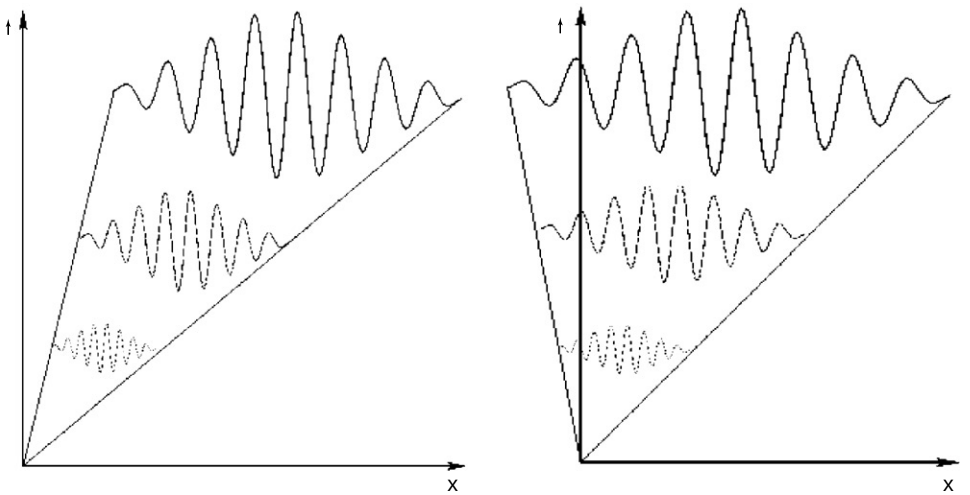

Fig. 2. Schematic representation of the concepts of convective (left) and absolute (right) instability of *parallel* flows, whose basic state is independent of the downstream coordinate.

mainly focussing on accuracy and efficiency are presented in Section 3. Global instability analysis results of the problems highlighted in Fig. 1, alongside bluff-body global instabilities and evidence of the potential role of global eigenmodes in turbulent flow are presented in Section 4. Concluding remarks on achievements and potential future advances of global instability theory are furnished in Section 5. Motivated by the realisation that accurate basic states are essential for the success of the subsequent global instability analysis, a suite of validated algorithms for the accurate and efficient recovery of some two-dimensional basic flows of significance to aeronautics is presented in the appendix.

2. Theory

2.1. Decompositions and resulting linear theories

Central to linear flow instability research is the concept of decomposition of any flow quantity into an $O(1)$ steady or time-periodic laminar so-called *basic* flow upon which small-amplitude three-dimensional disturbances are permitted to develop. In order to expose the ideas in the present paper but without loss of generality, and unless otherwise stated, incompressible flow is considered throughout and attention is mainly focussed on steady basic flows. Physical space is three-dimensional and the most general framework in which a linear instability analysis can be performed is one in which three spatial directions are resolved and time-periodic small-amplitude disturbances, inhomogeneous in all three directions, are superimposed upon a steady $O(1)$ basic state, itself inhomogeneous in space. This is consistent with the separability in the governing equations of time on the one hand and the three spatial directions on the other. We term this a *three-dimensional* global, or TriGlobal, linear instability analysis, in line with the dimensionality of the basic state. The relevant decomposition in this context is

$$\mathbf{q}(x,y,z,t) = \bar{\mathbf{q}}(x,y,z) + \varepsilon\tilde{\mathbf{q}}(x,y,z,t) \tag{1}$$

with $\bar{\mathbf{q}} = (\bar{u},\bar{v},\bar{w},\bar{p})^{\mathrm{T}}$ and $\tilde{\mathbf{q}} = (\tilde{u},\tilde{v},\tilde{w},\tilde{p})^{\mathrm{T}}$ representing the steady basic flow and the unsteady infinitesimal perturbations, respectively. On substituting (1) into the governing equations, taking $\varepsilon \ll 1$ and linearising about $\bar{\mathbf{q}}$ one may write

$$\tilde{\mathbf{q}}(x,y,z,t) = \hat{\mathbf{q}}(x,y,z)\mathrm{e}^{\mathrm{i}\Theta_{3\mathrm{D}}} + \text{c.c.}, \tag{2}$$

with $\hat{\mathbf{q}} = (\hat{u},\hat{v},\hat{w},\hat{p})^{\mathrm{T}}$ representing three-dimensional amplitude functions of the infinitesimal perturbations, Ω being a complex eigenvalue and

$$\Theta_{3\mathrm{D}} = -\Omega t \tag{3}$$

being a complex phase function. Complex conjugation is introduced in (2) since $\hat{\mathbf{q}}, \Omega$ and their respective complex conjugates are solutions of the linearised equations, while $\tilde{\mathbf{q}}$ is real. The three-dimensional eigenvalue problem resulting at $O(\varepsilon)$ is not tractable numerically at Reynolds numbers of relevance to aeronautics, as will be discussed shortly.

Simplifications are called for, in the most radical of which the assumptions $\partial\bar{\mathbf{q}}/\partial x \ll \partial\bar{\mathbf{q}}/\partial y$ and $\partial\bar{\mathbf{q}}/\partial z \ll \partial\bar{\mathbf{q}}/\partial y$ are made, effectively neglecting the dependence of the basic flow $\bar{\mathbf{q}}$ on x and z; further, the basic flow velocity component $\bar{v}$ is also neglected. The first, in conjunction with the second, best-known as *parallel-flow* assumption, permit considering the decomposition

$$\mathbf{q}(x,y,z,t) = \bar{\mathbf{q}}(y) + \varepsilon\hat{\mathbf{q}}(y)\mathrm{e}^{\mathrm{i}\Theta_{1\mathrm{D}}} + \text{c.c.} \tag{4}$$

This Ansatz is typical of and well-validated in linear instability of external aerodynamic flows of boundary layer or shear layer type. In axisymmetric geometries the analogous Ansatz[1] decomposes all flow quantities into basic flow and disturbance amplitude functions depending on the radial spatial direction alone and assumes independence of the basic flow on the azimuthal and axial spatial directions. The latter two spatial directions are taken to be homogeneous as far as the linear disturbances are concerned. No special reference to the latter Ansatz will be made, since it conceptually belongs to the same class as (4). In (4) $\hat{\mathbf{q}}$ are one-dimensional complex amplitude functions of the infinitesimal perturbations and Ω is in general complex. Two classes of flows are currently being considered within (4), discriminated by the phase function $\Theta_{1\mathrm{D}}$. In the first class,

$$\Theta_{1\mathrm{D}} = \Theta_{\mathrm{OSE}} = \alpha x + \beta z - \Omega t, \tag{5}$$

where α and β are wavenumber parameters in the spatial directions x and z, respectively.

Introduction of a harmonic decomposition in these directions implies homogeneity of the basic flow in both x and z; furthermore, a basic flow velocity vector of the form $(\bar{u}(y),0,\bar{w}(y))^{\mathrm{T}}$ ensures separability of the linearised equations and their consistency with the decomposition (4). Mathematical feasibility and numerical tractability of the resulting ordinary-differential-equation-based eigenvalue problem has made (4) and (5) the basis of exhaustive studies, in the span of the last three quarters of last century, of a small class of flows which satisfy these assumptions. Substitution into the incompressible continuity and Navier–Stokes equations results in a system which may be rearranged into the celebrated Orr–Sommerfeld and Squire equations, while the Rayleigh equation is obtained in the limit $Re \to \infty$ [2]. We term this class of instability theory an *one-dimensional* linear analysis, again by reference to the dimensionality of the basic state. Most representative wall-bounded flow of this class, in which the viscous (Orr–Sommerfeld) type of theory resulting from

[1] $\mathbf{q}(r,\theta,z,t) = \bar{\mathbf{q}}(r) + \varepsilon\hat{\mathbf{q}}(r)\mathrm{e}^{\mathrm{i}\Theta_{1\mathrm{D}}} + \text{c.c.}$

decomposition (4) has been applied, is the flat-plate boundary layer [31]; the free shear layer is the prototype example of open system in which the respective inviscid limit of the theory is applicable [32]. A note is in place here, namely that treating physical space as being homogeneous in two out of its three directions results in the (wrong) identification of linear instabilities exclusively with wave-like solutions of the linearised system of governing equations (e.g. the Tollmien–Schlichting waves in Blasius flow); potential of confusion is generated in that small-amplitude nonperiodic *linear* disturbances may be associated with a nonlinear flow phenomenon [33].

Several attempts have been made to circumvent the restriction of a parallel basic flow and thus enlarge the scope of the instability problems which may be addressed by the linear theory based on (4) and (5). The most successful effort to-date in the context of boundary-layer type flows is the PSE concept, introduced and recently summarised by Herbert [5]. Analogously with the classic linear theory based on (4) and (5), one spatial direction of the basic flow is resolved. By contrast to this linear theory, though, the basic flow in the context of PSE is permitted to grow *mildly* in one or both remaining spatial directions. The linear instability problem is thus parabolised and may be solved efficiently by space-marching numerical procedures.

The second class of flows satisfying (4) is thus obtained by taking the velocity-component $\bar{v}$ into account and considering locally, i.e. at a specific x-location,

$$\Theta_{1D} = \Theta_{PSE} = \int_{x_0}^{x} \alpha(\xi) - \mathrm{d}\xi + \beta z - \Omega t. \tag{6}$$

Implicit here is the WKB-type of assumption of the existence of two scales on which the instability problem is studied, one slow upon which the basic flow develops and one fast on which the instability problem is considered. Strictly speaking, $\hat{\mathbf{q}}$ in (4) must be written as a function of the slowly-varying x-scale, which has been avoided in order for the capturing of 'most' of the streamwise variation in the instability problem in the phase function (6) to be stressed. Specifically, $\alpha(x)$ is a slowly varying in the streamwise direction x wavenumber which is intended to capture practically all streamwise variations of the disturbance on the fast scale. A normalisation condition which removes the ambiguity existing on account of the two streamwise scales was introduced by Bertolotti et al. [34]

$$\int_0^{y_e} \hat{\mathbf{q}}^{\dagger} \frac{\partial \hat{\mathbf{q}}}{\partial x} \mathrm{d}y = 0. \tag{7}$$

The superscript † refers to the complex conjugate and y_e stands for the upper boundary of the discretised domain. In line with the terminology introduced earlier, the PSE is a *quasi-two-dimensional* approach to linear instability analysis. The scope of mildly growing basic flows for which the quasi-two-dimensional linear analysis may be applied without changing the mathematical character of the system of equations describing flow instability into an elliptic problem is steadily being extended; a recent example is offered by the favourable comparison of PSE and DNS results in a laminar boundary layer which encompasses a steady closed recirculating flow region [35].

Between the two extremes (1) and (4) one may consider a basic flow in which $\partial\bar{\mathbf{q}}/\partial z \ll \partial\bar{\mathbf{q}}/\partial x$ and $\partial\bar{\mathbf{q}}/\partial z \ll \partial\bar{\mathbf{q}}/\partial y$. The decomposition

$$\mathbf{q}(x,y,z,t) = \bar{\mathbf{q}}(x,y) + \varepsilon\hat{\mathbf{q}}(x,y)\mathrm{e}^{\mathrm{i}\Theta_{2D}} + \text{c.c.} \tag{8}$$

in which the basic flow $\bar{\mathbf{q}} = (\bar{u},\bar{v},\bar{w},\bar{p})^{\mathrm{T}}$ is a steady solution of the *two-dimensional* continuity and Navier–Stokes equations and

$$\Theta_{2D} = \beta z - \Omega t \tag{9}$$

is thus considered. While the idea of decomposition in this approach is shared with that in the classic Orr–Sommerfeld type of linear analysis, the key difference with the latter theory is that here three-dimensional space comprises an *inhomogeneous* two-dimensional domain which is extended periodically in z and is characterised by a wavelength L_z, associated with the wavenumber of each eigenmode, β, through $L_z = 2\pi/\beta$. The corresponding linear eigenmodes are three-dimensional functions of space, inhomogeneous in both x and y and periodic in z. The symmetries of the basic flow $\bar{\mathbf{q}}$ determine those of the amplitude functions $\hat{\mathbf{q}}$ while in the limit $\partial\bar{\mathbf{q}}(x,y)/\partial x \to 0$ the analysis based on (8) and (9) yields the eigenfunctions predicted by (4) and (5). It is clear, however, that wave-like instabilities, solutions of the ordinary-differential-equation-based linear instability theory which follows (4) and either (5) or (6) are only one small class of the disturbances which solve the partial-differential-equation-based two-dimensional generalised eigenvalue problem resulting from (8) and (9) as will be shown by several examples in Section 4. The instability analyses reported herein have (8) and (9) as their departure point. On grounds of the resolution of two spatial directions, x and y, and in line with the terminology introduced earlier, the linear analysis following (8) and (9) is coined a *two-dimensional* global, or BiGlobal, linear instability theory.

2.2. On the solvability of the linear eigenvalue problems

Formulation of the three-dimensional global linear eigenvalue problem is straightforward; however, its numerical solution is not feasible with present-generation computer architectures at Reynolds numbers encountered in aeronautical applications. Indeed, coupled resolution of d spatial directions requires

storage of arrays each occupying

$$4 \times 2^6 \times N^{2\times d} \times 10^{-9} \text{ Gbytes}$$

of core memory in primitive variables formulation and 64-bit arithmetic, if N points resolve each spatial direction. The size of each array is doubled if 128-bit arithmetic is deemed to be necessary [36]. If a numerical method of optimal resolution power for a given number of discretisation points is utilised, such as spectral collocation, experience with the one-dimensional eigenvalue problem suggests that in excess of $N = 64$ must be used for adequate resolution of eigenfunction features in the neighbourhood of critical Reynolds numbers that are typical of boundary layer flows. The resulting estimates for the sizes of the respective matrices are

$$\sim 17.6 \text{ Tbytes}, \ \sim 4.3 \text{ Gbytes and } \sim 1.0 \text{ Mbytes},$$

if $d = 3, 2$ and 1, respectively, i.e. when decompositions (1), (8) or (4) are considered. It becomes clear that while the classic linear local analysis ($d = 1$) requires very modest computing effort and is indeed part of industrial prediction toolkits, the main memory required for the solution of the three-dimensional linear EVP is well beyond any currently available or forecast computing technology. An additional subtle point regarding decomposition (1)–(3) is that, from the point of view of a linear instability analysis, solution of the three-dimensional linear generalised eigenvalue problem which results from substitution of this decomposition into the incompressible Navier–Stokes and continuity equations and subtraction of the basic-flow related terms (themselves satisfying the equations of motion) may be *uninteresting*; the very existence of a three-dimensional steady state solution $\bar{\mathbf{q}}$ is synonymous with stability of *all* three-dimensional perturbations $\hat{\mathbf{q}}$, i.e. the imaginary part of all eigenvalues Ω defined in (3) is negative. On the other hand, a global instability analysis based on decomposition (8) and (9) is well feasible using current hardware and algorithmic technology and is the focus of the present review.

2.3. Basic flows for global linear theory

Before presenting the different forms that the eigenvalue problem of two-dimensional linear theory assumes, some comments on the basic flow $\bar{\mathbf{q}}$ are made. A two-dimensional basic state will be known analytically only in exceptional model flows; in the vast majority of cases of industrial interest it must be determined by numerical means. However, an accurate basic state is a prerequisite for reliability of the instability results obtained; if numerical residuals exist in the basic state (at $O(1)$) they will act as forcing terms in the $O(\epsilon)$ disturbance equations and result in erroneous instability predictions. In their most general form the $O(1)$ equations resulting from (8) and (9) are the two-dimensional equations of motion

$$\mathscr{D}_x\bar{u} + \mathscr{D}_y\bar{v} = 0, \tag{10}$$

$$\bar{u}_t + \bar{u}\mathscr{D}_x\bar{u} + \bar{v}\mathscr{D}_y\bar{u} = -\mathscr{D}_x\bar{p} + \mathscr{K}\bar{u}, \tag{11}$$

$$\bar{v}_t + \bar{u}\mathscr{D}_x\bar{v} + \bar{v}\mathscr{D}_y\bar{v} = -\mathscr{D}_y\bar{p} + \mathscr{K}\bar{v}, \tag{12}$$

$$\bar{w}_t + \bar{u}\mathscr{D}_x\bar{w} + \bar{v}\mathscr{D}_y\bar{w} = -\partial\bar{p}/\partial z + \mathscr{K}\bar{w}, \tag{13}$$

where

$$\mathscr{K} = 1/Re(\mathscr{D}_x^2 + \mathscr{D}_y^2), \tag{14}$$

$\mathscr{D}_x^2 = \partial^2/\partial x^2$ and $\mathscr{D}_y^2 = \partial^2/\partial y^2$. The need to perform a direct numerical simulation for the basic field is in remarkable contrast with the OSE/PSE type of linear analyses, in which the basic flow is either known analytically (e.g. plane Poiseuille or Couette flow), is obtained by solution of systems of ordinary differential equations or, at most, solution of the nonsimilar boundary layer equations. Depending on the global instability problem considered, limiting cases may exist in which the solution of the basic flow required for a global instability analysis may also be obtained by relatively straightforward numerical methods. In the simplest of cases the basic flow is known analytically. However, in general a DNS will be required to solve (10)–(13). The quality of the solution of (10)–(13) critically conditions that of the global linear eigenvalue problem; results of sufficiently high quality must be obtained for the basic flow velocity vector $\bar{\mathbf{q}}$ prior to attempting a global instability analysis.

Two simplified cases of system (10)–(13) deserve mention, one of a *parallel* basic flow which has a single velocity component $\bar{w}$ along the homogeneous z-direction while $\bar{u} = \bar{v} \equiv 0$ and one of a basic flow defined on the Oxy plane, having nonzero components $\bar{u}$ and $\bar{v}$ and $\bar{w} \equiv 0$ or $\partial\bar{w}/\partial z \equiv 0$. In the first case the Poisson problem

$$\mathscr{K}\bar{w} = \partial\bar{p}/\partial z \tag{15}$$

must be solved. With current algorithmic and hardware technologies a two-dimensional Poisson problem may be integrated numerically to arbitrarily high accuracy. Tatsumi and Yoshimura [14], Ehrenstein [16] and Theofilis et al. [37] solved (15) to obtain the basic flows for their respective analyses, which will be described in what follows.

It is more efficient to address the vorticity transport equation alongside the relation between streamfunction and vorticity,

$$\frac{\partial\zeta}{\partial t} + \left\{\frac{\partial\psi}{\partial y}\frac{\partial\zeta}{\partial x} - \frac{\partial\psi}{\partial x}\frac{\partial\zeta}{\partial y}\right\} - \mathscr{K}\zeta = 0, \tag{16}$$

$$\mathscr{K}\psi + \frac{1}{Re}\zeta = 0, \tag{17}$$

rather than solving the system of four equations (10)–(13) in the second case, where $\zeta = -\partial\bar{u}/\partial y + \partial\bar{v}/\partial x$ is the vorticity of the basic flow and ψ is its streamfunction, for which $\bar{u} = \partial\psi/\partial y$ and $\bar{v} = -\partial\psi/\partial x$ holds. Theofilis et al. [38], Hawa and Rusak [39] and Theofilis [40] provide examples of global analyses in which the basic state was obtained using the system (16) and (17). In case the basic state comprises a third velocity component $\bar{w}$ for which $\partial\bar{w}/\partial z \equiv 0$ holds, this velocity component can be calculated from

$$\frac{\partial\bar{w}}{\partial t} + \left\{\frac{\partial\psi}{\partial y}\frac{\partial\bar{w}}{\partial x} - \frac{\partial\psi}{\partial x}\frac{\partial\bar{w}}{\partial y}\right\} - \mathscr{K}\bar{w} = 0, \tag{18}$$

subject to appropriate boundary conditions (e.g. [37]). Note that (16), (17) and (18) are decoupled such that the latter equation can be solved after $(\bar{u}, \bar{w})$ have been determined. In view of the significance of the basic state for two-dimensional global linear instability analysis, the appendix is used to present an efficient two-dimensional DNS algorithm for the solution of (16) and (17); the same algorithm can be also used for solution of (18).

In an aeronautical engineering context an important flow is that of a boundary layer encompassing a closed recirculation region, i.e. "bubble" laminar separation. The first model for this flow was provided by the free-stream velocity distribution of Howarth [41]

$$U_\infty = \beta_0 - \beta_1 x, \tag{19}$$

where β_0, β_1, x and U_∞ are dimensional quantities. Details of the derivation and accurate numerical solution of the nonsimilar boundary layer equation which results from the free-stream velocity distribution (19) are also provided in the appendix. There, an accurate algorithm for the numerical solution of the appropriate governing equation will also be discussed.

An alternative method for obtaining the basic flow is experimentation using modern field measurement techniques, such as particle image velocimetry, and analysis of the data by appropriate algorithms (e.g. [42,43]). Care has to be taken when using experimentation in that the measured field corresponds to $\mathbf{q}$ in (1). There are two caveats; first, $\mathbf{q}$ may contain an unsteady component that must be filtered out before a steady basic state $\bar{\mathbf{q}}$ is obtained, as will be discussed in what follows. Second, the dependence of $\mathbf{q}$ on the three spatial coordinates must be examined in order to ensure satisfaction of the condition $\partial\bar{\mathbf{q}}/\partial z \equiv 0$ along an appropriately defined homogeneous spatial direction. On account of the fact that field resolution in the measurements is typically too coarse for subsequent analyses[2] it is recommended to model the experimental data, for example by use of two-dimensional DNS, compare the modelled results with measurements at different locations and, on satisfactory conclusion, proceed with the analysis. Prime examples of such modelling have been performed in the framework of the classic analysis of trailing vortex instability by Crow [44] and the recent efforts of de Bruin et al. [45], Crouch [46] and Fabre and Jacquin [47] in the same area. Either experiment or computation will ultimately deliver a basic state $\bar{\mathbf{q}}$ the global linear instability of which is now examined.

[2] In case of wall-bounded flows proximity to solid surfaces is an additional limitation to resolution.

2.4. The linear disturbance equations at $O(\varepsilon)$: a Navier–Stokes based perspective

A step back from decomposition (8) and (9) is first taken and homogeneity of space in the z-direction is retained as the only assumption. This results in the coefficients of the linearised disturbance equations at $O(\varepsilon)$ being independent of the z-coordinate, in which an eigenmode decomposition may be introduced, such that

$$\tilde{\mathbf{q}}(x, y, z, t) = \mathbf{q}'(x, y, t)\mathrm{e}^{\mathrm{i}\beta z} + \text{c.c.} \tag{20}$$

with $\mathbf{q}' = (u', v', w', p')^{\mathrm{T}}$. Complex conjugation is introduced in (20) since β is taken to be real in the framework of the present temporal linear nonparallel analysis, $\tilde{\mathbf{q}}$ is real while $\mathbf{q}'$ may in general be complex. One substitutes decomposition (20) into the equations of motion, subtracts out the $O(1)$ basic-flow terms and solves the linearised Navier–Stokes equations (LNSE)

$$-\frac{\partial u'}{\partial t} + [\mathscr{L} - (\mathscr{D}_x\bar{u})]u' - (\mathscr{D}_y\bar{u})v' - \mathscr{D}_x p' = 0, \tag{21}$$

$$-\frac{\partial v'}{\partial t} - (\mathscr{D}_x\bar{v})u' + [\mathscr{L} - (\mathscr{D}_y\bar{v})]v' - \mathscr{D}_y p' = 0, \tag{22}$$

$$-\frac{\partial w'}{\partial t} - (\mathscr{D}_x\bar{w})u' - (\mathscr{D}_y\bar{w})v' + \mathscr{L}w' - \mathrm{i}\beta p' = 0, \tag{23}$$

$$\mathscr{D}_x u' + \mathscr{D}_y v' + \mathrm{i}\beta w' = 0, \tag{24}$$

where the linear operator is

$$\mathscr{L} = (1/Re)(\mathscr{D}_x^2 + \mathscr{D}_y^2 - \beta^2) - \bar{u}\mathscr{D}_x - \bar{v}\mathscr{D}_y - \mathrm{i}\beta\bar{w}. \tag{25}$$

Here the nonlinearities in $\mathbf{q}'$ are neglected for numerical expediency, making LNSE a subset of a DNS approach. The basic flow may be taken either as steady or unsteady and obtained from a solution of (10)–(13). The issue of appropriate boundary conditions for the LNSE approach will be addressed in conjunction with the subsequent discussion of solution of the partial-derivative eigenvalue problem (EVP).

Early global flow instability analyses employed the LNSE concept to recover linear instabilities of nonlinear basic flow. Kleiser [48], Orszag and Patera [49], Brachet and Orszag [50] and Goldhirsch et al. [51] used this approach in which the desired instability results can be obtained by post-processing the DNS results during the regime of linear amplification or damping

of small-amplitude disturbances, for instance from different logarithmic derivatives of the DNS solution (e.g. [52]). More recently, Collis and Lele [53] and Malik [54] have utilised the LNSE concept in subsonic three-dimensional and hypersonic two-dimensional flows. Provided the third spatial direction could be neglected altogether, LNSE results are related with the linear development of the two-dimensional eigenmodes of the global EVP ($\beta = 0$). If the homogeneous spatial direction is resolved using a Fourier spectral method the three-dimensional ($\beta \neq 0$) global flow eigenmodes are actually the two-dimensional Fourier coefficients of the decomposition and can be monitored during the simulation. Otherwise, if a different discretisation of the homogeneous spatial direction is used, the development of all but the least-stable/most-unstable global flow eigenmode may be obscured.

In the important class of a time-periodic basic state that takes the form

$$\bar{\mathbf{q}}(x,y,t) = \bar{\mathbf{q}}(x,y,t+T) \tag{26}$$

and the global eigenmodes may be derived from (21)–(24) using Floquet theory, taking the form

$$\mathbf{q}'(x,y,t) = \mathrm{e}^{\sigma t} \sum_{n=-N}^{N} \hat{\mathbf{q}}(x,y)\mathrm{e}^{\mathrm{i}\delta t}, \quad \text{where } \delta = \frac{2\pi}{T}. \tag{27}$$

Floquet theory was introduced to study the linear instability of nonlinearly modified basic states by Herbert [55–57], whose EVP results were reproduced in DNS by Orszag and Patera [49], Gilbert [58] and Zang and Hussaini [59]. More recently, the linear analyses of Henderson and Barkley [23], Barkley and Henderson [24] and the subsequent nonlinear analyses of Henderson [60] and Barkley et al. [61] on the instability of steady flow on an unswept infinitely long circular cylinder, in which the entire Bénard–Kármán vortex street constitutes the time-periodic basic state, are examples of Floquet analyses.

Although it is difficult to compare directly, the conceptual advantage of a DNS/LNSE-based global instability analysis over the EVP approach is that both the linear and the nonlinear development of the most unstable eigendisturbances, as well as the issue of receptivity [62], can be studied in a unified manner. Its disadvantage compared with the EVP is that a DNS/LNSE approach is substantially less efficient than the numerical solution of the EVP in performing parametric studies. It has to be stressed, however, that the nontrivial solution of a partial derivative EVP, in which two spatial directions are coupled, in conjunction with the continuous development of efficient approaches for the performance of DNS do not permit making definitive statements as to the choice of an optimal approach for global instability analysis.

2.5. The different forms of the partial-derivative eigenvalue problem (EVP)

If the two-dimensional basic state is a steady solution of the equations of motion, the linear disturbance equations at $O(\varepsilon)$ are obtained by substituting decomposition (8) and (9) into the equations of motion, subtracting out the $O(1)$ basic flow terms and neglecting terms at $O(\varepsilon^2)$. In the present temporal framework, β is taken to be a real wavenumber parameter describing an eigenmode in the z-direction, while the complex eigenvalue Ω, and the associated eigenvectors $\hat{\mathbf{q}}$ are sought. The real part of the eigenvalue, $\Omega_\mathrm{r} \equiv \Re\{\Omega\}$, is related with the frequency of the global eigenmode while the imaginary part is its growth/damping rate; a positive value of $\Omega_\mathrm{i} \equiv \Im\{\Omega\}$ indicates exponential growth of the instability mode $\tilde{\mathbf{q}} = \hat{\mathbf{q}}\mathrm{e}^{\mathrm{i}\Theta_{2D}}$ in time t while $\Omega_\mathrm{i} < 0$ denotes decay of $\tilde{\mathbf{q}}$ in time. The system for the determination of the eigenvalue Ω and the associated eigenfunctions $\hat{\mathbf{q}}$ in its most general form can be written as the complex nonsymmetric generalised EVP

$$[\mathscr{L} - (\mathscr{D}_x\bar{u})]\hat{u} - (\mathscr{D}_y\bar{u})\hat{v} - \mathscr{D}_x\hat{p} = -\mathrm{i}\Omega\hat{u}, \tag{28}$$

$$-(\mathscr{D}_x\bar{v})\hat{u} + [\mathscr{L} - (\mathscr{D}_y\bar{v})]\hat{v} - \mathscr{D}_y\hat{p} = -\mathrm{i}\Omega\hat{v}, \tag{29}$$

$$-(\mathscr{D}_x\bar{w})\hat{u} - (\mathscr{D}_y\bar{w})\hat{v} + \mathscr{L}\hat{w} - \mathrm{i}\beta\hat{p} = -\mathrm{i}\Omega\hat{w}, \tag{30}$$

$$\mathscr{D}_x\hat{u} + \mathscr{D}_y\hat{v} + \mathrm{i}\beta\hat{w} = 0, \tag{31}$$

subject to appropriate boundary conditions, which will be addressed shortly.

Simplifications of the partial-derivative EVP (28)–(31) valid for certain classes of basic flows are discussed first. One such case arises when the wavenumber vector $\beta\mathbf{e}_z$ is perpendicular to the plane on which the basic flow $(\bar{u},\bar{v},0,\bar{p})$ develops. The absence of a basic flow z-velocity component in the linear operator in conjunction of the redefinitions

$$\tilde{\Omega} = \mathrm{i}\Omega, \tag{32}$$

$$\tilde{w} = \mathrm{i}\hat{w} \tag{33}$$

result in the following generalised real nonsymmetric partial derivative EVP after linearisation and subtraction of the basic-flow related terms:

$$[\mathscr{M} - (\mathscr{D}_x\bar{u})]\hat{u} - (\mathscr{D}_y\bar{u})\hat{v} - \mathscr{D}_x\hat{p} = \tilde{\Omega}\hat{u}, \tag{34}$$

$$-(\mathscr{D}_x\bar{v})\hat{u} + [\mathscr{M} - (\mathscr{D}_y\bar{v})]\hat{v} - \mathscr{D}_y\hat{p} = \tilde{\Omega}\hat{v}, \tag{35}$$

$$+\mathscr{M}\tilde{w} - \beta\hat{p} = \tilde{\Omega}\tilde{w}, \tag{36}$$

$$\mathscr{D}_x\hat{u} + \mathscr{D}_y\hat{v} - \beta\tilde{w} = 0, \tag{37}$$

where

$$\mathscr{M} = (1/Re)(\mathscr{D}_x^2 + \mathscr{D}_y^2 - \beta^2) - \bar{u}\mathscr{D}_x - \bar{v}\mathscr{D}_y. \tag{38}$$

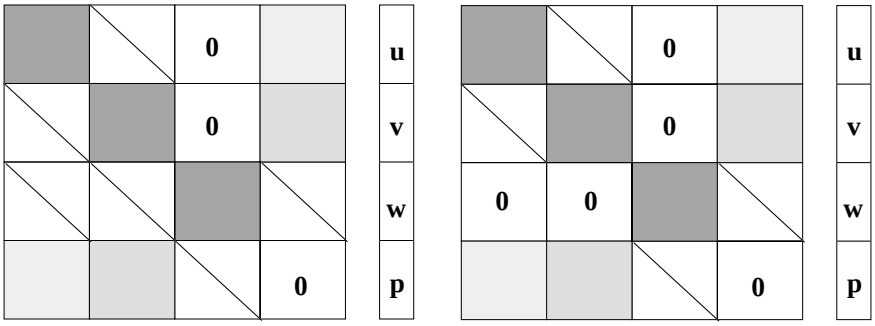

Fig. 3. Structure of the complex (left) and the real (right) matrix **A** in (55) resulting from numerical discretisation of (28)–(31) and (34)–(37), respectively.

From the point of view of a numerical solution of the EVP, formulation (34)–(37) enables storage of real arrays alone, as opposed to the complex arrays appearing in (28)–(31). Although this may appear a trivial point, freeing half of the storage required for the coupled numerical discretisation of two spatial directions results in the ability to address flow instability at substantially higher resolutions using (34)–(37) as opposed to those that could have been addressed based on (28)–(31). This ability is essential in case high Reynolds numbers are encountered and/or resolution of strong gradients in the flow is required. This point has been clearly manifested in the difficulties encountered in the problem of global linear instability analysis in the classic lid-driven cavity flow. While smaller than the original EVP system (34)–(37) still consists of four coupled equations. The dense structure of the LHS of (28)–(31) and (34)–(37) is presented in Fig. 3. From a physical point of view (34)–(37) delivers real or complex conjugate pairs of eigenvalues, which points to the existence of *stationary* ($\Re\{\tilde{\Omega}\}=0$) or *pairs* ($\pm\Re\{\tilde{\Omega}\}\neq 0$) of disturbances, *travelling in opposite directions* along the z axis.

A reduction of the number of equations that need be solved is possible in a class of basic flows $(0,0,\bar{w},\bar{p})^{\mathrm{T}}$ which possess one velocity component alone, the spanwise velocity component $\bar{w}$ *along* the direction of the wavenumber vector $\beta\mathbf{e}_z$. In this case the EVP may be re-written in the form of the generalised Orr–Sommerfeld and Squire system,

$$\mathscr{E}\hat{u}=\mathscr{O}\hat{w}, \tag{39}$$

$$\mathscr{E}\hat{v}=\mathscr{O}\hat{u}, \tag{40}$$

where

$$\mathscr{E}=-\left[\frac{\mathrm{i}}{\beta}\mathscr{N}+(\bar{w}-\Omega/\beta)\right](\mathscr{D}_y^2-\beta^2)+(\mathscr{D}_y^2\bar{w}) \tag{41}$$

and

$$\mathscr{O}=\left[\frac{\mathrm{i}}{\beta}\mathscr{N}+(\bar{w}-\Omega/\beta)\right]\frac{\partial^2}{\partial x\partial y}-(\mathscr{D}_x\bar{w})\mathscr{D}_y-(\mathscr{D}_y\bar{w})\mathscr{D}_x-\frac{\partial^2\bar{w}}{\partial x\partial y} \tag{42}$$

with

$$\mathscr{N}=(1/Re)(\mathscr{D}_x^2+\mathscr{D}_y^2-\beta^2). \tag{43}$$

This form of the two-dimensional global EVP was first presented and solved by Tatsumi and Yoshimura [14]. Compared with the original EVP (28)–(31), the two discretised Eqs. (39) and (40) have 2^2 lower storage requirements and demand 2^3 shorter runtime for their solution if the standard QZ algorithm is used for the recovery of the eigenspectrum. However, the appearance of fourth-order derivatives in the generalised Orr–Sommerfeld and Squire system as opposed to second-order derivatives in the original EVP may result in a higher number of discretisation points per eigenfunction being necessary for results of the former problem to be of comparable quality as those of the latter, so that the above estimates of savings may not be fully realisable in practice.

An important subclass of two-dimensional eigenvalue problems deserves being mentioned separately since it arises frequently in applications where physical grounds exist to treat one of the two resolved spatial directions as homogeneous and resolve it by a discrete Fourier Ansatz. As a matter of fact the first successful extension of the classic linear theory based on (4), coined by Herbert [57] a *secondary* instability analysis, solves eigenvalue problems of this class. In case one spatial direction, say x, is taken to be periodic the two-dimensional eigenvalue problem can be formulated by considering an expansion of the eigenmodes using Floquet theory [63]

$$\hat{\mathbf{q}}(x,y)=\mathrm{e}^{\mathrm{i}\delta x}\sum_{n=-N}^{N}\tilde{\mathbf{q}}_n(y)\mathrm{e}^{\mathrm{i}n\alpha x}. \tag{44}$$

This is feasible if the basic state $\bar{\mathbf{q}}$ is a consistently defined homogeneous state, usually composed of an x-independent laminar profile and a linear or nonlinear superposition of an x-periodic primary disturbance. What sets this class of eigenvalue problems conceptually apart from the straightforwardly formulated systems (28)–(31), (34)–(37) or (39) and (40), besides being of utility in the particular situation of one periodic spatial direction, is that the simplicity of the boundary conditions of this class of global eigenvalue problems is not matched by that of their formulation. As a matter of fact, the number of Fourier coefficients in (44) needed to converge x-periodic global eigenmodes in typical applications of aeronautical interest is such that the effort of formulating the EVP using Floquet theory (c.f. [64]) may not be justified compared with a direct solution of the global EVP ((28)–(31)) in which the periodic direction is treated numerically using appropriate expansions [65].

A brief discussion of inviscid instability analysis is warranted here, since the simplest form of the two-dimensional EVP can be obtained in the $Re\to\infty$ limit, if physical grounds exist on which an inviscid linear analysis can be expected to recover the essential flow instability mechanisms. Some justification is provided by inviscid analyses of compressible flow instability in flat-plates and bodies of revolution (in either case resolving one spatial dimension), which was shown to deliver results in full qualitative and good quantitative agreement with the considerably more elaborate numerical solution of the corresponding viscous problem [31].

In the incompressible limit, straightforward manipulation of the linearised system of disturbance equations under the assumption of existence of a single basic flow velocity component in the direction of flow motion, $\bar{w}$, results in a single equation to be solved, the generalised Rayleigh equation first solved by Henningson [66] and subsequently by Hall and Horseman [67], Balachandar and Malik [68] and Otto and Denier [69] in the form:

$$Re\mathcal{N}\hat{p}-\frac{2\bar{w}_x\hat{p}_x}{\bar{w}-\Omega/\beta}-\frac{2\bar{w}_y\hat{p}_y}{\bar{w}-\Omega/\beta}=0. \tag{45}$$

This real EVP presents the lowest storage and operation count requirements for the performance of a global linear instability analysis, since in a temporal framework it is linear in the desired eigenvalue $c=\Omega/\beta$ and hence demands solution of one as opposed to the four coupled equations of the original problem, thus being optimal from the point of view of the ability to devote the available computing resources to the resolution of a single eigenfunction $\hat{p}$; all components of the disturbance velocity eigenvector may be recovered from $\hat{p}$ and its derivatives.

In compressible flow, the same assumption of a single velocity component $\hat{w}$, together with an equation of state

$$\kappa M^2\hat{p}=\bar{\rho}\hat{T}+\bar{T}\hat{\rho}, \tag{46}$$

also leads to the single equation

$$\begin{aligned}Re\mathcal{N}\hat{p}&+\left[\left(\frac{\bar{p}_x}{\kappa\bar{p}}-\frac{\bar{\rho}_x}{\bar{\rho}}\right)-\frac{2\beta\bar{w}_x}{(\beta\bar{w}-\Omega)}\right]\hat{p}_x\\&+\left[\left(\frac{\bar{p}_y}{\kappa\bar{p}}-\frac{\bar{\rho}_y}{\bar{\rho}}\right)-\frac{2\beta\bar{w}_y}{(\beta\bar{w}-\Omega)}\right]\hat{p}_y\\&+\left[\frac{\bar{\rho}(\beta\bar{w}-\Omega)^2}{\kappa\bar{p}}\right]\hat{p}=0.\end{aligned} \tag{47}$$

However, this equation is cubic in either of Ω or β, in a temporal or spatial framework, respectively. Numerical solution as a matrix eigenvalue problem in this case requires use of the companion matrix approach [70] such that the leading dimension of the inviscid eigenvalue problem is only a factor 3/5 smaller than that of the corresponding viscous problem. This in turn makes the choice of approach to follow for a global instability analysis less straightforward than in incompressible flow. Theofilis (unpublished) has solved (47) in the course of an instability analysis of compressible flow over an elliptic cone.

The boundary conditions for the disturbance pressure must be modified compared with those of a viscous analysis, to reflect the inviscid character of the analysis based on the partial-differential-equation (45) and (47). However, in all four aforementioned incompressible inviscid global analyses one spatial direction was treated as periodic, which considerably simplified the numerical solution of the problem in that no issues of appropriate boundary conditions in this direction or their compatibility with those in the other resolved spatial direction arise. This is no longer the case if both resolved spatial directions are taken to be inhomogeneous. Further, in view of the well-established results of the one-dimensional inviscid linear instability theory, attention needs to be paid to the issue of critical layer resolution [32]; such theoretical considerations extending the concept of a critical layer in two spatial dimensions are currently not available. Comparisons between viscous and inviscid solutions of the two-dimensional eigenvalue problem are also presently absent.

2.6. *Boundary conditions for the inhomogeneous two-dimensional linear EVP*

The subspace of admissible solutions of the EVPs (28)–(31), (34)–(37), (39) and (40) or (45) can be determined by imposition of physically plausible boundary conditions. Two types of boundaries may be distinguished, namely closed and open boundaries, respectively, corresponding to either solid-walls or any of far-field, inflow or outflow boundaries. Some

guidance for the boundary conditions to be imposed in the two-dimensional EVP at solid walls and far-field boundaries is offered by the classic one-dimensional linear analysis. At solid walls, viscous boundary conditions are imposed on all disturbance velocity component in all but the inviscid EVP; the viscous boundary conditions for the disturbance velocity components read

$$\hat{u} = 0, \quad \hat{v} = 0, \quad \hat{w} = 0, \tag{48}$$

$$\hat{u}_s = 0, \quad \hat{v}_s = 0, \quad \hat{w}_s = 0 \tag{49}$$

with subscript s denoting first derivative along the tangential direction. In the free-stream, exponential decay of all disturbance quantities is expected. The boundary condition (48) is imposed at a large distance from the wall by use of homogeneous Dirichlet boundary conditions on all disturbance velocity components and pressure, or by use of asymptotic boundary conditions which permit considerable reduction of the integration domain. However, in view of the stretching transformation of wall-normal coordinates, which is typically applied to resolve near-wall structures of the eigenmodes, imposition of asymptotic boundary conditions near a solid wall does not necessarily imply substantial savings in the size of the discretised problem compared with that which results from considering a domain in which homogeneous Dirichlet boundary conditions are imposed at large distances from the solid wall. Homogeneous Dirichlet boundary conditions are also imposed on the disturbance velocity components at a solid wall and a far-field boundary in case one spatial direction is treated as periodic.

Boundary conditions for the disturbance pressure at a solid wall do not exist physically; instead the compatibility condition

$$\frac{\partial \hat{p}}{\partial x} = \mathscr{K}\hat{u} - \bar{u}\frac{\partial \hat{u}}{\partial x} - \bar{v}\frac{\partial \hat{u}}{\partial y}, \tag{50}$$

$$\frac{\partial \hat{p}}{\partial y} = \mathscr{K}\hat{v} - \hat{u}\frac{\partial \hat{v}}{\partial x} - \hat{v}\frac{\partial \hat{v}}{\partial y} \tag{51}$$

can be collocated. Homogeneous Dirichlet boundary conditions can be imposed on the disturbance pressure at a free boundary, or on its first derivative in the direction normal to the boundary.

At inflow one may use homogeneous Dirichlet boundary conditions on the disturbance velocity components; this *choice* corresponds to studying disturbances *generated* within the examined basic flowfield. The study of global linear instability in the laminar separation bubble [35] is based on such an approach. Other choices are possible, for example based on information on *incoming* perturbations obtained from linear local (5) or nonlocal (6) analysis. This freedom highlights the potential of the partial-derivative EVP approach to be used as a numerical tool for receptivity analyses alongside the more commonly used (and substantially more expensive) spatial DNS approach.

Care has to be taken in case the free boundary is taken too close to regions where the disturbance eigenmodes are still developing. Analytically known asymptotic boundary conditions, derived from the governing equations and taking into account the form of the basic flow at the boundary, is the method of choice in this case, when the boundary is located at a region where the basic flow has reached a uniform value. Typical example is the free-stream in boundary layer flow. However, in the course of solution of the two-dimensional EVP a closure boundary may be necessary at regions where the basic flow is itself developing. This may for instance occur at the downstream free boundary in boundary layer flow.

At an outflow boundary one encounters an ambiguity with respect to the boundary conditions to be imposed on the disturbance velocity components analogous to that encountered in spatial DNS. In the latter case, one solution presented by Fasel et al. [71] is imposition of boundary conditions based on incoming/outgoing wave information. Specifically, one may impose

$$\partial\hat{\mathbf{q}}/\partial x = \pm \mathrm{i}|\alpha|\hat{\mathbf{q}}, \tag{52}$$

to ensure propagation of wave-like small-amplitude disturbances $\hat{\mathbf{q}}$ into or out of the integration domain. Although this approach has been successfully used in cases the eigenmode structure merges uniformly into a wave-like linear disturbance (e.g. [72]) imposition of this solution may be restrictive in general, since a wave-like solution is only one of the possible disturbances developing in the resolved two-dimensional domain. This is certainly not the most interesting instability, from a physical point of view, in the context of a global instability analysis of two problems discussed in what follows, that of global instability in the laminar separation bubble [35] and the swept attachment-line boundary layer [73,18]. Furthermore, even if one is interested only in wave-like solutions, the wavenumber α in (52) is an a priori unknown quantity.

An alternative to analytic closure at an open boundary is imposition of numerical boundary conditions which extrapolate information from the interior of the calculation domain. Such conditions have been imposed by several investigators who showed extrapolation to perform adequately in a variety of flow problems. Theofilis [18] and Heeg and Geurts [74] employed linear extrapolation along the chordwise direction x of the swept attachment-line boundary layer, while Härtel et al. [75,76] used this approach in their studies of gravity-current head and obtained very good agreement with DNS results, as shown in Fig. 4. Finally, linear extrapolation of results from the interior of the domain was used in the separation bubble global instability analyses of Theofilis et al. [35]. One obvious criterion for

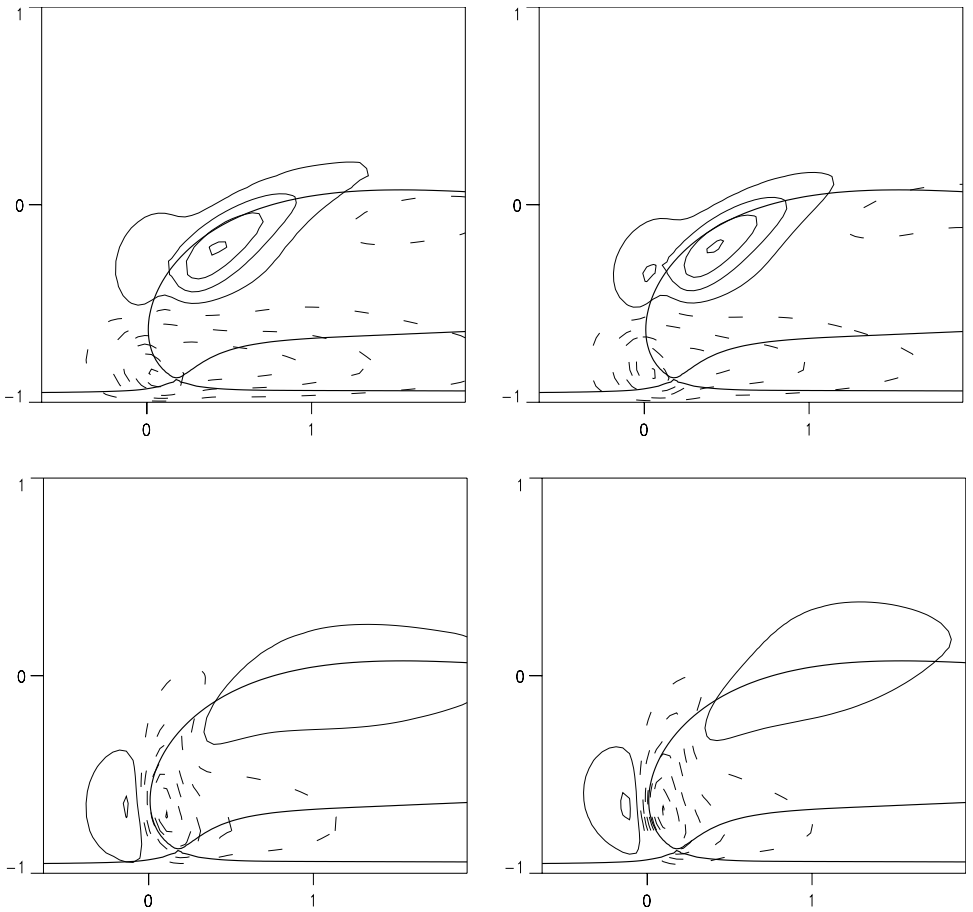

Fig. 4. Comparison of global eigenmodes obtained by DNS (left column) and solution of the two-dimensional eigenvalue problem (right column) in the gravity-current head [75].

the adequacy of this approach and reliability of the results it delivers is the insensitivity of the eigenvalues obtained on the order of the extrapolation. Experience has shown that if the location of the closure boundary is not affecting the simulation results, linear extrapolation will suffice.

In case the linear analysis is based on solution of Eq. (45) inviscid boundary conditions for pressure at solid walls must close the system of equations [66,67],

$$\frac{\partial \hat{p}}{\partial y} = 0 \quad \text{at } y = 0 \text{ and } y \to \infty, \tag{53}$$

where y denotes the spatial coordinate normal to a solid surface. Finally, when symmetries exist in the steady basic state upon which instability develops, it is tempting to reduce the computational cost of the partial derivative EVP by considering that the disturbance field inherits these symmetries. The domain on which the disturbance field is defined is then divided into subdomains according to the symmetries of the basic flow and the eigenproblem is solved on one of these subdomains, after imposing boundary conditions at the artificially created internal boundaries, which express the symmetries of the basic flow. The partial-derivative EVP in the rectangular duct [14], Görtler vortices [67] and swept attachment-line boundary layer [73] has used this approach. Unless supported by theoretical arguments (derived for instance using Lie-group methods) it is far from clear that the disturbance field should satisfy the symmetries of the basic flow and one should be cautious whether imposition of symmetries on the disturbance field constrains the space of solutions obtained and inhibits classes of potentially interesting eigensolutions from manifesting themselves in the global eigenspectrum.

3. Numerical methods

3.1. The two-dimensional basic flow

The choice of numerical method for the BiGlobal eigenvalue problem is crucial for the success of the

computation. Several reasons contribute to this assertion. With respect to the provision of a two-dimensional basic flow, it has been stressed that this should be an accurate solution of the equations of motion at $O(1)$. This implies the need for convergence in the two resolved spatial coordinates and, if applicable, in time. It may at first sight appear a straightforward task to achieve these goals, given the maturity of existing algorithms for the solution of the two-dimensional equations of motion and the ever increasing capabilities of modern hardware. Indeed, a wide palette of methods exist in the literature, but the mixed success of their results might be an indication of the little attention that has been paid to the following points.

First, the need may arise for the basic flow to be obtained on much finer a grid than that on which the subsequent analysis is feasible in order for information to be reliably interpolated on the latter grid. Second, a complete parametric study of the BiGlobal instability analysis problem requires the provision of basic flows at sufficient Reynolds number values, until a neutral loop can be constructed with reasonable degree of refinement. Third, a more subtle point is worthy of being highlighted here. In case of integration in time until a steady state is obtained and starting from a low Reynolds number at which convergence in time is quickly achieved, one notes that increasingly long time-integrations are necessary as the Reynolds number increases. As a matter of fact straightforward rearrangement of (8) and (9) delivers an estimate of the time T_{A_1/A_2} necessary (under linear conditions) for the least stable BiGlobal mode present in the numerical solution to be reduced from an amplitude A_1 to A_2. This may be calculated using

$$T_{A_1/A_2} = \ln(A_1/A_0)/(-\Omega_i), \tag{54}$$

where Ω_i is the damping rate of the mode in question. The worst case scenario in a time-accurate integration is that the solution will lock-in the least-stable BiGlobal eigenmode which develops upon $\tilde{\mathbf{q}}$ and has $\beta = 0$ throughout the course of the simulation [77]; an upper bound for the time necessary for the steady-state to be obtained may then be calculated by (54) in which Ω_i is the damping rate of this mode. Defining, for example, convergence as the reduction of an $O(1)$ residual by 10 orders of magnitude results in an integration time of $T_{10^{-10}} \approx 23/|\Omega_i|$. This is a conservative estimate since it is occasionally observed that other stronger damped eigenmodes will come into play early in the simulation and the least-damped eigenmode will only determine the late stages of the convergence process. However, with $\Omega_i \to 0$ as conditions for amplification of the two-dimensional BiGlobal eigenmode ($\beta = 0$) are approached the integration time in the DNS until convergence in time is achieved could be substantial. Consequently, terminating the time-integration for the basic state prematurely, on grounds of computational expediency, will be reflected in erroneous BiGlobal instability analysis results.

Even on modern hardware, a combination of these reasons can result in the limit of feasibility of a BiGlobal instability analysis quickly being reached on account of poor choice of numerical approach for the solution of the basic flow problem; not only accurate but also efficient methods for the calculation of the basic state are called for. Description of numerical approaches for solving the unsteady equations of motion is beyond the scope of the present paper; the interested reader is referred to a number of recent articles and monographs (e.g. [78–80]) on the issue. In the appendix a well-validated DNS approach based on spectral collocation on rectangular grids is presented, which has been shown to fulfill the aforementioned prerequisites of accuracy and efficiency in a variety of open- and closed-system flows. Additionally, an algorithm for the numerical solution of the nonsimilar boundary-layer equations is presented, the results of which form inflow conditions for the DNS of one of the most common instability problems in aeronautics, that of separated boundary layer flow.

3.2. The eigenvalue problem

As far as the eigenvalue problem is concerned, if the BiGlobal instability analysis is performed using a DNS methodology, the above comments apply in addition to aggravation of the cost of the analysis on account of parametric studies at different β values. On the other hand, if an EVP is solved, consensus appears to emerge that the classic approach of using variants of the QZ algorithm which delivers the full eigenvalue spectrum is inefficient and even on present-day hardware may constrain the analysis to Reynolds numbers of $O(10^2)$. Numerical discretisation of the two spatial directions of any of the alternative formulations of the EVP, for instance using the collocation derivative matrices (107) and (108) and imposition of the appropriate boundary conditions, results in a matrix eigenvalue problem of the form

$$\mathbf{A}X = \Omega\mathbf{B}X. \tag{55}$$

The major challenge associated with the BiGlobal instability analysis is the size of this generalised nonsymmetric, in general complex, matrix eigenvalue problem. While the absence of $\bar{w}$ results in the ability to formulate a real EVP, the storage requirements of the discretised problem are still formidable. Typical resolutions for adequate description of the spatial structure of BiGlobal eigenfunctions require the solution of upwards of 1000 coupled linear equations for each component of the disturbance eigenvector $\hat{\mathbf{q}}$. Clearly, the numerically least demanding formulation is the inviscid generalised Rayleigh equation (45) followed by the generalised Orr–Sommerfeld and Squire system (39) and

(40). In its most general form, however, the dense structure of matrix **A** in (55) schematically shown in Fig. 4 does not permit further simplifications and one must rely on adequate computing power in order to solve the two-dimensional eigenvalue problem.

Two aspects of the numerical solution must be addressed independently. The first concerns methods for the spatial discretisation of the linear system. Several alternatives have been used in the literature. An indicative list contains finite-difference [81,74], finite-volume [82,83] and finite-element approaches [11,84,85], spectral Galerkin/collocation methods [86,14,73,87], spectral element methods [24,88] and mixed finite-difference/spectral schemes [66,69]. A detailed description of either numerical method is beyond the scope of the present review and can be found in the original references.

The second aspect concerns methods for the recovery of the eigenvalue. Since interest from a physical point of view is in the leading eigenvalues, use of the classic QZ algorithm [15] which delivers the full spectrum is either inefficient or impractical. The reason is that this algorithm requires the storage of four arrays, two for the discretised matrices in (55) and two for the returned results. Even less efficient when used as the only means of eigenvalue computation are iterative techniques based on the inverse Rayleigh [15] or the less-known Wieland [89] algorithms. Nevertheless, if the full spectrum is required, the QZ algorithm is one of the viable alternatives that may be used and has indeed delivered accurate results when combined with a spectral method for the discretisation of the spatial operator (e.g. [14,73]). Further iterative methods in this vein are the schemes used in [66,67,69].

Krylov subspace iteration (e.g. [19,50,90]), on the other hand, provides efficient means of recovering an arbitrarily large window of either leading or interior eigenvalues of a matrix at a fraction of both the memory and the computing time requirements of the QZ algorithm. Several BiGlobal instability analyses to-date have used the Arnoldi algorithm, which solves either the generalised EVP or a standard EVP resulting from the so-called shift-and-invert strategy which converts (55) to

$$\hat{\mathbf{A}}X = \mu X, \quad \hat{\mathbf{A}} = (\mathbf{A} - \lambda\mathbf{B})^{-1}\mathbf{B}, \quad \mu = \frac{1}{\Omega - \lambda}, \tag{56}$$

where λ is a shift parameter. In solving the original generalised EVP one may take advantage of the sparsity of **A** and the simple structure of **B**; this advantage is lost when one uses the shift-and-invert algorithm. In return one gains the ability to store a single array, which may be decisive for the success of the computation.

The outline of the Arnoldi algorithm for the standard eigenvalue problem, including the calculation of the Ritz vectors which approximate the eigenvectors of the original eigenvalue problem, is presented in Table 1. The algorithm itself is both vectorisable and parallelisable. Lehoucq et al. [91] have provided open-source vector and parallel versions of the Arnoldi algorithm which have been used successfully, amongst others, by Wintergerste and Kleiser [92]. On the other hand, hand-coded versions of the algorithm have reached performance of over 4 Gflops on a single-processor NEC SX-5 supercomputer, without optimisation [87,40,35,93]. Further efficiency gains can be achieved by parallelizing the most CPU time consuming element of the algorithm, namely calculation of the inverse of matrix **A**.

Worthy of mention is a particular aspect of subspace iteration methods, which has been employed in combination with finite-element discretisation of the spatial operator by Morzynski et al. [85], namely preconditioning of the problem combined with a real-shift inverse Cayley transformation. The advantage of the latter transformation is that it permits reducing the eigenvalue computations from complex to real arithmetic, which in turn permits devoting the freed memory to either resolve the flow better at a certain Reynolds number or attain substantially larger Reynolds numbers in comparison with an eigenvalue computation based on complex arithmetic. Yet another modern method for the calculation of large-scale eigenvalue problems, the

Table 1
One variant of the Arnoldi algorithm, including calculation of the Ritz vectors

- Compute $\hat{A} = A + \mathrm{i}\lambda$ and overwrite $\hat{A}$ by its LU-decomposition
- Compute the entries $h_{i,j}$ of the Hessenberg Matrix $\bar{H}_m$

Initialize $\begin{cases} \hat{r}_0 = [1, 1, \ldots, 1]^{\mathrm{T}}, & r_0 \coloneqq \hat{r}_0/\|\hat{r}_0\|_2, \\ h_{0,0} = \|\hat{r}_0\|_2, & \bar{V}_0 = r_0 \end{cases}$

For $j = 0, \ldots, m-1$ do

Set $r_j \coloneqq (B, r_j)$

Use $\hat{A}$ to solve (55)

For $i = 0, \ldots, j$ do $\begin{cases} h_{i,j} \coloneqq (\bar{V}_i, r_j) \\ r_j \coloneqq r_j - h_{i,j}\bar{V}_i \end{cases}$

Form $h_{j+1,j} = \|r_j\|_2$ and $\bar{V}_{j+1} = r_j/h_{j+1,j}$

- Compute the eigenvalues of $H_m \equiv \bar{H}_m$−last row using the QZ
- Select an interesting eigenvalue and calculate its Ritz vector $q = (\bar{V}, y)$

Jacobi–Davidson algorithm for polynomial-eigenvalue problems [94], deserves mention. This algorithm can be used if the two-dimensional eigenvalue is addressed in the framework of a spatial analysis, i.e. an approach which takes Ω in the original EVP or in any of the derivatives of system (28)–(31) as a real parameter and seeks to calculate a complex eigenvalue β and associated eigenvectors $\hat{\mathbf{q}}$. Rearranging terms in the two-dimensional EVP one obtains a quadratic eigenvalue problem of the form

$$\mathbf{A}X + \beta\mathbf{B}X + \beta^2\mathbf{C}X = 0. \tag{57}$$

The size of the matrices involved precludes application of the classic companion-matrix approach [70] in conjunction with the Arnoldi algorithm.[3] The Jacobi–Davidson algorithm, on the other hand, solves polynomial eigenvalue problems directly, without the need to convert them to larger linear eigenvalue problems. As in the Arnoldi algorithm, efficient solution approaches can be used for the residual linear operations involved. Furthermore, it is feasible to use domain decomposition in conjunction with the Jacobi–Davidson algorithm and consequently both vectorise and parallelise the entire procedure for the calculation of the two-dimensional spatial eigenvalue spectrum in complex geometries.

However, a word of caution is warranted regarding a 'spatial' BiGlobal eigenvalue problem from a physical point of view. The spatial concept is well-defined only in the case of two-dimensional instabilities in the framework of (4) and (5), where the real part of the sought eigenvalue corresponds to the wavenumber of an instability *wave*. If two spatial directions are resolved, the eigenmodes will *not* possess a wave-like character in the general case [33] and it is not clear whether the concept of a complex β can be simply borrowed from its counterpart terminology in one-dimensional linear analysis. By contrast to the temporal BiGlobal linear analysis, which has produced several results which compare very well with both experiment and DNS in a variety of inhomogeneous flows, no such example is known in spatial BiGlobal theory. Furthermore, from a numerical point of view Heeg and Geurts [74] have documented that the computing effort of a spatial BiGlobal eigenvalue problem solved with the Jacobi–Davidson algorithm scales with the size of the problem solved raised to a power between two and three; this could become excessive compared with the cost of the respective temporal problem. In short, the issues of physical interpretation of the results and of affordability of the algorithm for the solution of the EVP should be resolved before one embarks upon a spatial BiGlobal linear analysis.

For further details and variants of subspace iteration methods the interested reader is referred to [19]; it suffices here to mention that subspace iteration methods are slowly establishing themselves as methods of choice for the solution of problems which deal with matrices of large leading dimension both in a fluid-mechanics context [20–22] and in other areas of engineering where they replace traditional fixed-point iteration methods (e.g. [95–97]).

[3] And even less so in conjunction with the QZ.

3.3. On the performance of the Arnoldi algorithm

Returning to the Arnoldi algorithm for the temporal BiGlobal eigenvalue problem, the question of its performance which has been addressed by Nayar and Ortega [98] is revisited here. The reason is that these authors claimed that choosing the shift parameter λ is nontrivial and, ideally, prior information on it is required in order for reliable results to be obtained. This statement is put in perspective by reference to the one-dimensional eigenvalue problem which results from substitution of the Ansatz (4) into (28)–(31). As test case the classic problem of linear stability in plane Poiseuille flow at $Re = 7500, \alpha = 1$ [99] is chosen; the dependence of the flow on the spanwise direction z is neglected.

The one-dimensional linear stability system is solved using both the QZ and the Arnoldi algorithms, in order to assess the performance of the latter with respect to the dimension of the Hessenberg matrix m and the shift parameter λ. The problem is discretised by 64 Chebyshev collocation points; the QZ algorithm delivers the unstable eigenvalue $\Omega = 0.24989154 + \mathrm{i}0.00223497$ [99]. The discretisation is then kept constant and Hessenberg matrices of order $m = 8$ and 16 are constructed. The shift-and-inverted Arnoldi problems are solved at $\lambda = (\lambda_0 \pm \Delta\lambda, 0)$, and $(\lambda_0, \pm\Delta\lambda)$ with $\lambda_0 = 0$ and 1 and $\Delta\lambda = 0.1$; results are presented in Table 2.

Worthy of discussion in this table are a number of facts. First, the Arnoldi algorithm is capable of delivering an approximation to the desired eigenvalue using arbitrary (but reasonable) shifts at $m = 8$, i.e. from solution of an eigenvalue problem the size of which is orders of magnitude smaller than the original problem. This is the primary desirable property which gave impetus to the multitude of applications on which

Table 2
The effect of λ on the accuracy of the eigenvalue obtained by a spectral method and the Arnoldi algorithm using a complex shift-and-invert strategy

$\lvert\lambda - \Omega\rvert$	◇		○	
	Ω_r	$10^2 \times \Omega_i$	Ω_r	$10^2 \times \Omega_i$
0.27	0.24996772	0.221510	0.24989154	0.223497
0.15	0.24989150	0.223459	0.24989154	0.223497
0.27	0.24989934	0.224441	0.24989154	0.223497
0.35	0.24975903	0.213338	0.24989154	0.223497

Krylov subspace dimension ◇ $m = 8$, ○ $m = 16$.

algorithms of this class are currently being applied. Second, at fixed m the degree to which the true eigenvalue Ω is approximated is systematically demonstrated to be a function of the distance between it and the shift parameter λ. If the latter happens to be very close to the true eigenvalue the approximation at low m is very well acceptable. Third, irrespective of the radius λ of the disk centred at Ω an increase of the number of Arnoldi iterations and, consequently, of the size of the Hessenberg matrix m significantly improves the approximation to Ω that the Arnoldi algorithm delivers. In other words, the decisive parameter determining the accuracy of the computations is not an arbitrary shift parameter λ but the distance in the complex plane between λ and an unknown desired eigenvalue Ω which, in turn, is a function of m, so that a large enough m eliminates the need for a priori information on λ. Indeed, one of the safest ways to identify a correct eigenvalue of the original problem is its independence of λ at a given m.

These conclusions carry weight when solving the two-dimensional eigenvalue problem (28)–(31) also. The flow problem here is the two-dimensional counterpart of plane Poiseuille flow, namely flow in a rectangular duct driven by a constant pressure gradient along the homogeneous direction z. The aspect ratio is taken $A = 100$ and the parameters $Re = 10^4, \alpha = 1$ [100] are chosen. The ability of the Arnoldi algorithm to deliver the most interesting part of the eigenspectrum at a fraction of the computing effort required by the QZ algorithm is documented on two different platforms in Table 3. The first observation is that use of the QZ also for the two-dimensional eigenvalue problem at discretisations dictated by the resolution of near-wall features of the eigenmodes is entirely inappropriate on the workstation, while it requires significant CPU resources on the supercomputer. On the other hand, the Arnoldi algorithm is substantially more efficient in terms of both memory and CPU requirements on both platforms, enabling the use of a workstation for this numerically challenging problem. The substantial memory savings materialised by the Arnoldi algorithm become increasingly attractive from an efficiency point of view as the resolution of the eigenvalue problem increases.

Fig. 5 shows a comparison of the eigenspectra obtained by the two algorithms. A notable result is the excellent agreement of the most interesting (from a physical point of view) most unstable/least stable part of the discrete eigenspectrum. Several converged eigenvalues have been obtained by using a low subspace dimension $m = 64$ in the example solved. Doubling m results in additional converged eigenvalues, while the overall runtime requirement remains an order of magnitude lower than that of the QZ. The splitting of the tail of the continuous spectrum is known to represent a numerical problem of the type of arithmetic used [36]; however, use of 128-bit arithmetic for the two-dimensional eigenvalue problem is not feasible on present-day hardware for all but Reynolds numbers of at most $O(10^2)$. Further discussion of numerical aspects of the eigenvalue problem is beyond the scope of the present article and will be presented elsewhere in due course.

4. Results of BiGlobal flow instability analysis

The wide spectrum of the outlined methodologies has been used to establish basic flows for linear BiGlobal instability analysis. At the simplest level, an analytic solution may be available; only a small number of such flows exist. At a higher level of complexity ordinary differential equation systems must be solved; nonsimilar boundary-layer type of flows represent the next level of sophistication. Finally, in the most general case a two-dimensional DNS methodology on arbitrary

Table 3
Comparison of core memory and runtime requirements for the numerical solution of (7) using the Arnoldi algorithm against a solution of (6) based on the QZ algorithm

Resolution	Arnoldi $(\mathbf{A}-\lambda\mathbf{B})^{-1}\mathbf{BX} = \mu\mathbf{X}$					QZ $\mathbf{AX} = \Omega\mathbf{BX}$		
	Memory (Mb)	Runtime (s)				Memory (Mb)	Runtime (s)	
		$\diamond$	$\bigcirc$	$\triangleleft$	$\triangleright$		$\oplus$	$\otimes$
12×12	9	1.46	2.69	2.00	2.97	23	40	108
16×16	23	3.97	6.31	8.38	10.98	63	85	765
20×20	51	10.32	14.18	26.46	32.60	145	220	2873
24×24	101	41.73	58.23	70.06	82.05	291	440	8617
28×28	183	84.59	108.69	164.07	185.64	525	990	22 029
32×32	292	164.62	199.06	349.62	383.01	879	3100	51 270

Runs on a NEC SX-4 supercomputer using subspace dimension $\diamond$ $m = 64$ and $\bigcirc$ $m = 128$ (Arnoldi) and $\oplus$ QZ, and on an EV6/500 MHz Alpha workstation using subspace dimension $\triangleleft$ $m = 64$, $\triangleright$ $m = 128$ (Arnoldi) and $\otimes$ QZ.

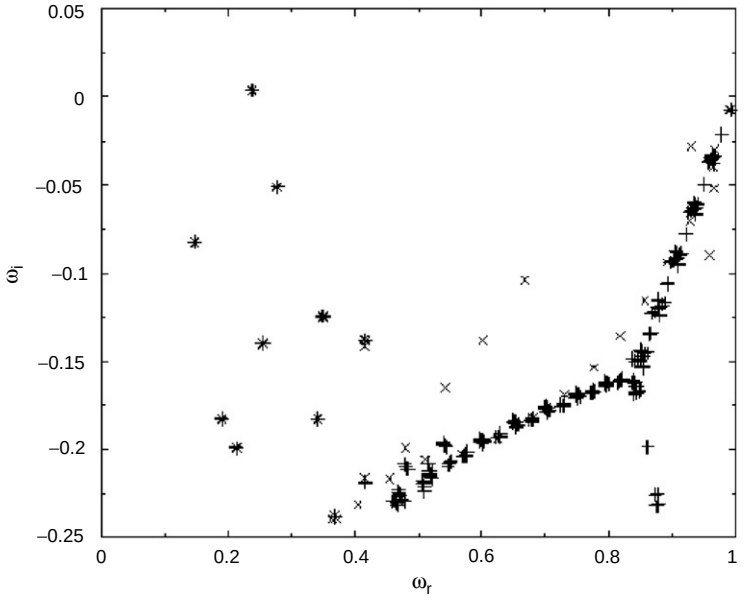

Fig. 5. Comparison of eigenvalues obtained by numerical solution of the two-dimensional EVP by the QZ algorithm (+) and Arnoldi iteration (×) in rectangular duct flow at aspect ratio $A = 100$ and parameter values $Re = 10^4, \beta = 1$ [99].

geometries is necessary to recover the basic flow to be analysed by BiGlobal linear theory. In certain cases the numerical results have been corroborated by comparison with experiment. Commensurate with ever increasing computing hardware capabilities, the BiGlobal instability analyses have also employed all alternative forms of the eigenvalue problem discussed in Section 2.5. Here, almost exclusively problems of relevance to external and internal aerodynamics will be discussed, mainly concentrating on the flows schematically depicted in Fig. 1.

4.1. The swept attachment line boundary layer

4.1.1. The basic flow

Starting at the attachment-line boundary layer region, schematically depicted in Fig. 6, one notes that laminar flow control methodologies on wings and fins should aim at prediction of the state at which the flowfield is found in the attachment-line before attempting to control the flow downstream of this region. The basic incompressible flow can be modelled by the swept Hiemenz exact solution of the steady equations of motion if curvature is neglected. This steady flow consists of the solution of a system of ordinary differential equations which can be solved in a straightforward manner [41,101]. Global instability analyses employing solution of the two-dimensional eigenvalue problem (28)–(31) have been presented by Lin and Malik [73], Theofilis [18] and Heeg and Geurts [74]. Secondary stability analyses of the swept Hiemenz flow employing Floquet analysis have monitored a basic flow composed of linear superposition of the least-damped eigenmode upon the swept Hiemenz basic state along the attachment line Theofilis and Dallmann [102] or quasi two-dimensional linear theory Janke and Balakumar [103]. If curvature in the attachment-line region is not negligible, a basic flow of the nonsimilar boundary layer class may be sought and analysed, as done by Lin and Malik [17].

4.1.2. The eigenvalue problem

This boundary layer is attractive from a theoretical point of view in that it represents an exact solution of the incompressible equations of motion in either its unswept [104] or swept configuration and instability analyses may thus be performed in a mathematically consistent manner. Thorough discussions of the instability of this flow are provided by [101,105–107] and more recently by [108,109,52]. In the first one-dimensional linear theory analysis, Görtler [110] postulated that the linear instabilities developing upon the (unswept) Hiemenz basic flow inherit the symmetry of this basic flow. According to the Görtler-Hämmerlin (GH) [110,111] instability Ansatz,

$$\hat{u} = x\tilde{u}(y)\mathrm{e}^{\mathrm{i}(\beta z-\omega t)}, \tag{58}$$

$$\hat{v} = \tilde{v}(y)\mathrm{e}^{\mathrm{i}(\beta z-\omega t)}. \tag{59}$$

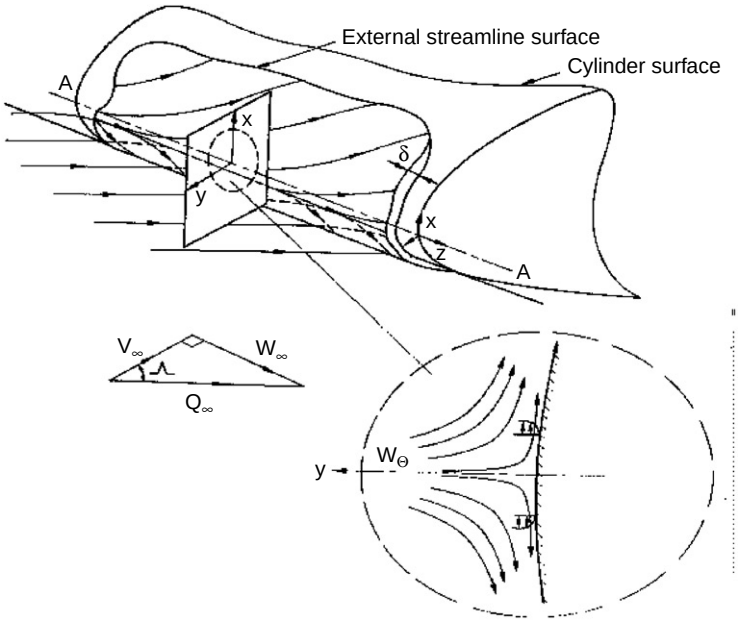

Fig. 6. Schematic representation of the swept attachment-line boundary layer [105,52].

This idea was extended to the swept Hiemenz flow by Hall et al. [101] who additionally assumed

$$\hat{w} = \tilde{w}(y)\mathrm{e}^{\mathrm{i}(\beta z-\omega t)} \tag{60}$$

and solved an ordinary-differential-equation-based linear eigenvalue problem of class (4) and (5) to recover a critical Reynolds number $Re_{\mathrm{crit}} \approx 581$. This compares very well with the results of both experiments performed under linear conditions and several two- and three-dimensional DNS studies; however, in the presence of large-amplitude disturbances in the flow, subcritical instability has been observed experimentally and in DNS at a much lower $Re \approx 245$ value [105,107].

Theofilis and Dallmann [102] employed the shape assumption [57] for the secondary instability problem and, staying within the bounds imposed by this approach, showed that amplitudes of the primary (decaying) GH mode of $O(1\%)$ are sufficient to excite secondary instability of both fundamental and subharmonic type at $Re > 250$, as shown in Fig. 7. On the other hand, motivated by the discrepancy in linear critical Reynolds numbers Lin and Malik [73,17], formulated and solved the two-dimensional eigenvalue problem (28)–(31) in which the assumption on the form of the disturbances in the streamwise direction x has been relaxed. These investigators utilised the symmetries of the basic flow in their analysis and discovered new BiGlobal eigenmodes in the swept Hiemenz case, the frequencies of which were documented as being very close to, while their growth rates were found to be smaller than the respective quantities of the GH eigenmode. In this respect, the new modes cannot be held responsible within a linear framework for subcritical instability in the swept Hiemenz flow.

Theofilis [18] solved the partial-derivative eigenvalue problem without utilising the symmetries of the basic flow and documented the chordwise variation of the new modes with respect to x. He went on to analyse the spatial structure of the BiGlobal eigenmodes, the first three of which are shown in Fig. 8. All BiGlobal flow eigenmodes were classified into two families of symmetric and antisymmetric modes, discriminated by their chordwise dependence. The analytical description of the chordwise structure of the BiGlobal eigenmodes in terms of polynomials in x was utilised to derive two ordinary-differential-equation-based eigenvalue problems for the symmetric

$$\{\mathscr{P} - 2M\bar{u} + \mathrm{i}\beta Re\Omega\}\tilde{u}_{2M-1} - \bar{u}'\tilde{v}_{2M-2} = 0, \tag{61}$$

$$2(2M-1)[\bar{u}\mathscr{D} + \bar{u}']\tilde{u}_{2M-1} + \{\mathscr{R} + (2M-1)\bar{u}'' + \mathrm{i}\beta Re\Omega[\mathscr{D}^2 - \beta^2]\}\tilde{v}_{2M-2} = 0, \tag{62}$$

and the antisymmetric modes

$$\{\mathscr{P} - (2M+1)\bar{u} + \mathrm{i}\beta Re\Omega\tilde{u}_{2M}\}\tilde{u}_{2M} - \bar{u}'\tilde{v}_{2M-1} = 0, \tag{63}$$

$$4M\{\bar{u}\mathscr{D} + \bar{u}'\}\tilde{u}_{2M} + \{\mathscr{R} + 2M\bar{u}'' + \mathrm{i}\beta Re\Omega[\mathscr{D}^2 - \beta^2]\}\tilde{v}_{2M-1} = 0. \tag{64}$$

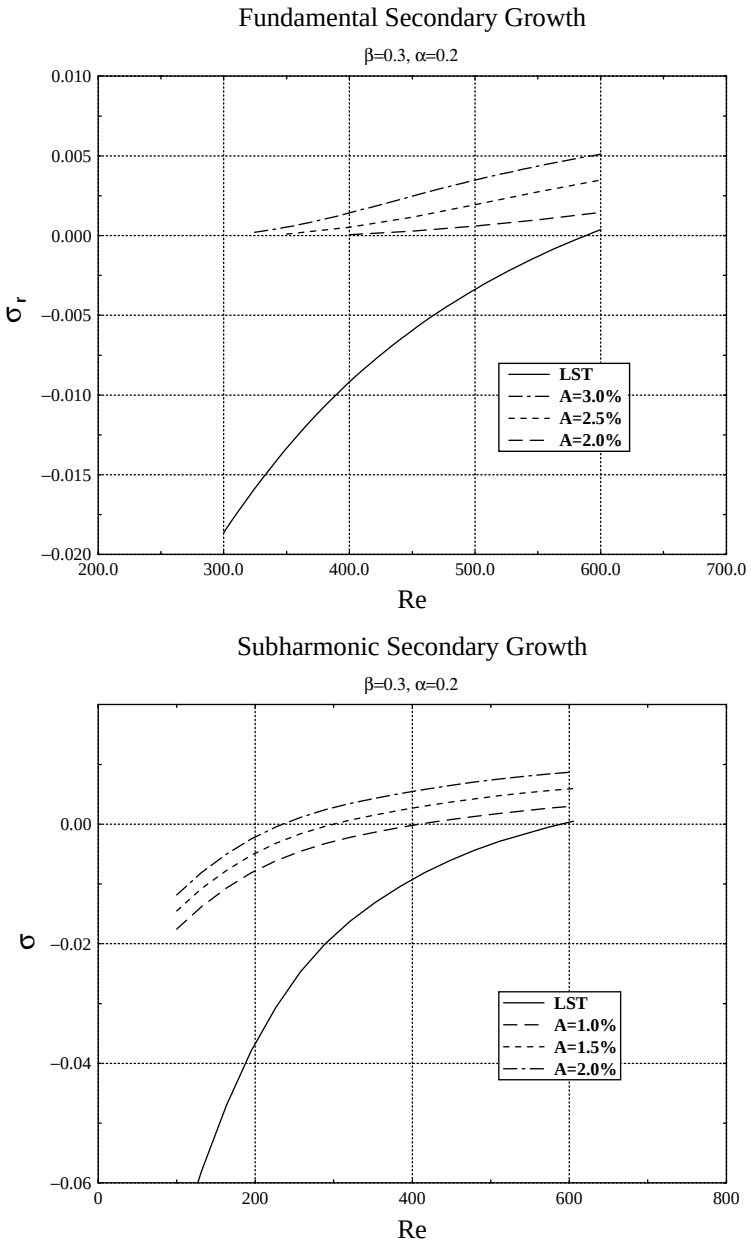

Fig. 7. Secondary instability in the swept Hiemenz flow [102].

Here $(\bar{u},\bar{v},\bar{w})^{\mathrm{T}}$ denotes the swept Hiemenz basic flow, $M=1,2,\ldots$ denotes the discrete BiGlobal eigenmodes,

$$\mathscr{P}=\mathscr{D}^2-\bar{v}\mathscr{D}-\beta^2-\mathrm{i}\beta Re\bar{w},$$

$$\begin{aligned}\mathscr{R}=&\mathscr{D}^4-\bar{v}\mathscr{D}^3-[2(M-1)\bar{u}+\bar{v}'+\mathrm{i}\beta Re\bar{w}+2\beta^2]\mathscr{D}^2\\&+[\bar{u}'+\beta^2\bar{v}]\mathscr{D}+2(M-1)\beta^2\bar{u}+\beta^2\bar{v}'\\&+\beta^4+\mathrm{i}\beta^3 Re\bar{w}+\mathrm{i}\beta Re\bar{w}'',\end{aligned}$$

where $\mathscr{D}\equiv \mathrm{d}/\mathrm{d}y$. These systems allow the calculation of the BiGlobal instability in the attachment-line region and recover the eigenvalues of the temporal partial-derivative eigenvalue problem results at a fraction of the cost of solving (28)–(31). When written as a spatial eigenvalue problem (61)–(64) yield results which are in excellent agreement with those of the spatial DNS of the attachment-line region [112] or the results of the corresponding spatial partial-derivative eigenvalue

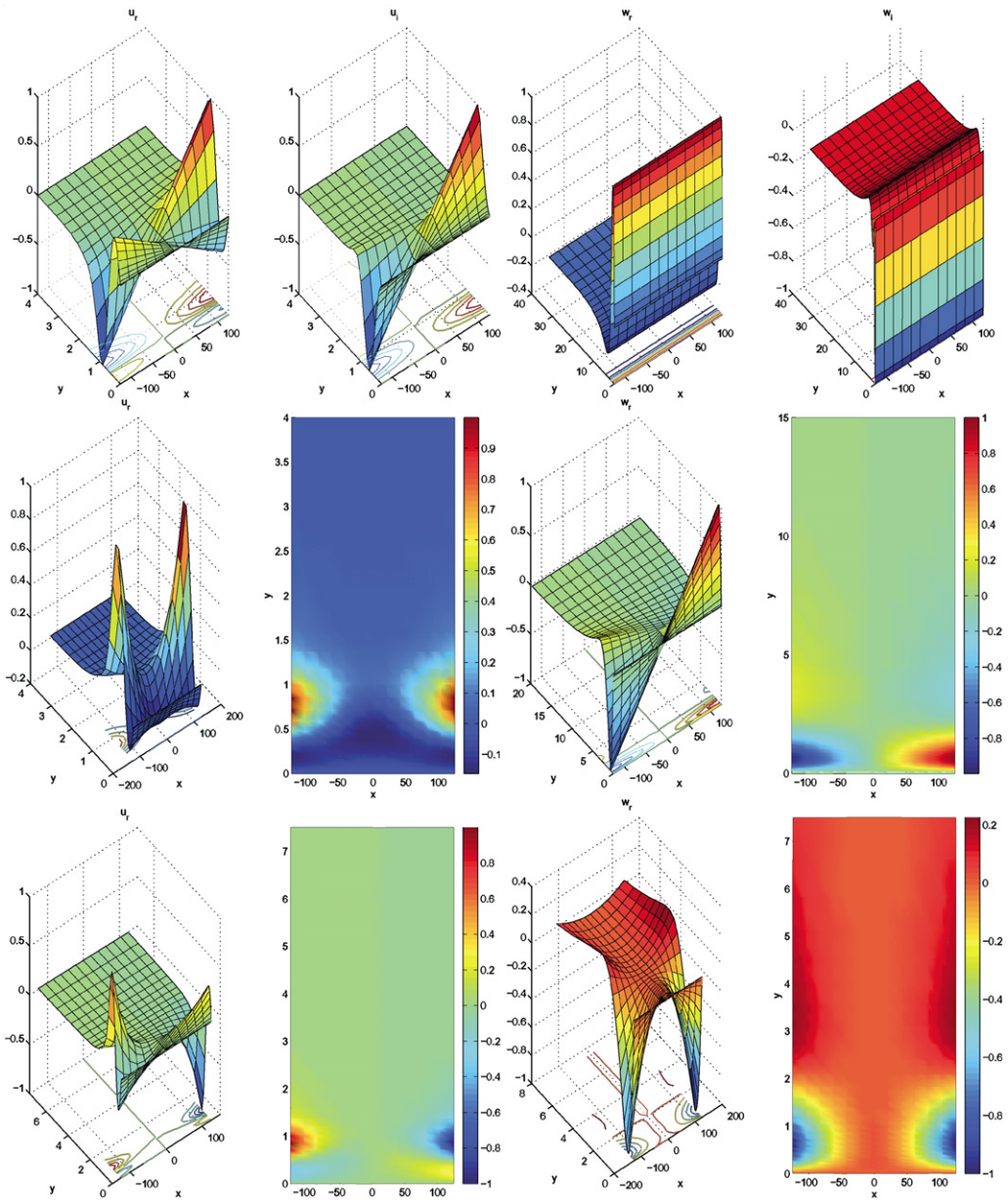

Fig. 8. Upper: The spatial structure of $\Re\{\hat{u}\}$, $\Im\{\hat{u}\}$, $\Re\{\hat{w}\}$ and $\Im\{\hat{w}\}$, of the Görtler-Hämmerlin (GH) mode, recovered as *solution* of the two-dimensional eigenvalue problem (28)–(31). Middle: The spatial structure of components of the disturbance eigenvectors pertinent to the global eigenmode A1. Lower: Same result for S2. Left two columns $\Re\{\hat{u}\}$, right two columns $\Re\{\hat{w}\}$.

problem in this flow. The supergeometric decay of the amplitude functions of all model eigenmodes as $M \to \infty$, which accounts for finite results being delivered by the three-dimensional extension of the GH model, is shown in Fig. 9 at a particular set of values of the parameters (Re, β). Fedorov (unpublished) has independently arrived at the prediction of the instability results of [73] through WKB analysis, which delivers results equivalent to those obtained by solution of the one-dimensional eigenvalue problem (61)–(64). A discussion of linear and nonlinear instability in the three-dimensional swept Hiemenz flow, including direct numerical simulations initialised on the extended GH model eigenfunctions may be found in [113]. Bertolotti [114] in his work on the connection of attachment-line and crossflow instabilities showed that the polynomial modes (61)–(64) are the only families of linear disturbances relevant to instability in the attachment-line region itself. The spatial BiGlobal

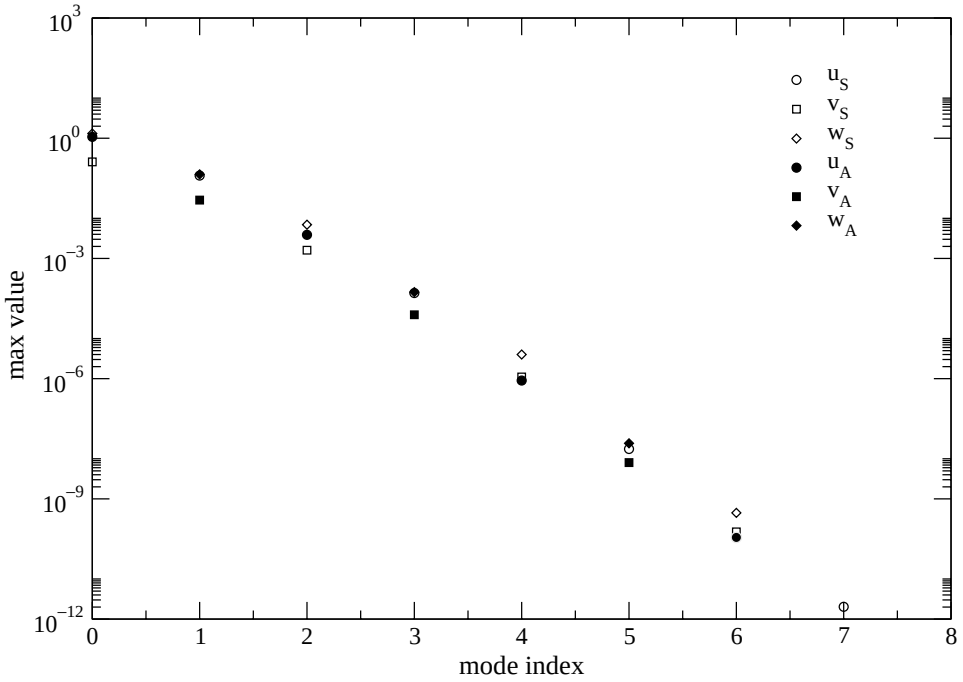

Fig. 9. Maximum values of amplitude functions of the extended GH model against mode index m at $Re = 800, \beta = 0.255$. u_S, v_S, w_S, p_S and u_A, v_A, w_A, p_A denote maximum values of $\tilde{u}_m, \tilde{v}_m, \tilde{w}_m, \tilde{p}_m$ of symmetric and antisymmetric modes, respectively.

eigenvalue problem has been solved by Heeg and Geurts [74]. An interesting characteristic of this work from a numerical point of view is its use of a high-order finite-difference method in conjunction with Jacobi–Davidson iteration; the latter permits solving eigenvalue problems in which the eigenvalue appears either linearly or nonlinearly at the same computing effort. Finally, Lin and Malik [17] departed from the swept-Hiemenz flow model and addressed the problem of instability in the attachment-line region taking curvature into account and solving the respective two-dimensional eigenvalue problem. In line with analogous results using the one-dimensional eigenvalue problem, curvature was found to stabilise the flow.

In summary, BiGlobal instability analysis has delivered the full-spectrum of attachment-line eigenmodes relevant to laminar-turbulent flow transition on account of linear mechanisms. Owing to the simple nature of the model basic flow it has been possible to model the EVP results by solution of (61–64), thus aiding their incorporation into engineering-prediction toolkits.

4.2. The crossflow region on a swept wing

4.2.1. The basic flow

Moving downstream of the attachment line on to the portion of the flowfield where different degrees of deflection of the flow in the freestream and in the boundary layer result in the latter having an inflectional profile, as schematically depicted in Fig. 10, a well-understood primary inviscid linear instability mechanism of the class (4) is encountered [115]. The amplification of this primary instability leads to a saturated nonlinear basic state, identified as the well-known stationary or travelling crossflow vortices [116–118].

The basic flow on this portion of a swept wing is obtained by superposition of results of one-dimensional linear theory upon a boundary layer solution at arbitrarily low levels [119,120] or by three-dimensional DNS [92]. Other investigations solve the nonsimilar boundary layer equations upon which the crossflow vortex primary instability is superimposed as a result of PSE computation [65,103]. Yet another possibility which circumvents the need to solve the receptivity problem associated with PSE is superposition of nonlinear saturation states of the primary linearly unstable solutions upon the latter [64]. However, Haynes and Reed [121] have shown that the nonlinear PSE is the methodology which delivers best agreement with experiment as far as the saturated nonlinear crossflow-vortex basic flow is concerned. All subsequent BiGlobal instability analyses define a local coordinate system in which the basic flow plane is locally normal to the axis of the primary crossflow vortices. A visualisation of this basic flow taken from the DLR experiment on crossflow instability [118] is presented in Fig. 11.

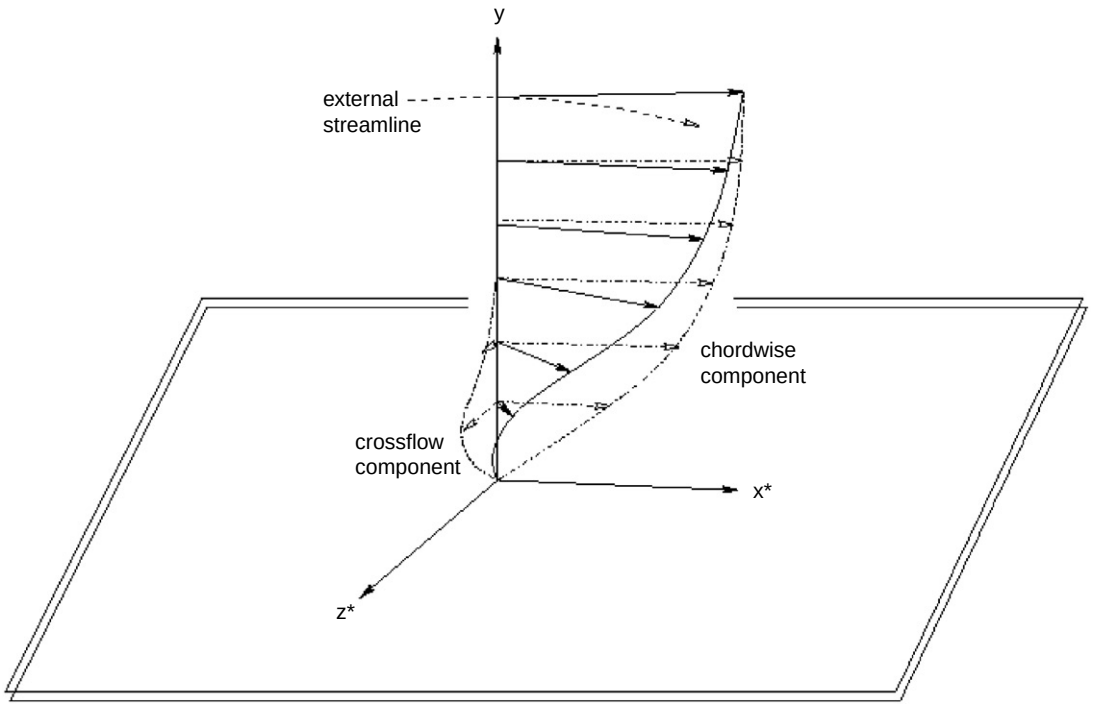

Fig. 10. Schematic representation of a 3D boundary layer velocity profile [115].

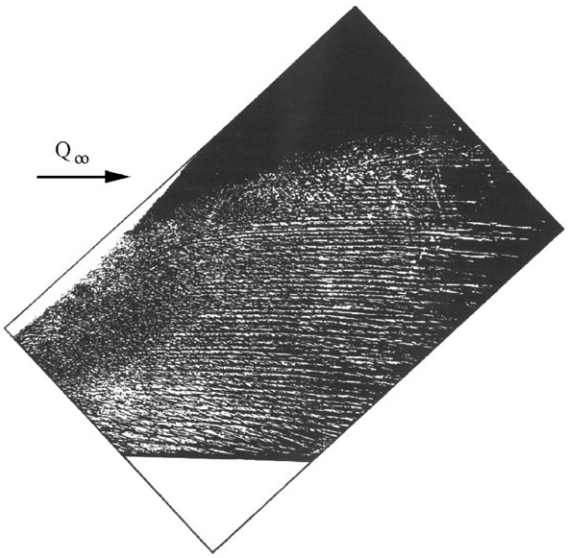

Fig. 11. Flow visualisation of crossflow vortices, taken from the experiment on the DLR swept wing [118].

4.2.2. The eigenvalue problem

The significance of crossflow vortices for swept wings has prompted intense investigation into instability mechanisms leading to breakdown of the nonlinear saturated basic state to turbulent flow. The first experimental evidence that a high-frequency secondary instability is responsible for transition of the flow to turbulence was provided in the swept cylinder experiments of Poll [122], while Kohama et al. [123] were the first to identify this mechanism on a swept wing. Subsequent experimental [124–126] and a multitude of numerical work has confirmed the existence of high-frequency secondary instability, linear amplification of which rapidly leads the flow to breakdown and turbulence. Reibert et al. [124], Saric et al. [127] and Saric and Reed [128] went on to exploit this phenomenon and offer efficient technological solutions for laminar flow control in incompressible and supersonic swept wing flows, respectively. High-frequency secondary instability has been addressed theoretically in a number of papers, notably the DNS work of Hoegberg and Henningson [129], Wintergerste and Kleiser [92] and Wassermann and Kloker [130] and the analyses of Fischer and Dallmann [119], Fischer et al. [120], Malik et al. [65], Wintergerste and Kleiser [92], Janke and Balakumar [103] and Koch et al. [64]. In all analyses the two-dimensional eigenvalue problem has been solved by taking the homogeneous flow direction to be aligned with the axis of the crossflow vortices and resolving the other two spatial directions using a Fourier Ansatz in the direction parallel to the wall. The crossflow vortex

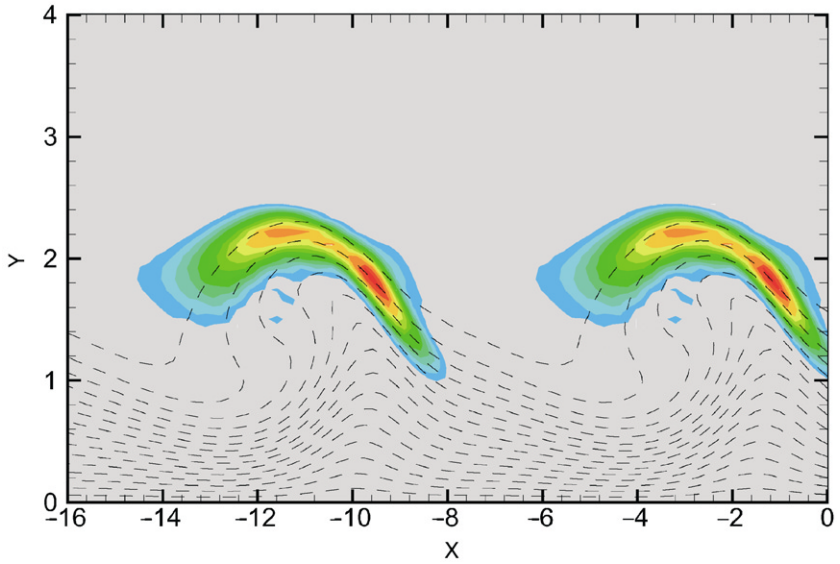

Fig. 12. Saturated stationary primary crossflow vortex and superimposed secondary instability structure for the DLR-Experiment at $x/c = 0.60$ [103].

axis is assumed to be straight, an assumption which can be a posteriori justified by reference to the wavelengths of the amplified high-frequency secondary disturbances.

A BiGlobal eigenvalue problem was formulated and solved by Malik et al. [65], using a Krylov subspace iteration method. The BiGlobal eigenmodes could be classified in two families, while the predicted frequencies of the two dominant modes were found to peak between 3.5 and 4.5 kHz. The spatial structure of these modes was found to be consistent with available experimental results. One such result, showing (in colour) the structure of the high-frequency secondary instability superimposed upon the crossflow vortices (dashed lines) is shown in Fig. 12. However, Malik et al. [65] stressed that in order for reliable transition-prediction criteria to be provided, additional work is necessary on at least two fronts, receptivity of the flow during the stages prior to linear growth of the primary disturbances and the correlation of transition onset location and onset of the secondary instability. They pointed out that one possible means to achieve this is through DNS which takes into account onset of high-frequency secondary instability, interaction of stationary and travelling crossflow disturbances and nonlinearity. A step in this direction was taken by Hoegberg and Henningson [129] while work is in progress by Wintergerste and Kleiser [92].

The latter authors studied the BiGlobal eigenvalue problem by expanding the eigenfunctions into finite Fourier–Chebyshev series, in view of the periodic nature of the problem in the lateral spatial direction. Use of the Arnoldi algorithm described in Section 3.2 was found to be essential for convergence of the results in this work. During the early stages of the DNS computation of the basic state, only low-frequency $O(10^2)$ Hz secondary disturbances were found. As the amplitude of the crossflow vortex rose beyond 10% high-frequency secondary instability appeared, in line with the results of Fischer et al. [120] who used the simplifying assumption of a basic flow modified by model linear primary eigenfunctions, as opposed to the DNS-obtained basic state of [92]. As a matter of fact two modes I and II were found by the latter authors in the BiGlobal eigenspectrum, corresponding to frequencies $f = 2134$ and $f = 510$ Hz, respectively. The corresponding phase velocities were found to be $c_{\mathrm{ph}} \approx 0.76$ and 0.41, respectively. The spatial structure of the high-frequency secondary instability eigenmodes corresponds to elongated vortices located above the centre of the crossflow vortex, at an angle of $\theta \approx 70^\circ$ to it. As time progresses the instability amplifies in an explosive manner.

Janke and Balakumar [103] and Koch et al. [64] used Floquet theory along the lines of (44) to solve the BiGlobal eigenvalue problem. The first work focussed on the existence of multiple roots of the eigenvalue problem and the claim was put forward that this could explain the origin of high-frequency instability and the time-dependent occurrence of an exponential growth of travelling disturbances observed in experiment. In the second work, it was first stressed that the model basic flow utilised had a universal character in terms of it being independent of the receptivity problem. Earlier findings on the large number of Fourier components in

the Floquet analysis necessary to converge the high-frequency secondary instability solution were confirmed. The results of the BiGlobal eigenvalue problem were then interpreted and, despite the clear association of the most amplified BiGlobal mode with a well-understood instability, the possibility was left open that absolute instability mechanisms may be at play and the need for further studies to understand the laminar-turbulent transition phenomenon was stressed. In summary, DNS analyses and the BiGlobal eigenvalue problem has permitted new physical insight into the secondary instability problem of crossflow vortices, otherwise accessible only to DNS. Further quantification of the phenomenon and utilisation of its results to arrive at theoretically founded predictions of laminar-turbulent breakdown on swept wing configurations is currently underway on both sides of the Atlantic.

4.3. Model separated flows

A comprehensive and rather recent (in terms of the effort spent of the problem) review of separated flow instability is presented by Dovgal et al. [131]. These investigators considered several configurations of aerodynamic interest in which boundary layer separation occurs. A unifying characteristic of their approach, though, has been that a separation bubble was viewed as an *amplifier* of incoming disturbances. Indeed, it has been known for several decades that disturbances entering the separated flow region will experience explosive amplification even before reaching the bubble itself. Theories based on (4) and either of (5) or (6) and, of course, DNS can be used to describe these instabilities. However, the mechanisms discussed in [131] do not preclude the possibility of instability other than that covered by these theories. Indeed, Dovgal and Sorokin [132] have examined experimentally flow being a backwards facing step and observed two modes of instability, one associated with amplified shear-layer disturbances and one associated with vortex-shedding type of BiGlobal instability. The interpretation of instability results in separated flow is far from being understood in a conclusive manner; the interested reader is referred to Boiko et al. [133] for background information on either instability mechanism.

A significant theoretical development in this area has been the identification of the potential of a closed laminar separation region to act as a *generator* of

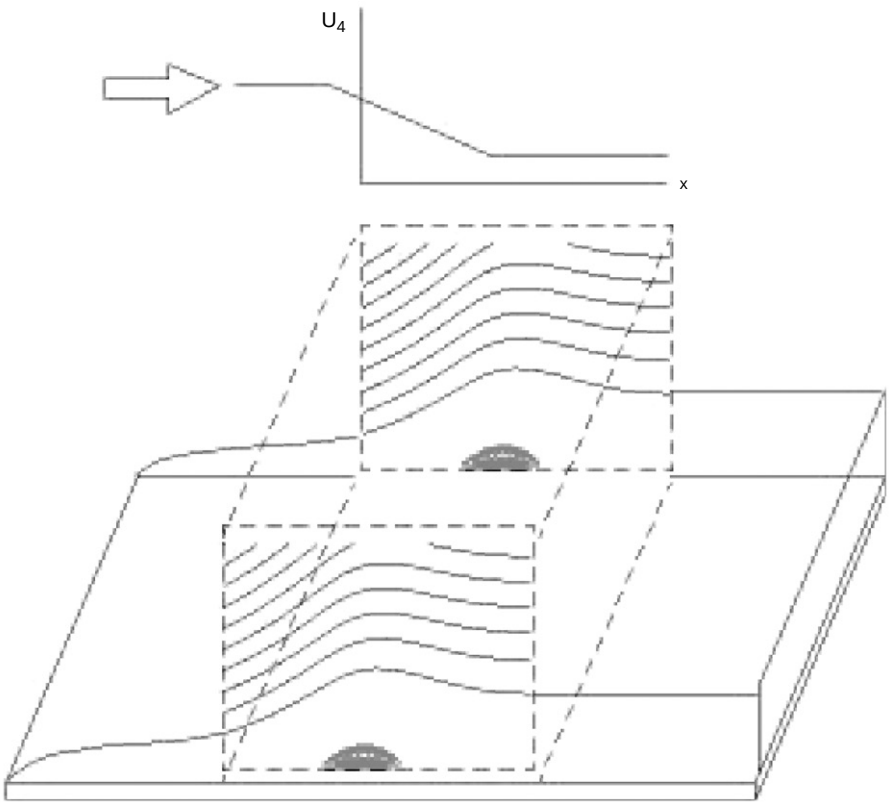

Fig. 13. Schematic representation of the concept of a global instability analysis of model separation-bubble flows.

eigendisturbances and support BiGlobal instability in the absence of incoming disturbances [134]. Further detailed studies of the phenomenon using two different model flows have been addressed independently by Hammond and Redekopp [135] and Theofilis et al. [35]; the concept employed in either case is sketched in Fig. 13.

4.3.1. The basic flow

In the work of Hammond and Redekopp [135] the generic mechanism of BiGlobal instability[4] was demonstrated on the analytical model

$$\bar{u}(\eta) = f'(\eta, \beta_0) - a\eta e^{-(\eta-\eta_0)/\eta_0}, \tag{65}$$

where f is the solution to the Falkner–Skan equation[5] subject to the boundary conditions

$$f(0) = f'(0) = 0, \quad f'(\eta \to \infty) = 1, \tag{66}$$

where the parameters a, β_0 and η_0 independently control the strength of the backflow velocity and the depth of the reversed-flow, which has been chosen to have circular-arc dividing streamlines.

The mixed finite-difference/spectral algorithm described in the appendix was used for the solution of the boundary-layer equations in the BiGlobal instability analysis of laminar separated flow model presented by Theofilis et al. [35]. These authors solved the nonsimilar boundary-layer equation (A.7) to obtain the inflow boundary condition at $\xi = 0.05$ for the subsequent two-dimensional DNS of the separated flow region; the algorithm also described in the appendix was used for the DNS, in which parameters were chosen to match those of Briley [137], while the inflow location was kept constant at $\xi_0 = 0.202$ to ensure a well-defined recirculation region [138]. The vorticity and two integral quantities of the closed separation bubble flowfield thus obtained are presented in Fig. 14. The total divergence of these results, defined as

$$d = \sum_{ix=0}^{Nx} \sum_{iy=0}^{Ny} \mathscr{D}_x \bar{u}(ix, iy) + \mathscr{D}_y \bar{v}(ix, iy), \tag{67}$$

is $d = 6.6 \times 10^{-8}$, implying satisfaction of the continuity equation to within 5×10^{-11} at this resolution.

4.3.2. The eigenvalue problems

Hammond and Redekopp [135] performed a global (in the classic sense) instability analysis within the framework of WKB theory, in which the basic state and its instabilities are assumed to develop on different spatial scales. This assumption facilitates the numerical work in that instead of the two-dimensional eigenvalue problem (34)–(37) a sequence of Orr–Sommerfeld equations may be solved at successive downstream locations within the bubble. However, instead of following the classic temporal or spatial OSE models, in the two-dimensional limit of which the parameters (α, Ω) in (5) are real/complex and complex/real respectively, the OSE problem for this type of global instability analysis is solved taking both α and Ω to be complex quantities. The dispersion relation

$$D(\alpha, \Omega; Re) = 0 \tag{68}$$

was used to compute a growth rate for BiGlobal instability through the requirement that the group velocity

$$\partial\Omega/\partial\alpha|_{\alpha_0} = 0 \tag{69}$$

at a particular α_0. Note, this dispersion relation contains parameters defined in (65). The instability analysis showed that model separated flow can become BiGlobally unstable when the peak reversed flow in the bubble reaches about 30% of the freestream value. These authors went on to associate their result with the experimental evidence on pitching aerofoils and dynamic stall that time-dependent large-scale dynamics lead to collapse of the separated flow region when the latter approaches about 40% of the free-stream value. The question of the shape of the BiGlobal eigenmode and its possible implication for flow control will be revisited in Section 4.12.

Theofilis et al. [35] have employed one-dimensional (OSE), quasi-two-dimensional (PSE) and two-dimensional (BiGlobal) analyses to study numerically the instability of incompressible steady laminar boundary-layer flow which encompasses a recirculation bubble. Both stationary and pairs of travelling linear instabilities were discovered, which are distinct from known solutions of the linear OSE or linear PSE instability theories, and can both become unstable at sufficiently high backflow strength, at the present parameters of the $O(10\%)$. It should be mentioned that at these parameters Tollmien–Schlichting instability has a wavelength which is an order of magnitude smaller than a typical scale of the BiGlobal eigenmode amplitude functions and its growth rates are approximately two orders of magnitude smaller than those of TS instability. A conjecture on the consequence of this disparity in amplification rates of the two instability mechanisms Theofilis [139] has suggested that, although the classic TS mechanism may act as a catalyst for laminar breakdown, attention must be paid to the control of BiGlobal instability of the flow as a precursor to vortex-shedding and a mechanism relevant to turbulent flow control, in a manner that will be discussed in what follows.

[4] This basic state is one in which the concepts of global instability, as used by earlier theoretical analyses of weakly nonparallel flows and in the present sense of inhomogeneous two-dimensional basic flows, coincide.

[5] A special case of the nonsimilar boundary layer equations (A.7) and prime denotes differentiation w.r.t. η. [136].

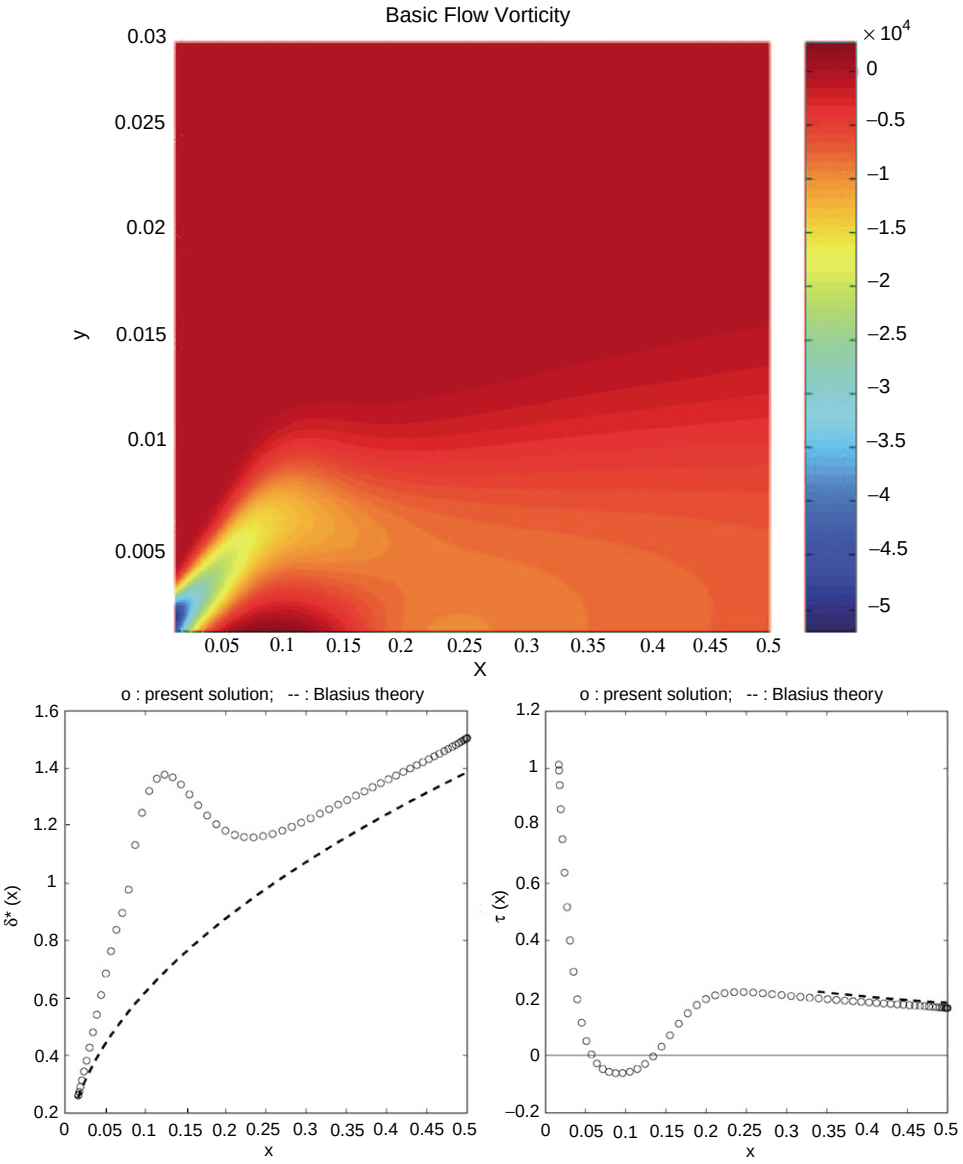

Fig. 14. Basic flow vorticity $\zeta = \partial\bar{v}/\partial x - \partial\bar{u}/\partial y$ (upper) and integral quantities of the [137] separation bubble.

The spatial structure of the most unstable BiGlobal eigenmode, recovered by solution of the real eigenvalue problem (34)–(37) at $Re \approx 1.7 \times 10^4$, is shown in Fig. 15. The innocuous nature of the primary separation line alongside the three-dimensionalisation of the primary reattachment region is shown in Fig. 16, where an isosurface of the disturbance vorticity is shown at an arbitrary level. The primary separation bubble is contained within the dashed lines and paths of particles released in the flow provide a qualitative demonstration of the effect of the BiGlobal eigenmode on the closed streamlines of the basic flow. The recovery of unstable eigenvalues in the problem at hand must be seen in the perspective of the artificial (from a physical point of view) homogeneous Dirichlet inflow boundary conditions. In practice, Tollmien–Schlichting instability in the flow under consideration is orders of magnitude stronger than the BiGlobal mechanism, at least in the bracket of parameters monitored by Theofilis et al. [35]. Recent numerical efforts [140] have independently confirmed the existence of BiGlobal instability at the parameters of [35], although later efforts (Hetsch, personal communication) have attributed the results of [140] to insufficient numerical resolution. This further

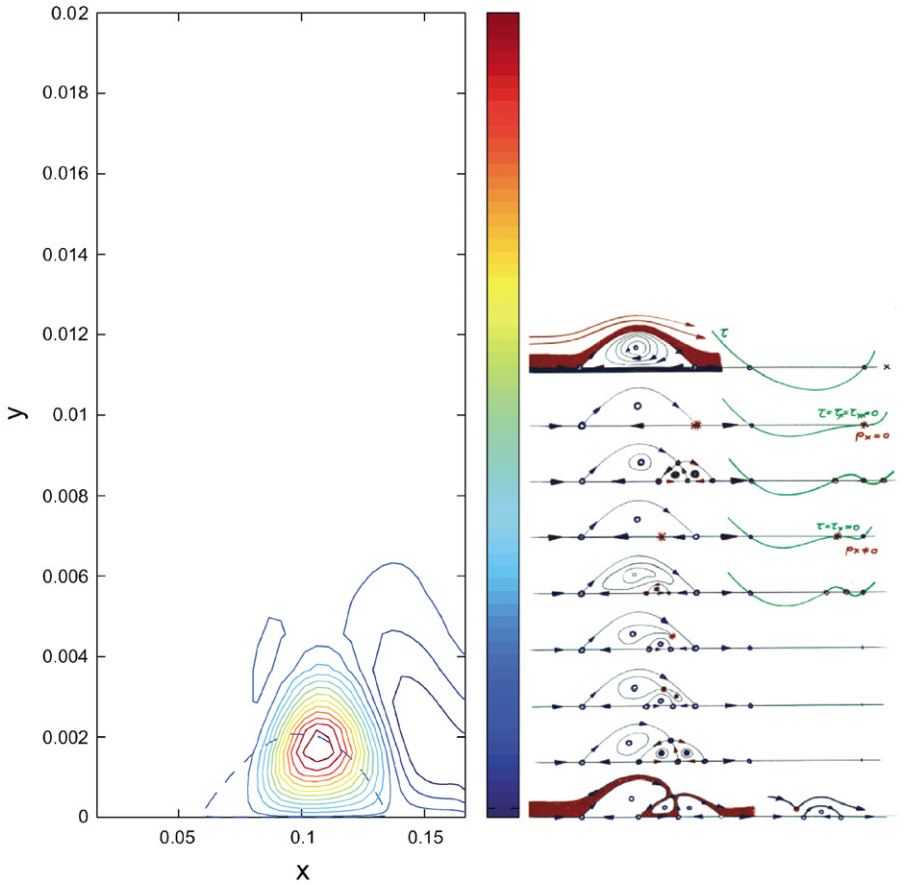

Fig. 15. Left: Amplitude functions of the dominant streamwise velocity component of the most unstable stationary global eigenmode $\hat{u}$; the location of the primary separation bubble is also noted by a dashed line. Right: Schematic representation of a mechanism for vortex shedding from a laminar separation bubble, on account of global instability [35].

underlines the need for *well-defined* models of separated (basic) flow prior to renewed efforts towards identification of critical conditions of the respective BiGlobal instability.

While it might be expected that recovery of BiGlobal instability should be relatively more straightforward in the course of DNS, the disparity of growth rates could make its experimental isolation difficult and may indeed explain why this mechanism has gone unnoticed despite decades of experimental efforts in this key problem. Aside from the relevance of the BiGlobal instability to laminar flow control, it has been conjectured by Theofilis et al. [35] that the BiGlobal instability mechanism discovered is related with and sheds light to the phenomenon of vortex-shedding by separation bubbles; the mechanism is also schematically depicted in Fig. 15. In experiments it is often found that the separation line remains stationary while the reattachment-zone is highly three-dimensional and unsteady, a result which is in line with that of the BiGlobal analysis [35]. Further, conjectures based on topological arguments regarding the origins of unsteadiness and three-dimensionality in separated flow [141] appear to be substantiated by the results of the analysis of Theofilis et al. [35].

4.4. *Separated flow at the trailing-edge of an aerofoil*

Investigation of flow separation behind streamlined and bluff bodies alike is a field of vigorous investigation, the payoff being that a better understanding of this phenomenon can lead to its improved modelling and, ultimately, to reliable flow-control strategies. At the Reynolds numbers of practical interest in external aerodynamics and turbomachinery the flow is typically found in a turbulent state; the various paths to transition in separated flow are subject of current research from experimental, theoretical and numerical points of view. A first step towards analysing BiGlobal

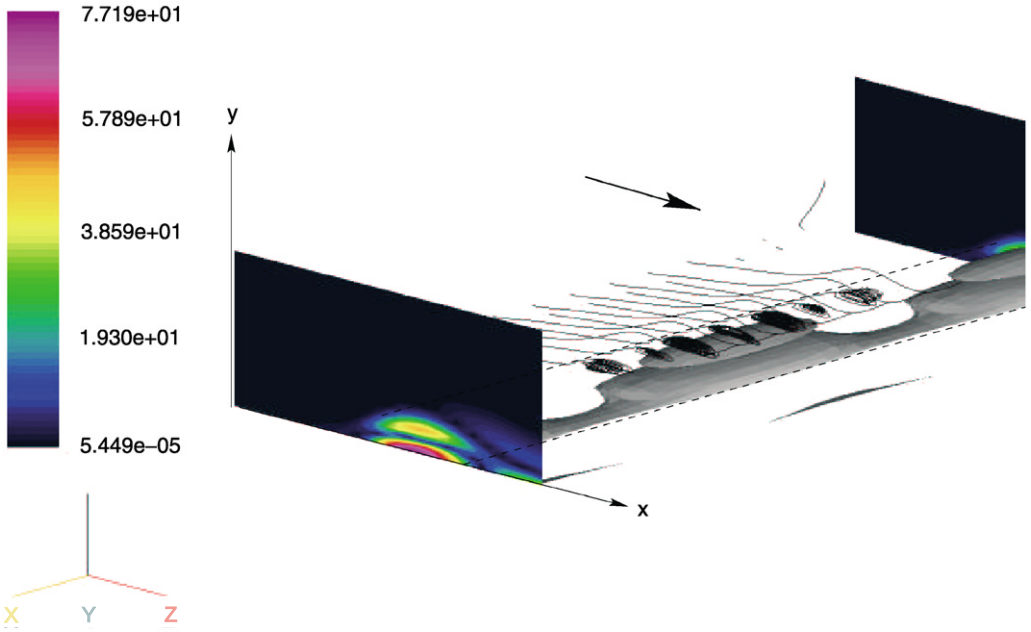

Fig. 16. Three-dimensionalisation of the reattachment line on account of global instability of the Briley separation bubble visualised as isosurfaces of the disturbance vorticity [139].

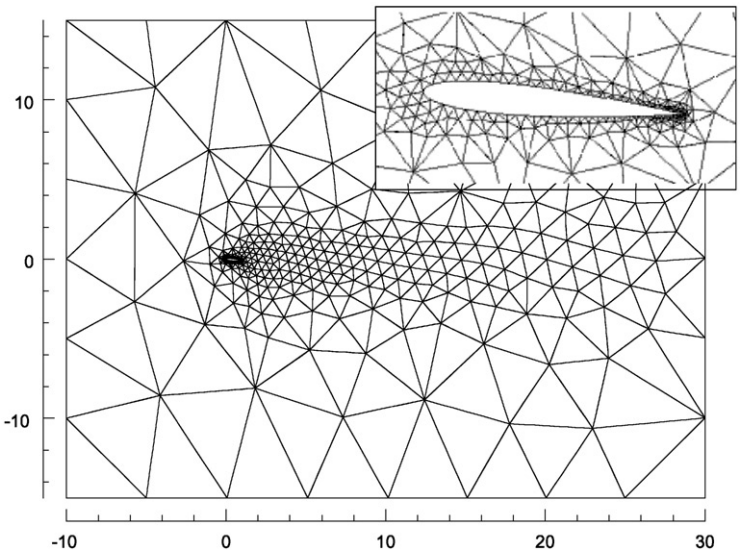

Fig. 17. Triangulation of the physical domain around a NACA 0012 aerofoil of unit chord [142].

instability of separated flow at the trailing-edge of an aerofoil was undertaken by Theofilis and Sherwin [142].

4.4.1. The basic flow

In this work the basic flow was computed by state-of-the-art spectral/*hp* element methods for DNS [78]; these methods combine the high accuracy of classical spectral techniques with the geometric flexibility of finite element methods by applying higher order polynomial expansions within a series of elemental sub-domains; in this manner spectral/*hp* element methods permit achieving the highest possible accuracy *per unit of computational power*.

Fig. 17 shows the discretisation of a NACA 0012 aerofoil at an angle of incidence of -5°. A large computational domain ($x^* \in [-10, 30] \times y^* \in [-15, 15]$) in

chord length c units was chosen to remove any influence of the artificial computational boundaries. A key point regarding the accuracy of this basic flow is that the geometry of the aerofoil was consistently described by isoparametric elements, e.g. the surface was represented by a similar order polynomial order within each element as that in the solver itself. The calculations were performed at a chord Reynolds number $Re_c = U_\infty c/\nu = 10^3$ where U_∞ is the magnitude of the free stream velocity, c is the chord length and ν is the kinematic viscosity of the fluid. The aerofoil was assumed to have a finite trailing-edge thickness of $0.003c$ and so the local Reynolds number based on the trailing-edge was $Re_{\rm tr} = 3$, which is well below typical bluff body vortex shedding values of approximately 50. At this Reynolds number one of the most interesting features of the flow is trailing-edge separation, visualised in Fig. 18. The highlighted part of the flow was extracted from the simulation data, rotated by an angle $\phi \approx -12^\circ$ and interpolated on a rectangular cartesian grid approximating a body-fitted coordinate system and extending between $x \in [0.714, 0.992] \times y \in [0.199, 0.2589]$ to form the basic flow of the BiGlobal instability analysis.

4.4.2. The eigenvalue problem

In a manner analogous to the model separated flow problems of Section 4.3 the two-dimensionality of the basic state suggests ability to solve the real eigenvalue problem (34)–(37). For reasons of numerical feasibility but also in order to monitor instability mechanisms potentially generated on account of the trailing-edge separated region in isolation from other instabilities present in this flow Theofilis and Sherwin [142] solved the two-dimensional eigenvalue problem using a rectangular standard Chebyshev grid mapped onto the highlighted part of the flow shown in Fig. 18 through an algebraic transformation. In order to prevent disturbances potentially existing upstream of the upstream boundary of the monitored domain from entering the trailing-edge region, homogeneous Dirichlet boundary conditions were imposed on all disturbance amplitude functions at this boundary. No slip conditions were imposed on the disturbance velocity components at the wall, where the compatibility conditions (50) and (51) were imposed on pressure. At the farfield boundary, homogeneous Dirichlet conditions have been imposed on all disturbance amplitude functions. Finally, at the outflow boundary a linear extrapolation procedure has been used.

The wavenumber parameter space was examined, taking the periodic spanwise extent of the domain $Lz/Lx \in [1/8, 32]$, where $Lx \approx 0.278$ is the streamwise extent of the separated region monitored, which results in $\beta \in [0.7, 180]$. Only damped eigenmodes have been found in this wavenumber range at this modest Reynolds number. The spatial structure of the spanwise disturbance velocity component $\hat{w}$ of the least damped eigenmode is shown in Fig. 19 at $Lz/Lx \approx 1$; as a matter of fact the qualitative structure of the least damped eigenmode is practically independent of β such that this

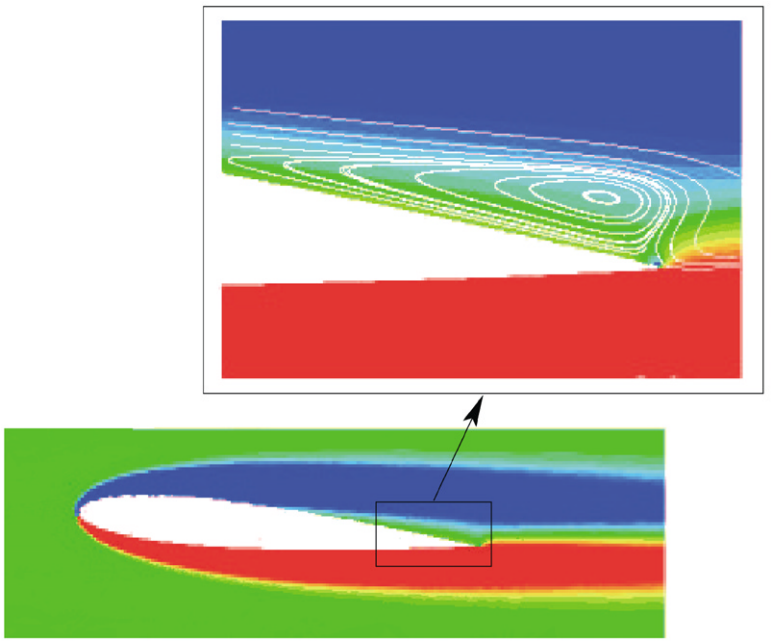

Fig. 18. Steady laminar separated in the trailing-edge of a NACA 0012 aerofoil at chord $Re = 10^3$ and angle of incidence -5° [142].

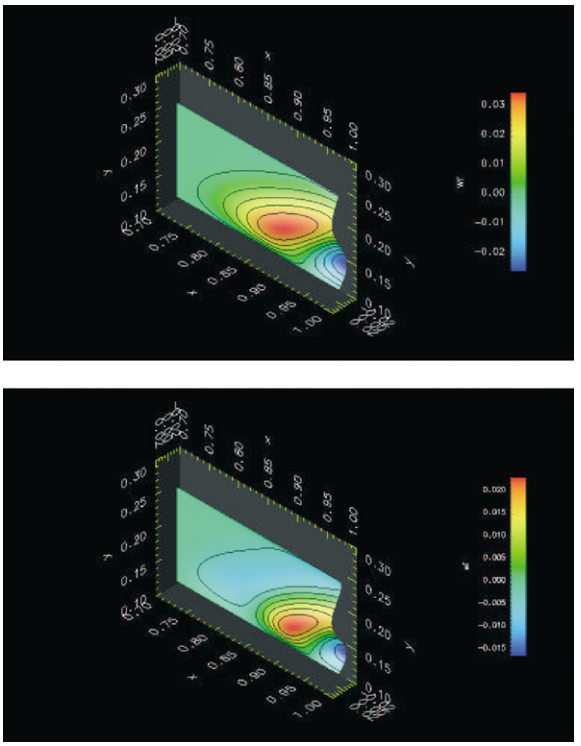

Fig. 19. Amplitude functions of the spanwise disturbance velocity component $\tilde{w}$ developing upon the basic flow of Fig. 18; upper $\Re\{\tilde{w}\}$, lower $\Im\{\tilde{w}\}$ [142].

result can be considered representative of those obtained at different wavenumber values. The $\hat{w}$ component of the BiGlobal eigenvector is interesting in that the actual three-dimensionalisation of the flow is determined by its structure when the eigenmode becomes unstable. The structure of $\tilde{w}$ is reminiscent of that found in the laminar separation bubble problem of Howarth/Briley, as discussed in the previous section; the basic flow recirculation zone will be split into two regions of fluid travelling in the opposite directions along the z-coordinate. The critical Reynolds number at which this will occur is the subject of current investigations.

The key discovery of global instabilities in separated flow alongside the prevalence of the phenomenon of flow separation in aeronautics warrant, in the author's view, renewed efforts in order to arrive at a more complete understanding of all instability mechanisms related to flow separation.

4.5. Flows over steps and open cavities

4.5.1. The basic flows

Open systems of practical importance in the context of aeronautics are the backward and forward facing steps, that over rectangular two-dimensional protrusions from a flat plate as well as open cavity configurations. All can be used as elementary models of parts of a high-lift configuration. Different methodologies have been followed for the recovery of the basic flow in these cases by the investigators who solved the respective BiGlobal instability problems. Barkley et al. [143] have used a spectral element discretisation of the backward facing step and Newton iteration for the two-dimensional basic state, which was obtained as the zeroth Fourier mode of the same three-dimensional spectral element numerical scheme also employed for the subsequent instability analysis. Stüer [82] and Stüer et al. [144] calculated the basic flow in the forward-facing step employing a second-order finite-volume method incorporating a projection step for the decoupled calculation of velocity and pressure fields. McEligot and co-workers [145] have produced benchmark experimental results for (three-dimensional) flow over a two-dimensional rectangular protrusion, covering Reynolds number ranges low enough so that well upstream and downstream of the protrusion essentially Blasius flow is established, up to such Reynolds numbers that flow is turbulent immediately downstream of the protrusion; no analysis of these experiments has been undertaken to-date.

The basic flow in open cavities of different aspect ratios was solved using 6th-order compact finite-differences [146] and a spectral multidomain algorithm [40] to recover solutions in compressible and incompressible open cavities, respectively. Interestingly, in both the backward facing step and the open cavity the shear layer emanating from the upstream corner becomes unsteady in two and unstable in three spatial dimensions in the context of the one-dimensional linear local theory discussed in Section 2. This has diverted attention of past investigations from the possibility of the entire two-dimensional separated flow in either the steps or the open cavity flows become unstable to three-dimensional spanwise periodic BiGlobal linear instabilities. The related conjecture is that a BiGlobal instability may act in these flows alongside the local instability, the origin of which is in the shear layer, in a manner analogous to that of separated flow on flat surfaces [135,35], and be responsible for the appearance of the currently little-understood so-called wake-mode instability [146]. Furthermore, if stores exist inside an open cavity the steady basic flow pattern is strongly affected; a demonstration can be found in Fig. 22. It may be inferred from this result that instability of the shear layer at the upstream wall may only partly be held responsible for the complex physical instability mechanisms encountered in experiments and three-dimensional simulations [9].

4.5.2. Eigenvalue problems and DNS-based BiGlobal instability analyses

Barkley et al. [143] have considered the stability of steady flow in a backward-facing step of inlet-to-outlet

height 1:2 in the range of Reynolds numbers (built with the centreline value of the parabolic velocity profile upstream of the step and the step height) $Re \in [450, 1050]$. They used DNS and a Krylov subspace iteration method for the determination of the most unstable eigenvalues, in both cases discretising space by a spectral-element method. One advantage of the latter is the ability to retain the same grid for both the basic flow and the eigenvalue problem but use the order of the expansion within elements to ensure convergence of the numerical results at modest resolution. These authors determined the critical conditions for the specific step geometry to be $Re_{\mathrm{crit}} = 750, \beta = 0.9$, i.e. the flow becomes three-dimensional to a BiGlobal eigenmode having a spanwise periodicity of approximately seven step heights. This critical Reynolds number value is substantially higher than those reported in experiments and DNS; however the intricate interplay of convective instability of the shear layer emanating at the lips of the step and BiGlobal instability of the entire recirculation bubble behind the step are far from being understood in a satisfactory manner for comparisons of the Reynolds number(s) to be made. The leading eigenmode of the BiGlobal instability has a spatial structure concentrated in the region immediately downstream of the step corner and, significantly, within the primary recirculation region, manifesting itself as a three-dimensionalisation of the basic-flow reattachment line. The latter aspect makes the BiGlobal instability mechanism in this flow qualitatively analogous to that of the pressure-gradient induced separation on a flat plate [35]. Barkley et al. [143] also addressed the issue of instability of the flow to two-dimensional BiGlobal eigenmodes. Based on extrapolation of damping-rate results these authors asserted that unsteadiness of the two-dimensional flow is expected beyond $Re = 1350$.

Stüer [82] and Stüer et al. [144] employed the same finite-volume algorithm used for the solution of the basic flow problem to calculate the BiGlobal instability of the forward-facing step. Their work covered a range of step-height based Reynolds numbers $Re \in [10, 200]$. On grounds of computing expediency these investigators have used the same grid for the calculation of the basic flow and the eigenvalue problem so their results cannot be considered definitive until confirmed by higher-resolution calculations or by a different high-order numerical method. In the parameter range examined, pertinent to a step-to-channel height ratio 0.5, they reported stability of the flow at $Re = 50$, instability of a stationary eigenmode at $Re = 100$ and instability of several travelling modes at $Re = 150$ and 200; they concluded that the 1:2 forward-facing step flow loses stability to three-dimensional travelling disturbances at $Re \approx 75$.

Theofilis [40] obtained incompressible flows over open cavities of different aspect ratios at Reynolds numbers which were chosen to be low enough such that no unsteadiness of the shear-layer was encountered. Characteristic results are shown in Fig. 20. Several models of the steady flowfield were analysed and the potential for BiGlobal instability of the flow, in the absence of shear-layer instability, was shown. At the other end of flow speeds, namely hypersonic flow, recent experimental and numerical investigations qualitatively relate flow over a so-called 'open' configuration of the open cavity with incompressible lid-driven rectangular cavity flow [147]. In the former case the shear layer formed at the upstream lip of the open cavity spans the entire width of the cavity and acts as a lid which isolates slow flow inside from that outside the open cavity. Inside the cavity the steady basic flow pattern resembles quite closely that of incompressible lid-driven cavity flow at moderate Reynolds number and comparable aspect ratios; the instability of the lid-driven cavity flow will be discussed in the next section.

Only DNS-based analyses of compressible open cavity flow are available [146,9]. Given the predominant role that the unsteady shear layer plays in this flow much effort is devoted towards analysing this essentially one-dimensional instability mechanism which can be formulated using (4) and either of (5) or (6), with appropriate acoustic forcing generated by interaction of the shear-layer with the downstream edge. However, the existence of a wake-mode instability [148] has raised intriguing questions, since its appearance cannot be explained using one-dimensional theory. Clearly a full understanding of all instability mechanisms, including those relevant to more complex cavities, is warranted. Some progress towards understanding was made by Colonius et al. [146], who found that the frequencies of oscillation of the wake-mode instability were nearly independent of the Mach number, over the range $0.2 < M < 0.8$, indicating that acoustic feedback did not play a role in the instability. They conjectured that wake-mode BiGlobal instability was related to a stronger recirculating flow within the cavity than that which exists in the shear-layer-mode.

Theofilis et al. [149] have analysed the steady two-dimensional basic state obtained in a length-to-depth ratio $L/D = 2$ cavity flow at incoming boundary layer displacement thickness $Re_\theta = 51$ and Mach number $M = 0.2$, shown in Fig. 20. The $\hat{u}$ disturbance velocity component of the least damped two-dimensional ($\beta = 0$) eigenmode of this flow is shown in Fig. 21; the most interesting characteristic of this BiGlobal eigenmode is its spatial shape, composed of a large-scale structure inside the cavity, reminiscent of the most unstable BiGlobal eigenmode in the lid-driven cavity (see below) and possibly related with the wake-mode, and a well-defined Tollmien–Schlichting instability developing on the downstream wall of the cavity. Moreover, this least-stable eigenmode shows no sign of a shear-layer related

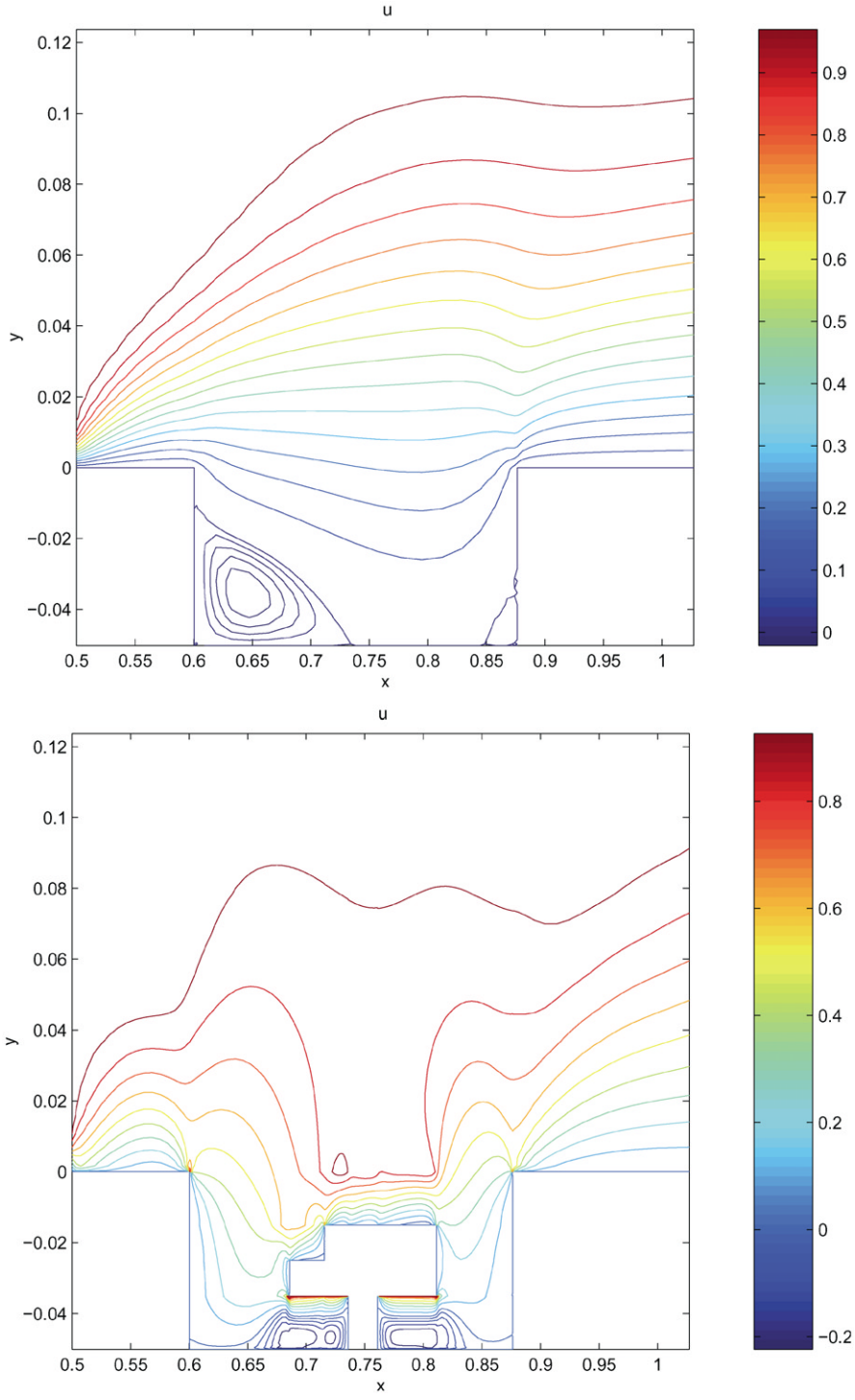

Fig. 20. Qualitative modification of the incompressible steady low-*Re* flow inside an open cavity on account of the presence of a model store.

eigenfunction. This counter-intuitive result is rather intriguing and points to the need for further work to quantify the relationship and relative significance of this BiGlobal instability mechanism with that in the shear-layer. This is even more compelling if an understanding of instability in 3D and/or full-store configurations is

to be achieved. This understanding is in the author's view a prerequisite for physically based efficient modelling and control in this flow.

4.6. Flow in lid-driven cavities

Three interesting classes of duct flows are schematically presented in Fig. 23; they correspond to pressure-driven flow in rectangular ducts having stationary walls (left) and duct flows driven by a lid which makes an angle ϕ with the axis Ox. The case $\phi = 0$ is the classic (rectangular) lid-driven cavity while $\phi = \pi/2$ corresponds to the two-dimensional analogon of Couette flow. All three classes have been studied in detail by Theofilis et al. [37].

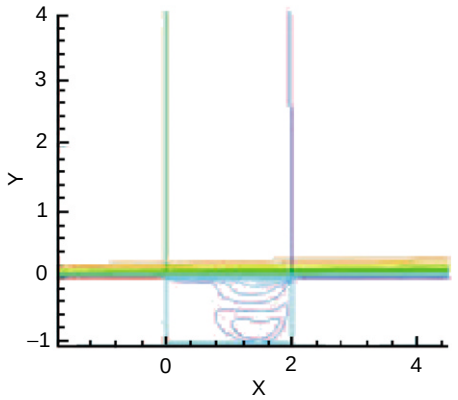

Fig. 21. Streamwise basic flow velocity component $\bar{u}$ of compressible flow in an open cavity [146,9].

4.6.1. The basic flows

The instability analysis in a lid-driven cavity flow, schematically depicted in Fig. 24, has clearly demonstrated the challenges presented by a BiGlobal linear analysis on account of poor resolution of the basic flow. The square lid-driven cavity has attracted considerable interest with respect to its BiGlobal linear instability by Ramanan and Homsy [81], Stüer [82], Ding and Kawahara [150,84] and Theofilis [40]. Ramanan and Homsy [81] used high-order accurate finite-differences, while Ding and Kawahara [150,84] used a finite-element methodology and Stüer [82] addressed this flow as part of the validations of a finite-volume algorithm. Theofilis [40] solved the basic flow problem using the spectral collocation algorithm of Appendix A. The accuracy of the obtained steady-state solutions has been assessed by comparison with the established works of Ghia et al. [151] and Schreiber and Keller [152] and converged basic states calculated at several Reynolds numbers and presented at $Re = 1000$ and 4000 in Table 4 demonstrate a satisfactory agreement with both benchmark works at the lower Re-value and especially with the Richardson extrapolated results of Schreiber and Keller [152] at the higher Reynolds number value monitored.

A different cavity flow configuration has been addressed by Kuhlmann and co-workers [83,153]. These authors considered basic flows set up by motion of two facing walls in opposite directions, which they monitored experimentally and analysed numerically. The

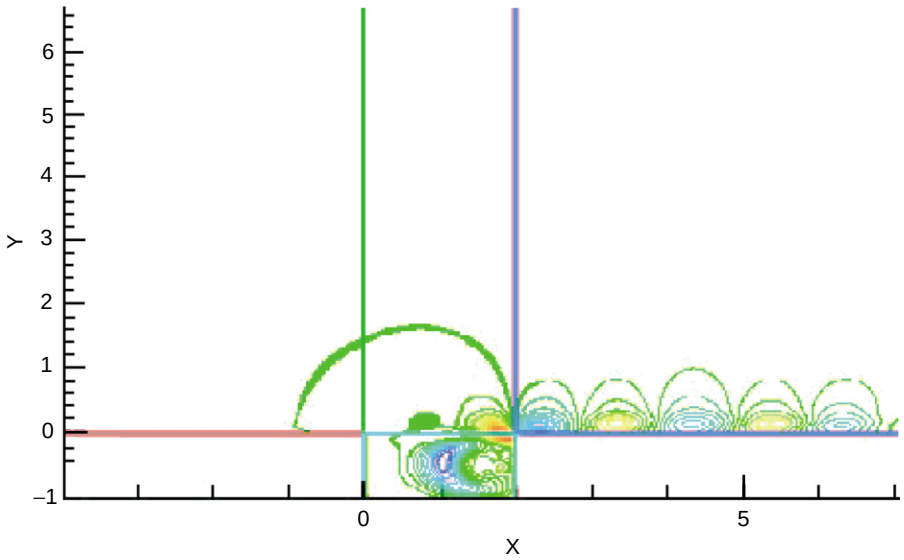

Fig. 22. Streamwise disturbance velocity component $\hat{u}$ in compressible flow over an open cavity at length-to-depth ratio 2, $Re_\theta = 51$ and $M = 0.2$ [149].

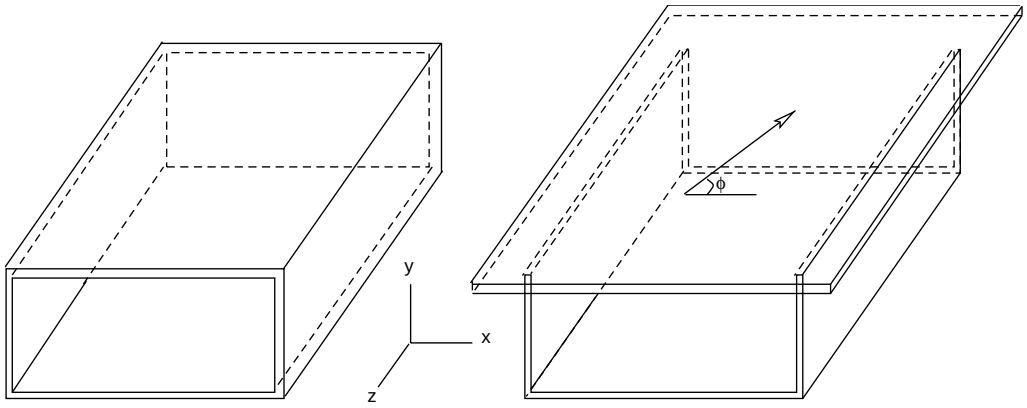

Fig. 23. Schematic representation of pressure-gradient driven flow in a duct with four stationary walls (left) and of flow driven by the motion of one wall which slides with constant velocity making an angle φ with the axis Ox (right).

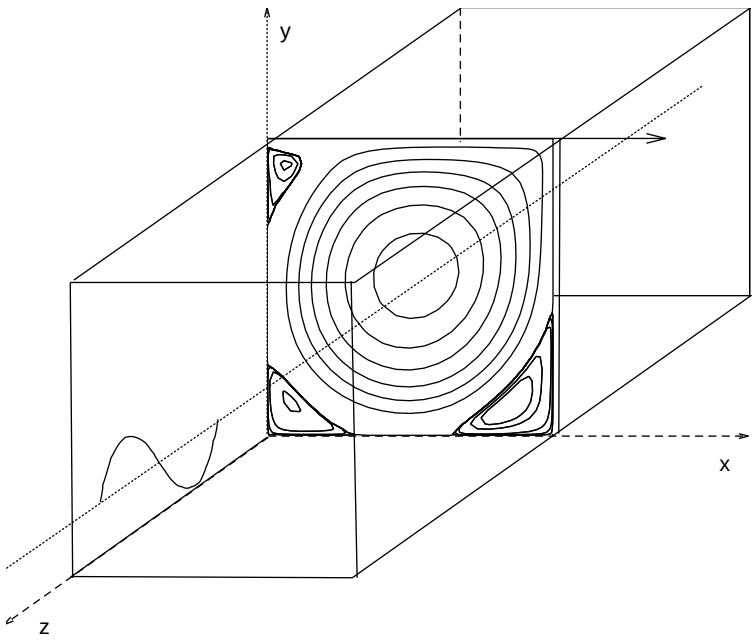

Fig. 24. Global instability analysis concept in a driven-cavity.

basic flow was described by two Reynolds numbers built with the aid of the speeds of the moving lids. Kuhlmann et al. [83] used a two-dimensional finite-difference/spectral-collocation DNS algorithm to calculate the basic states. To overcome the singularity in the boundary conditions at the junctions of stationary and moving cavity walls, these authors regularised the lid-velocity analytically and asserted that their chosen procedure affected the instability results maximally by a few percent. Furthermore, they justified the use of a two-dimensional solution procedure for the recovery of the basic state by comparison with experimental results in the neighbourhood of the plane of symmetry $z = 0$ of the configuration monitored. Based on their BiGlobal instability analysis results at the appropriate limit Kuhlmann et al. [83] questioned the accuracy of the BiGlobal instability analysis results of Ramanan and Homsy [81], thus raising renewed interest in the BiGlobal instability analysis of the classic (one-sided) lid-driven cavity flow.

4.6.2. *The eigenvalue problems*

This has been addressed by numerical solution of the real eigenvalue problem (34)–(37) in [150,84,82,40] or of

Table 4
Comparison of the interpolated values of our solutions on the maxima presented by [151] (GGS) and [152] (SK)

	$Re = 1000$							
	Primary		UL		LL		LR	
	ψ	ζ	ψ	ζ	$10^4\psi$	ζ	$10^3\psi$	ζ
GGS	−0.117929	2.04968			2.31129	−0.36175	1.75102	−1.1547
Present	−0.118902	2.06839			2.37806	−0.36575	1.77911	−1.1486
SK	−0.11894*	2.0677*			2.1700	−0.302000	1.700	−0.9990
Present	−0.118905	2.068234			2.3151	−0.312162	1.763	−1.0481
	$Re = 4000$							
	Primary		UL		LL		LR	
	ψ	ζ	ψ	ζ	$10^3\psi$	ζ	$10^3\psi$	ζ
SK	−0.12202*	1.9498*			1.1200	−1.0670	2.8000	−2.14500
Present	−0.122026	1.94960			1.2411	−1.1427	2.9228	−2.31944

An asterisk denotes Richardson-extrapolated data in the latter work.

a reduced form of this system in which a lower number of equations must be solved[6] in [81]. Furthermore, different numerical means, consistent with those used by the different investigators for the calculation of the basic flow, have been employed for the spatial discretisation of the eigenvalue problem. While the experimentally established stability of the two-dimensional basic state at low Reynolds numbers, i.e. two-dimensionality of the flow at these conditions [154], is reproduced in all available analyses, only those of Ding and Kawahara [84] and Theofilis [40] have produced consistent results at high Reynolds numbers as far as the third most unstable BiGlobal eigenmode is concerned. In the last work two additional eigenmodes were discovered, one stationary and one travelling. The critical parameters of the most unstable stationary mode $S1$ are $Re_{\mathrm{crit},S1} = 783$ at $\beta = 15.4$, those of the first travelling eigenmode $T1$ are ($Re_{\mathrm{crit},T1} = 845, \beta = 15.8$) while the respective parameters of the previously known mode $T2$ [84] are ($Re_{\mathrm{crit},T2} = 922, \beta = 7.4$). The frequency of the most unstable travelling mode $T1$ shows very good agreement with experimentally obtained frequency results of Benson and Aidun [155], as shown in Fig. 25. The spatial structure of two components of the (stable) two-dimensional ($\beta = 0$) eigenvector of a square cavity at $Re = 1000$ is shown in Fig. 26 with the values of the marked levels cited in Table 5; both the spanwise disturbance velocity component $\hat{w}$ and the disturbance pressure $\hat{p}$ are seen to acquire the vortical structure of the underlying two-dimensional basic flow [154]. The spatial structure of the most unstable three-dimensional eigenmode is shown in Fig. 27 as isosurfaces of the disturbance vorticity. It is interesting to note that such a structure might be confused with nonlinear flow behaviour in flow visualisations of experimental or DNS results, although it is the result of a BiGlobal *linear* mechanism.

The two-sided lid-driven cavity flow [83] is in certain ways analogous to the one-sided lid-driven cavity, but important differences also exist. The second Reynolds number introduces an additional control parameter in the problem. Keeping the two Reynolds numbers at the same value ('symmetric driving') Kuhlmann et al. [83] discussed the hysteresis loop encountered in the range $Re \in [234, 427]$ from the point of view of its instability to two-dimensional BiGlobal infinitesimal disturbances and showed that the flow is unstable within this bracket of Reynolds numbers and linearly stable at $Re < 234$, where it is found in a two-vortex state, as well as at $Re > 427$, where a cats eye structure is the prevalent flow configuration. However, the latter flow is unstable to three-dimensional perturbations, the critical conditions of which are a function of the cavity aspect ratio A. The minimum critical Reynolds number was found to be $Re \approx 190$ at $\beta = 2.4$ and $A = 1.45$. A different type of instability was also documented in the experiments, namely the appearance of multiple cells as the Reynolds number increases, which is another discriminating characteristic between the one- and two-sided lid-driven cavity flows. Finally, based on their experimental and numerical results, Kuhlmann et al. [83] proposed that in the two-vortex state the diameter D of the main inviscid vortex core scales linearly with the cavity aspect ratio, as opposed to $D \sim Re^{1/2}$ that Pan and Acrivos [156]

[6] Although higher-order derivatives appear, which are more challenging to represent numerically when using a moderate number of discretisation points.

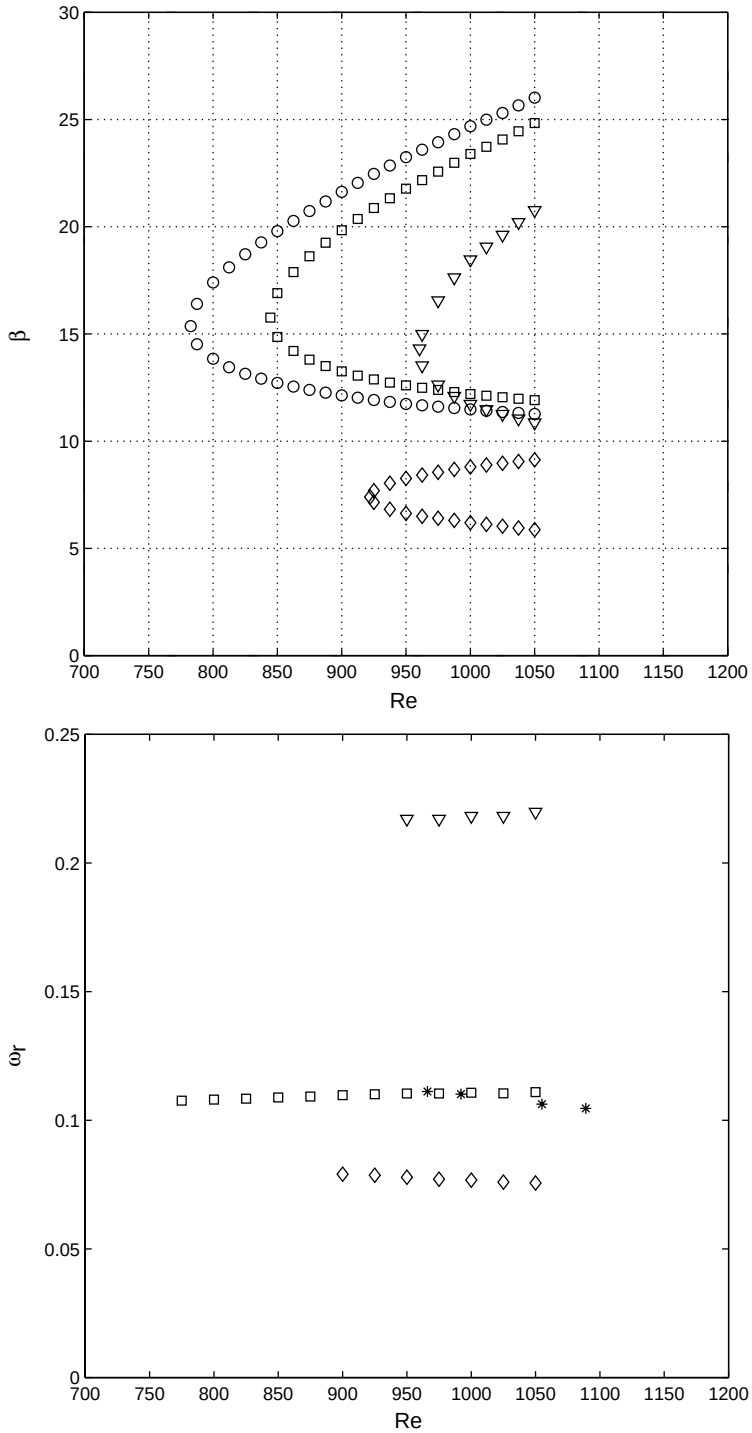

Fig. 25. Upper: theoretical neutral loops in the square lid-driven cavity. Lower: dependence of the frequency of the three most unstable global eigenmodes on Reynolds number and their comparison with experimental results of [155] denoted by star symbols; note, the most unstable mode is stationary, $\Omega_r \equiv 0$ [40].

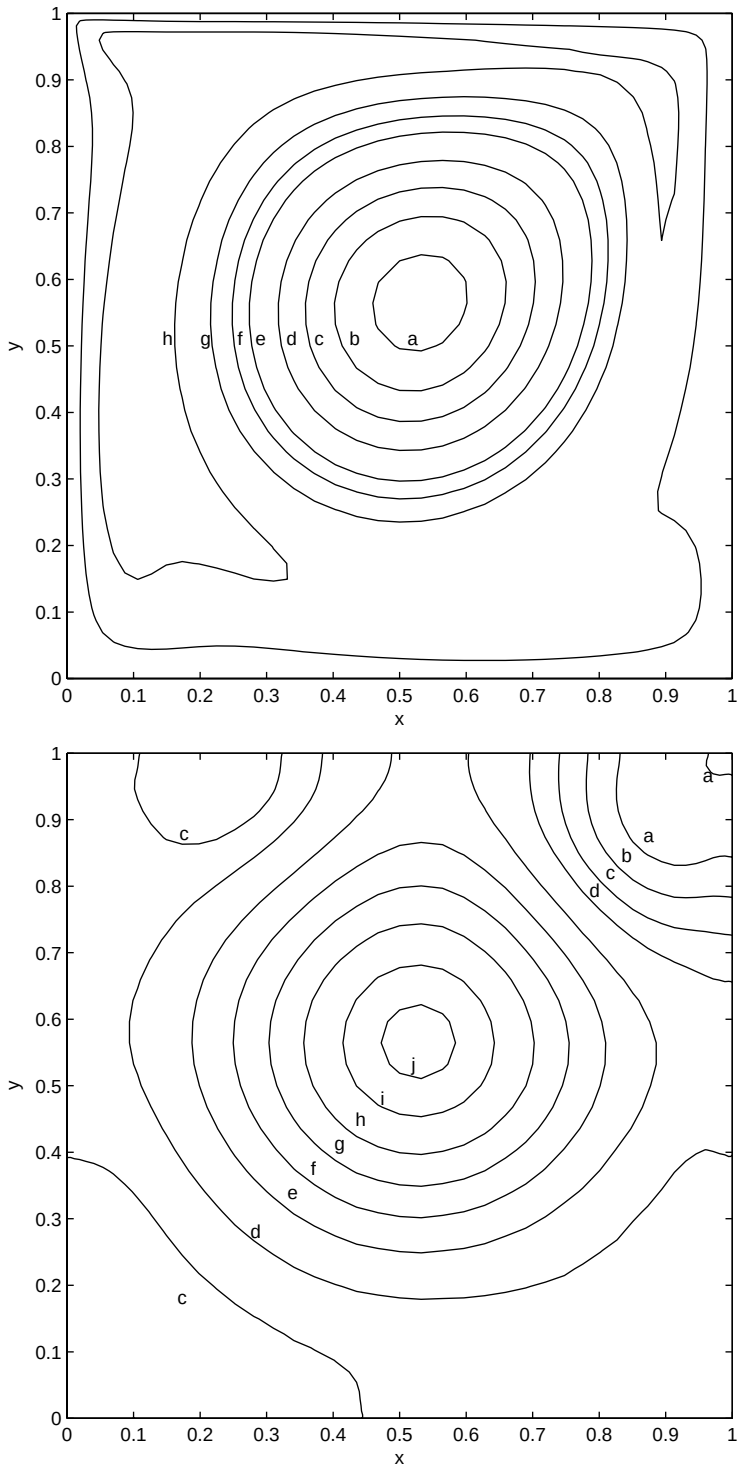

Fig. 26. Isolines of disturbance velocity component $\hat{w}$ and disturbance pressure $\hat{p}$ of the two-dimensional ($\beta = 0$) global mode at $Re = 10^3$ in a square lid-driven cavity [40].

Table 5
Isoline levels of the results of Fig. 25

$\hat{w}$	Symbol	a	b	c	d	e	f	g	h		
	Level	0.90	0.70	0.50	0.30	0.10	0.00	−0.10	−0.20		
$\hat{p}$	Symbol	a	b	c	d	e	f	g	h	i	j
	Level	0.90	0.80	0.70	0.60	0.45	0.30	0.15	0.00	−0.15	−0.20

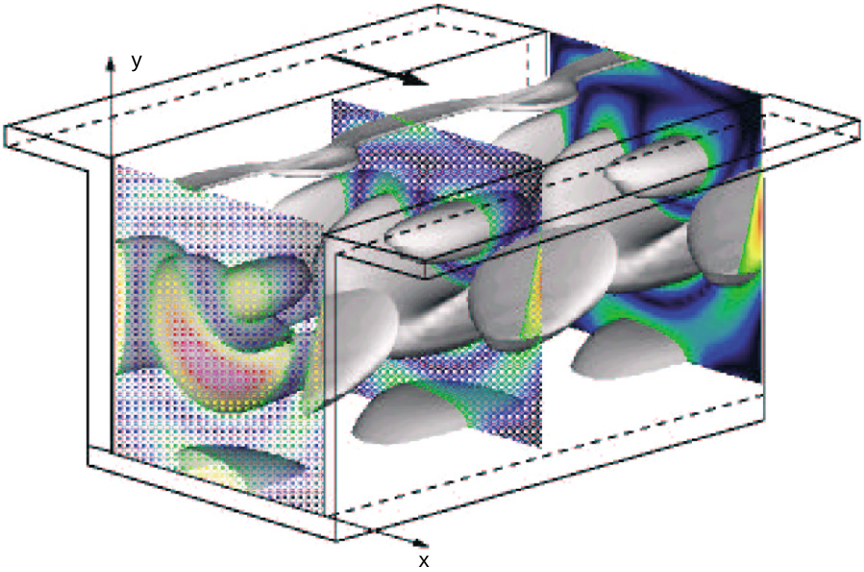

Fig. 27. Isosurface of disturbance vorticity magnitude in a square lid-driven cavity [40].

predicted in the limit $A \to \infty$ of an one-sided lid-driven cavity.

4.7. Flows in ducts and corners

4.7.1. Basic flows

Besides the handful of basic flows directly relevant to aeronautics which have been addressed by BiGlobal instability analysis to-date, several simple model flows which generalise analytically known one-dimensional steady profiles have been monitored with respect to their BiGlobal instability. Tatsumi and Yoshimura [14] studied the instability of flow in a rectangular duct, while Kerswell and Davey [157] addressed that of flow in a duct of elliptic cross section. The limit of large aspect ratio in the first flow and that of large eccentricity in the second approximate plane Poiseuille flow, while the case of unit eccentricity in the elliptic duct corresponds to one of the best known failures in the predictions of classic one-dimensional linear instability theory, namely Hagen–Poiseuille flow. In both the case of basic flow in a rectangular duct and that in the elliptic pipe analytic solutions are known for the single nonzero velocity component $\bar{w}$ set up when flow is driven by a constant pressure gradient along the homogeneous spatial direction z. In a rectangular duct defined in the domain $S = \{x \in [-A, A]\} \times \{y \in [-1, 1]\}$, where A is the aspect ratio (all lengthscales being nondimensionalised with respect to the duct semi-depth), the steady laminar flow is independent of z and possesses a velocity vector $(0, 0, \bar{w})^{\mathrm{T}}$. Taking the constant pressure gradient value $\mathrm{d}\bar{p}/\mathrm{d}z = -2$ and scaling the result with the value of $\bar{w}$ at the midpoint of the duct, the Poisson problem may be solved in series form [136]

$$\bar{w}(x, y) = 1 - y^2 - 4\left(\frac{2}{\pi}\right)^3 \sum_{n=0}^{\infty} \frac{(-1)^n}{(2n+1)^3} \times \frac{\cosh[(2n+1)\pi x/2]\cos[(2n+1)\pi y/2]}{\cosh[(2n+1)\pi A/2]}. \quad (70)$$

The plane Poiseuille basic flow result is retrieved from this expression in the limit $A \to \infty$. In the analysis of Theofilis et al. [37] the basic flow problem was solved numerically; an 8×8 Legendre collocation grid suffices to obtain a solution of the two-dimensional Poisson problem the relative deviation of which from the analytic solution is less than 10^{-8} while analyses were performed using upwards of 48^2 Legendre collocation

points. A different extension of the classic plane Poiseuille flow has been addressed by Ehrenstein [16] who solved the BiGlobal eigenvalue problem in a channel one wall of which was covered by riblets. Here the basic flow was obtained by solution of the appropriate two-dimensional Poisson problem (15), after an analytic description of the riblet geometry was provided.

Yet another two-dimensional duct flow which has a classic analytically known one-dimensional counterpart has been investigated recently with respect to its BiGlobal instability, namely wall-bounded Couette flow between parallel plates defined by $x\in[-A,A]$ and $y\in[-1,1]$ set up by keeping three walls at rest and permitting the fourth to move at a constant speed along the homogeneous direction, in the absence of a pressure gradient. Normalising the moving-wall speed to $\bar{w}(y=1)=1$ it is straightforward to solve the homogeneous two-dimensional Poisson equation (15) subject to inhomogeneous boundary conditions and derive an analytic solution for the basic flow $\bar{w}$ [37]

$$\bar{w}(x,y)=\sum_{n=0}^{\infty}\frac{4(-1)^n}{(2n+1)\pi}\frac{\sinh(2n+1)\pi(y+A)/2}{\sinh(2n+1)\pi A}\times\cos(2n+1)\pi x/2, \tag{71}$$

an expression which merges into the linear profile in the limit $A\to\infty$. Finally, flow in a sudden-expansion pipe has recently received attention with respect to its BiGlobal instability by Hawa and Rusak [39]. These investigators obtained the basic state in a slightly asymmetric channel numerically by solving (16) and (17) using finite-difference techniques before employing asymptotic expansions in the framework of a bifurcation analysis to address the instability problem.

Another problem of considerable relevance to aeronautical applications is that of boundary-layer flow in the junction of flat plates, an idealisation of corner flows encountered in external aerodynamics, notably at wing-body junctions and those of the rotor and hub of a propeller, as well as in junctions of wind-tunnel walls. Despite extensive efforts on the analytical/numerical description of the steady laminar boundary layer in this problem dating back to Carrier [158] the nonsimilar nonlinear nature of the governing equations is a source of a wealth of mathematically realisable and physically plausible solutions still being discovered Dhanak and Duck [159], Duck et al. [160]. The question which of the corner boundary layer basic flow solutions can be physically realisable may be addressed by BiGlobal instability analysis; two such efforts have been undertaken by Balachandar and Malik [68] and Parker and Balachandar [72]. The latter two works used steady laminar basic flows derived from a similar boundary-layer concept, with the two spatial coordinates x and y along the directions of the normals to the intersecting plates, as well as the streamwise direction z scaling uniformly with the inverse square-root of the Reynolds number built with z. The freestream velocity is taken to be of the form

$$W(z)=Cz^n \tag{72}$$

with C a constant and n an integer associated with the streamwise pressure gradient. A coupled set of inhomogeneous Poisson problems must be solved for the determination of the basic flow at a given downstream location z subject to boundary conditions, a detailed discussion of which is beyond the scope of the present review. It should be noted, however, that the analyses proceed by using a parallel-flow approximation, i.e. by neglecting streamwise variation of the three-dimensional steady laminar basic state set up by (72).

4.7.2. *The eigenvalue problems*

Tatsumi and Yoshimura [14], employing spectrally accurate numerical solutions of system (39) and (40), produced one of the early applications of viscous linear BiGlobal flow instability theory in an aerodynamics related configuration, that of pressure-gradient driven flow in a rectangular duct. Commensurate with the computing capabilities of the time, these authors took advantage of the symmetries of the basic flow in the duct and monitored eigendisturbances of odd or even parity across the axes, $x=0$ and $y=0$. In this manner accurate instability results could be produced at very large Reynolds numbers. From a physical point of view, it turned out that the plane Poiseuille flow, corresponding to an $A\to\infty$ duct, represents the most *unstable* flow configuration, while the limit of a square duct, $A=1$, was postulated to be linearly stable. Another paradox in the predictions of (BiGlobal) linear theory was thus added to the classic failure of the OSE-based analysis of Hagen–Poiseuille flow. From a numerical point of view, this flow is challenging on account of the need either to discretise a wide domain ($A\gg1$) at moderate Reynolds numbers or instability at moderate aspect ratios $A\approx1$ manifesting itself at large Reynolds numbers, rendering system (28)–(31) increasingly stiff. These challenges were shown by Theofilis [87] to be well met by the Arnoldi algorithm; the dependence of the eigenvalue (Ω_r,Ω_i) of mode I instability on β at $A=5$ is presented in Fig. 28; the spatial structure of the streamwise disturbance velocity component of this mode is shown in Fig. 29 where it can be seen that the symmetries imposed by Tatsumi and Yoshimura [14] are recovered as result of the calculations. However, the question which motivated the analysis of [14], namely subcritical instability of the rectangular duct flow [161] remains unanswered. One plausible explanation may be sought in the framework of subcritical instability of a nonlinearly modified basic state [56]; such an analysis would increase the size of the secondary BiGlobal eigenvalue problem by a factor

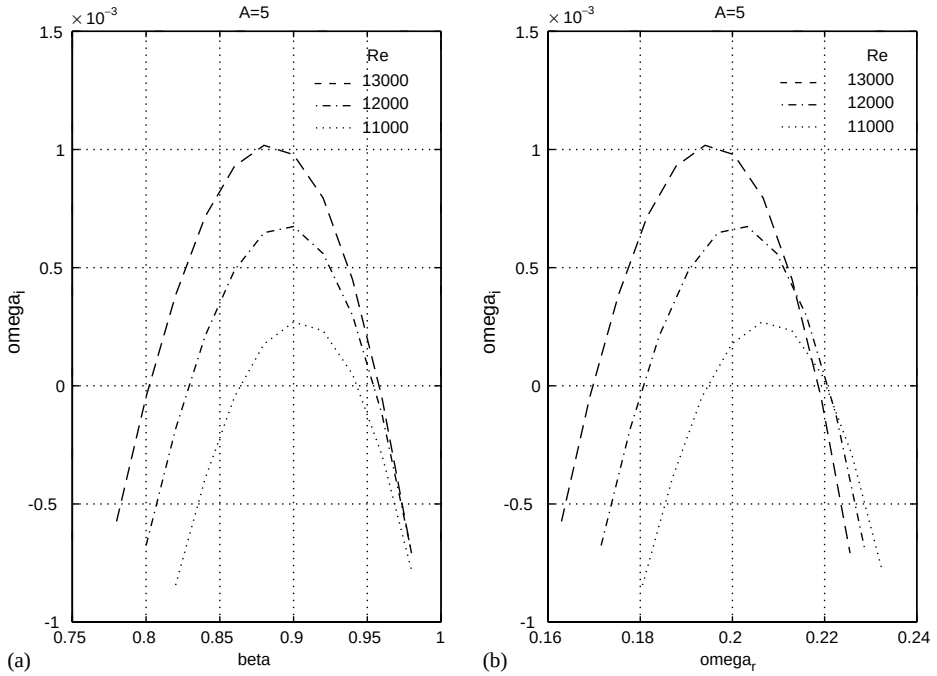

Fig. 28. Growth rate of mode I global instability as function of frequency in an $A = 5$ rectangular duct at three supercritical Reynolds numbers [14].

equal to the number of harmonics maintained in the secondary analysis and is currently beyond reach of a straightforward solution of the relevant extension to (28)–(31).

Another anomaly in the predictions of BiGlobal linear instability theory has been added by Theofilis et al. [37] who analysed the wall-bounded Couette flow (71). The eigenspectrum of (71) was found to have the familiar Y-shape of its one-dimensional analogon. The linear eigenmodes were found to comprise structures symmetric about $x = 0$ and concentrated at the top, middle or lower part of the domain; two typical eigenfunctions are shown in Fig. 30. However, a systematic search of the (Re, β) parameter space has yielded no linearly unstable modes, despite the presence of lateral walls. As a matter of fact, the wall-bounded version of this flow was found to be more stable than the classic linear profile. On the other hand, another duct geometry, that in an analytically prescribed U-grooved channel, could be analysed successfully with respect to its BiGlobal linear instability. Ehrenstein [16] used the Arnoldi algorithm to address the instability of this flow and predicted that a channel in which one wall was covered by riblets leads to a flow which is linearly more unstable than the plane Poiseuille flow. Further, he showed that an increase of the periodicity lengths of the riblets increases their instability and could recover pairs of counter-rotating vortices with a wavelength approximately that of the imposed riblet spacing, in line with analogous experimental observations.

Strong experimental evidence exists that the establishment of steady laminar corner flow is extremely sensitive to factors such as details of the geometry and shape of the leading-edge region as well as angle of incidence of the flow/streamwise pressure gradient. The conjecture put forward is that an instability mechanism is responsible for the wide discrepancies in the experimental literature; compilation of results at favourable pressure gradients and their extrapolation towards zero streamwise pressure-gradient conditions has yielded a critical Reynolds number based on distance from the leading edge of $O(10^2)$ [162]. The inviscid linear instability analysis of a model corner flow by Balachandar and Malik [68], performed by solution of the generalised Rayleigh equation (45), indeed delivered several unstable inviscid eigenmodes at zero streamwise pressure gradient. The issue of a critical Reynolds number remained outside the scope of this work and was addressed in the subsequent viscous BiGlobal linear instability analysis by Parker and Balachandar [72]. The latter work failed to identify inviscid instabilities at Reynolds numbers $Re < 5 \times 10^5$. Instead, a multitude of viscous BiGlobal modes, related with Tollmien–Schlichting instability away from the plates bisection, and a single inviscid so-called 'corner mode' were obtained in the latter work; the spatial structure of the

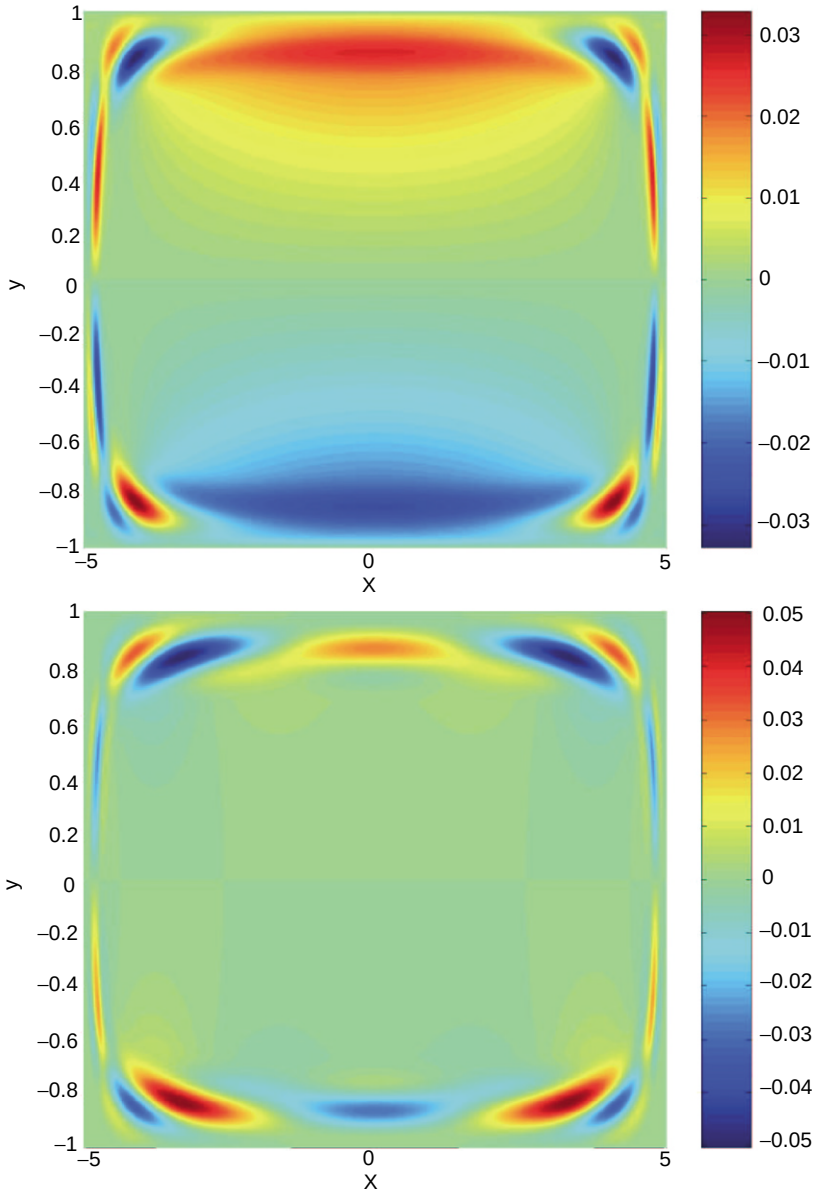

Fig. 29. Amplitude functions of the spanwise disturbance velocity component $\Re\{\tilde{w}\}$ in a $A = 5$ rectangular duct at critical conditions; upper: neutral eigenmode, lower: least damped eigenmode [87].

three most significant viscous modes is shown in Fig. 31, where the imposed symmetries can be observed as well as the TS structure that these BiGlobal eigendisturbances acquire away from the corner $\zeta = \eta = 0$. The wide gap between the critical Reynolds number conjectured from experiment and the theoretical predictions of [72], and the focus of the two available BiGlobal instability analyses on a similarity basic flow solution, in conjunction with the recent discovery of additional nonsimilar basic flows, suggest that the corner flow boundary layer problem and its BiGlobal linear instability will remain a challenging application for BiGlobal linear analysis in the foreseeable future.

4.8. Global instability of Görtler vortices and streaks

As a matter of fact, vortical flows have been the first to attract attention with respect to their BiGlobal elliptic linear instability. In the first analysis of its kind Pierrehumbert [10] reported the discovery of

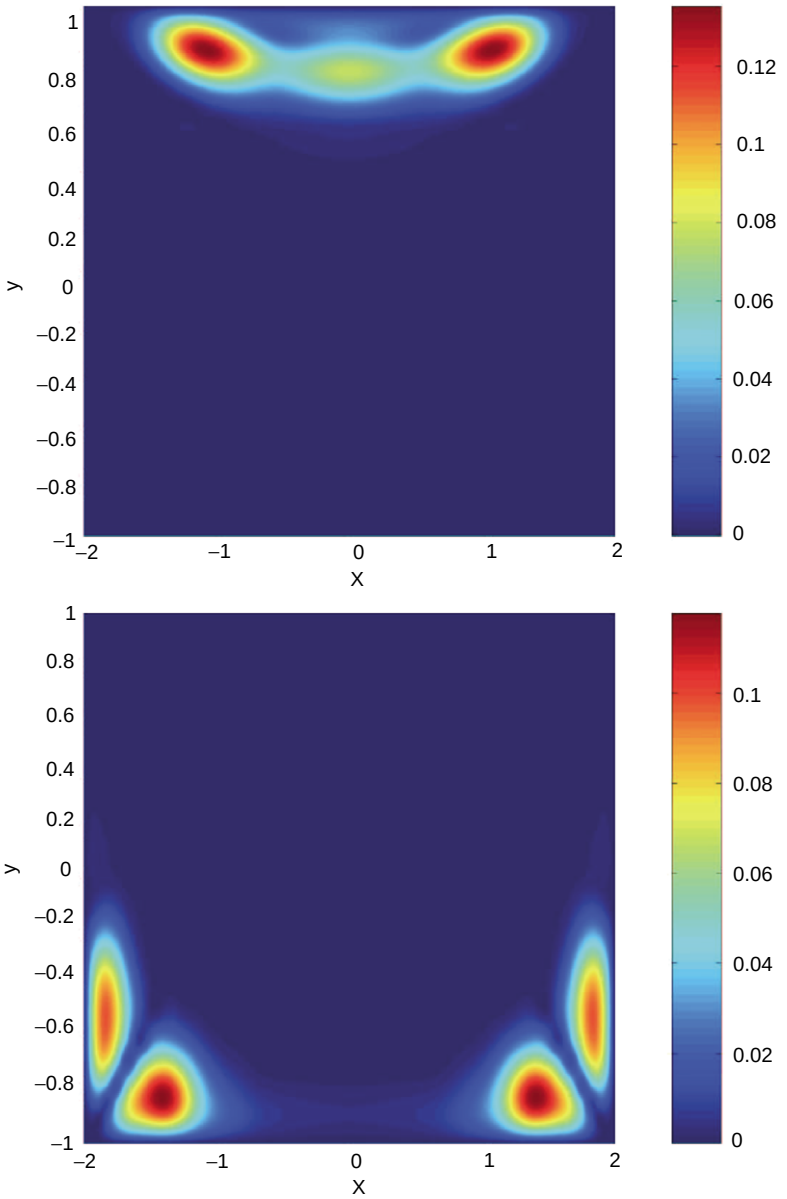

Fig. 30. Spatial structure of the spanwise disturbance velocity component $\Re\{\bar{w}\}$ of two eigenmodes in $A = 2$ wall-bounded Couette flow at $Re = 3200, \beta = 1$.

short-wavelength BiGlobal instability in inviscid vortex flow. Hall and Horseman [67] considered longitudinal Görtler vortices induced by wall curvature. This basic state was recovered as solution of the boundary-layer equations, starting the solution procedure at a location z_0 from the initial condition

$$\bar{w}(x, y) = y^6 \mathrm{e}^{-y^2/2x} \tag{73}$$

and integrating in z until the recovered basic flow supported BiGlobal instability in the subsequent analysis.

Within the context of algebraically growing solutions of the equations of motion, Brandt et al. [163] have recently addressed the instability of streaks formed in the boundary layer at high free-stream turbulence levels. The quasi-steady basic flow here is a single streak extracted from the three-dimensional DNS results of the same authors. Their BiGlobal instability analysis of the streak demonstrated that high-frequency secondary instability sets in and leads flow to breakdown and turbulence. It is interesting to note here that while the scenaria leading to crossflow vortex/streak formation

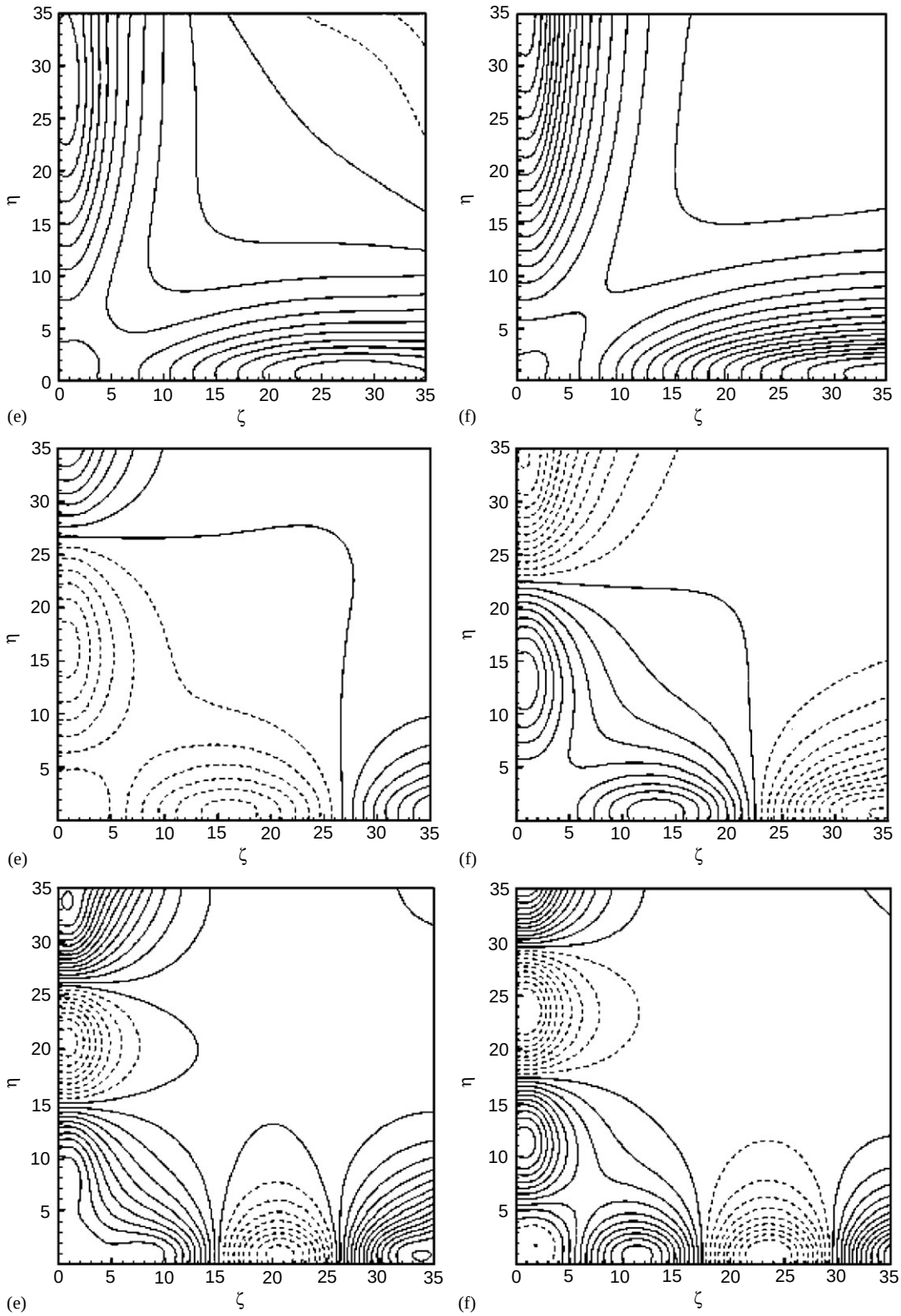

Fig. 31. Spatial structure of the real (left column) and imaginary (right column) parts of the streamwise disturbance velocity component $\hat{w}$ of the three most unstable viscous eigenmodes in corner flow instability as function of the transformed x and y coordinates, ζ and η, respectively [72], Upper to lower, modes I, II and III.

are fundamentally different, flow turbulence in both cases originates through a qualitatively analogous mechanism which can be described by BiGlobal linear theory.

4.9. The wake–vortex system

4.9.1. Basic flow models

In the course of current efforts to minimise the extent and strength of coherent vorticity in the wake of passenger aircraft during take-off and approach, the subject of instability of systems of trailing vortex models has received renewed attention. Since the key objective of the current efforts is to provide recommendations leading to reduction of aircraft-separation limits, currently of the order of a few minutes, focus of instability analyses is on mechanisms other than the classic Crow [44] instability, the long-wavelength nature of which excludes it from playing an active role in the sought process. Rather than the single pair of counter-rotating or co-rotating vortices, the stability of which has respectively been addressed by Crow [44] and Jiménez [164] attention is currently focussed on systems of multiple vortices produced by a flaps-down configuration. These flows can be modelled by linear superposition of isolated vortex tubes of prescribed circulation as schematically depicted in Fig. 32; however injecting such a system into the governing equations in general does not deliver a steady or time-periodic basic state in the sense of Section 2. Experimentation and numerical simulation are indispensable to understanding the basic flow character in this problem.

de Bruin et al. [45] have measured the (three-dimensional) wake behind a commercial aircraft model; assuming that the turbulence level in the wake was low, they used the two-dimensional field at a specific downstream location in the axial direction of the aircraft motion, z, as input for two-dimensional DNS calculations based on (16) and (17) and obtained very good agreement between experiment and DNS calculation at further downstream locations. The basic flow was found to be a time-periodic state in which each pair of starboard/port vortices rotates about the common centroid. A different approach has been followed by Rennich and Lele [165] who used the equilibrium condition

$$\left(\frac{b_2}{b_1}\right)^3+3\left(\frac{\gamma}{\Gamma}\right)\left(\frac{b_2}{b_1}\right)^2+3\left(\frac{b_2}{b_1}\right)+\left(\frac{\gamma}{\Gamma}\right)=0 \tag{74}$$

to relate the circulations Γ,γ and distances b_1,b_2 of the vortices, taking advantage of the well-known fact that satisfaction of (74) renders the configuration of Fig. 32 a quasi-stationary solution of the equations of motion in which the entire vortex system descends at a constant speed. Moreover, it has been argued that configurations having parameters which satisfy this equilibrium condition can be representative of a number of commercial aircraft wakes.

4.9.2. Analysis, numerical solutions and the eigenvalue problem

Crouch [46] addressed the instability of a basic flow composed of two pairs of co-rotating vortices, taking the first pair of signs for the circulation γ in Fig. 32. He employed the vortex-filament approach also used by Crow [44] and Jiménez [164] and numerical solutions of the initial value problem resulting from matching the induced velocities that the Biot–Savart law delivers with kinematic conditions resulting from temporal differentiation of the position vectors of the vortex system. The elegance of this approach lies in that the stability investigation may proceed analytically to a large extent. Its drawback is that the instability results delivered are relevant to the physical problem only for wavelengths that are long compared to the core size of the vortices and spurious instabilities may be predicted if this condition is violated. Taking this condition into consideration Crouch [46] proceeded by assuming that

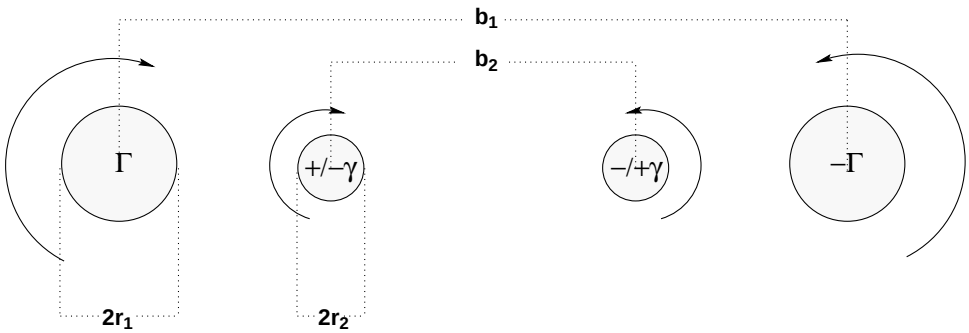

Fig. 32. One global instability analysis concept in a trailing vortex system.

the helical motion of the vortex pair on either side of the aircraft has a wavelength much larger than that of a developing instability and thus time is the only parameter characterising the motion of each vortex pair in the basic state; the periodic motion was treated by Floquet theory.

Three different instability mechanisms were discovered by Crouch [46]; they are depicted in Fig. 33 after one period of their respective evolution. The first is akin to Crow instability and corresponds to wavelengths and growth rates that are, respectively, too large and too small to be interesting for the wake–vortex minimisation problem (top of figure). The second mechanism corresponds to a new class of symmetric and antisymmetric disturbances (as viewed from the ground), which were discovered at shorter wavelengths, having growth rates up to twice as large as those of the Crow-like instabilities (middle of figure); as such, these instabilities may have an active role to play in the problem at hand. However, the third physical mechanism, transient growth of the wake–vortex system, has been identified to be the most promising one to be exploited for early breakdown of trailing vortices in the problem at hand. While this well-established in channel flows [166,167] route to transition is inactive at short wavelengths (scaling with the vortex spacing), at large wavelengths and/or when one vortex pair only is excited, it yields growth rates which can be an order of magnitude larger than those delivered by linear theory, leading the wake–vortex system to lose its coherence in a fifth of the time that the strongest of the linear mechanisms of the previous two types may do. Physically founded instability mechanisms have been experimentally verified on realistic wing configurations (Crouch, personal communication) as part of the effort of transitioning this theoretical knowledge to systems for wake–vortex control of commercial airliners.

Fabre and Jacquin [47] addressed a configuration composed of two pairs of counter-rotating vortices (i.e. considered the second pair of signs for γ in Fig. 32) subject to (74), which determines the positioning of the vortices once circulation is specified, i.e. modelled from experiment. These authors also used a vortex filament method for the instability analysis and complemented their linear theory by a transient growth study. In the case of a system of counter-rotating vortices too, linear instabilities additional to the Crow mode were discovered; the dependence of the (scaled) growth rates on wavenumber is shown in Fig. 34. The analogon of the Crow instability is denoted by the second symmetric mode S2, while it can be seen that the discovered modes S1 and A are respectively amplified by factors 10 and 5 stronger than S1; the spatial structure of the new eigenmodes is shown in Fig. 35. While interesting in their own right, these instabilities, of the classic elliptic nature first discussed theoretically by Pierrehumbert [10] and Bayly [86], they contribute little to the modification

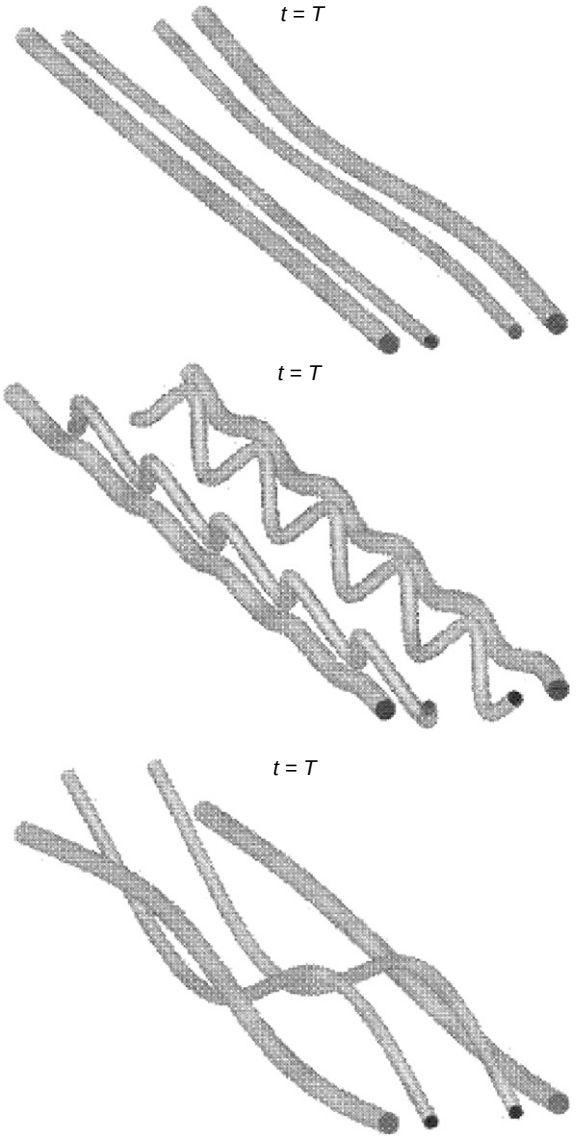

Fig. 33. Modification of the wake–vortex system on account of the mechanisms discussed by [46].

of the (stronger) outer vortices and attention must be focussed on mechanisms other than their BiGlobal linear instability in order to address the wake–vortex minimisation problem; work is in progress on this issue.

The restrictions of the vortex-filament approach and those implied by (74) may be relaxed when solving the two-dimensional eigenvalue problem (28)–(31). Jacquin et al. [93] have discussed applicability of the BiGlobal instability analysis concept by analysing basic flow systems constructed by linear superposition of pairs of co-rotating and counter-rotating Batchelor-like vortices

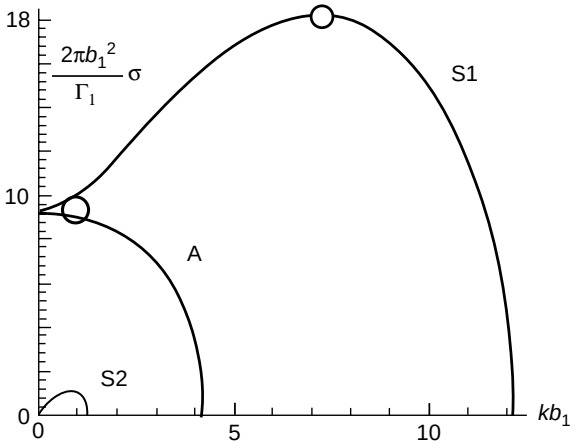

Fig. 34. Amplification rate $2\pi b_1/\Gamma_1\sigma$ against wavenumber kb_1 diagram of the short-wavelength instabilities S1 and A, amplified stronger than the [44] instability (S2), in a model wake–vortex system satisfying the equilibrium condition (74) [47].

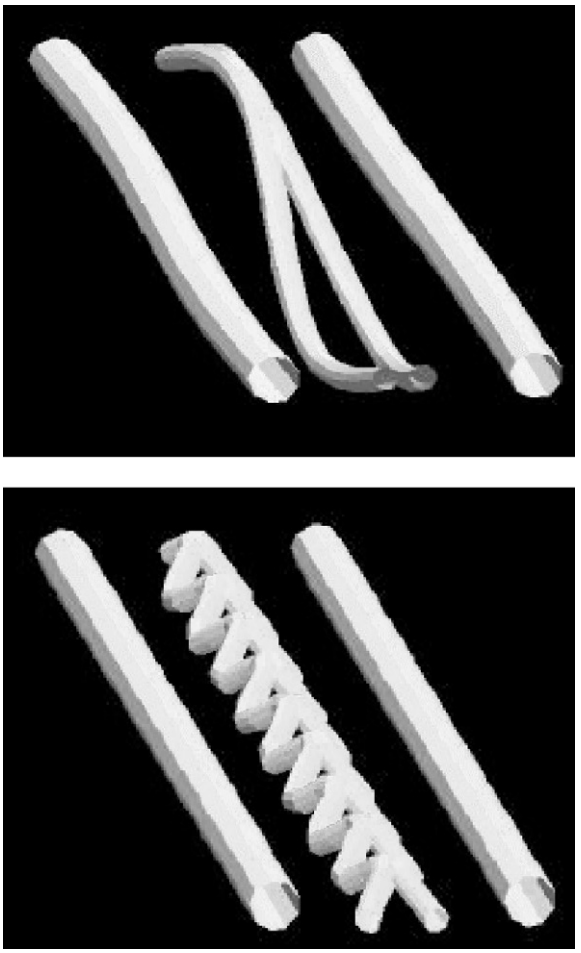

Fig. 35. Linear instability of the inner pair of vortices on account of the mechanism discovered by [47].

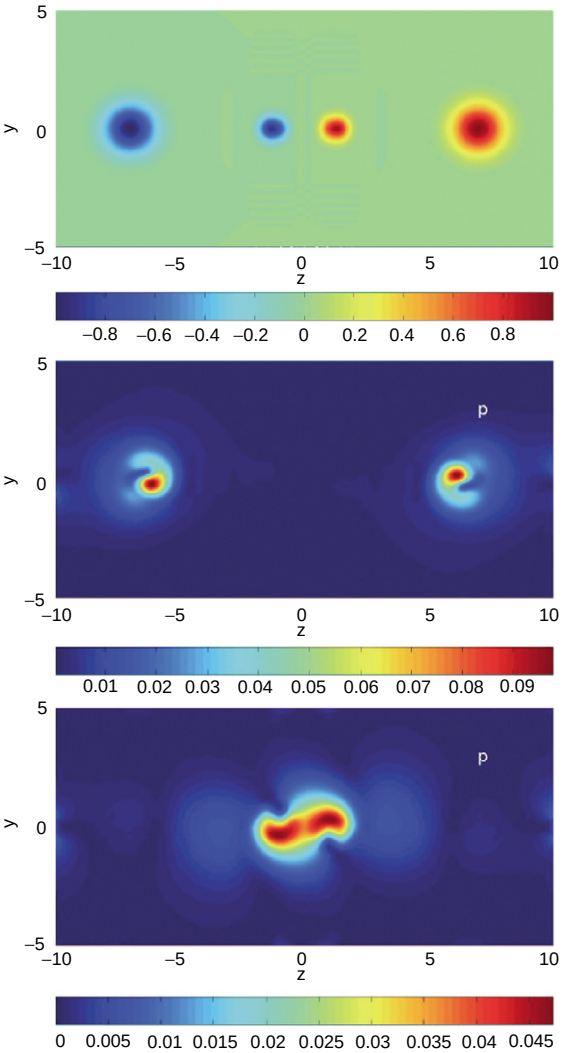

Fig. 36. Basic flows consisting of co-rotating or counter-rotating pairs of Batchelor vortices (upper) and the respective global instabilities in terms of the disturbance pressure amplitude function $\hat{p}$. Note, the homogeneous direction in this problem is denoted by z [93].

satisfying (74); the basic state is shown in the upper part of Fig. 36. Since the focus of that work, amongst others, was to demonstrate the potential of the BiGlobal eigenvalue problem from a qualitative point of view, a quasi-steady basic flow approximation was used. The amplitude functions of the $\hat{p}$ component of the most unstable eigenvector in either case are also plotted in Fig. 36. Either of the inner or outer pairs of vortices may be seen to be modified by the respective most unstable BiGlobal eigenmode. Further work to apply the theory of Section 2 to the wake–vortex problem is currently underway.

4.10. Bluff-body instabilities

4.10.1. Laminar flow past a circular cylinder

Bluff-body instability and transition is one problem in external aerodynamics, full understanding of which should, in the author's view, precede theoretically founded flow control methodologies. Insight into bluff-body three-dimensional instability has been gained by substantial progress made in the elementary configuration of an infinite cylinder from both an experimental [168] and a theoretical/numerical point of view, the latter employing accurate spectral-element DNS methodologies [169,23,24]. The linear stages of the transition process on the cylinder are now reasonably well-understood. A Hopf-bifurcation above a Reynolds number $Re = U_\infty D/\nu \approx 47$, establishes a time-periodic nominally two-dimensional state of the form (26) in which two-dimensional vortices having their axes parallel to that of the cylinder are shed. The Hopf bifurcation itself can be associated with instability of the $(\beta = 0)$-BiGlobal eigenmode superimposed upon the laminar two-dimensional steady-state circular cylinder solution prevailing at $Re < 47$. The instability of the time-periodic state is subsequently sought by Floquet theory. Barkley and Henderson [24] and Henderson and Barkley [23] have made essential contributions by identifying two distinct mechanisms, visualised in Fig. 37. Mode A instability sets in at $Re = 189$ and corresponds to a spanwise wavelength $L_z = 2\pi/\beta \approx 4D$; mode B instability is encountered at $Re = 259$ and has a characteristic wavelength of the order of the cylinder diameter; the spatial structure of both can be seen in Fig. 38. While the BiGlobal linear problem of circular cylinder instability may be considered closed, the nonlinear development of the BiGlobal eigenmodes A and B, including the question of energy transfer between them as the Reynolds number increases has continued receiving attention [23,61]. The earlier modelling efforts of Noack and Eckelmann [170] and co-workers as well as recent renewed efforts of the same investigators are also noted in this respect.

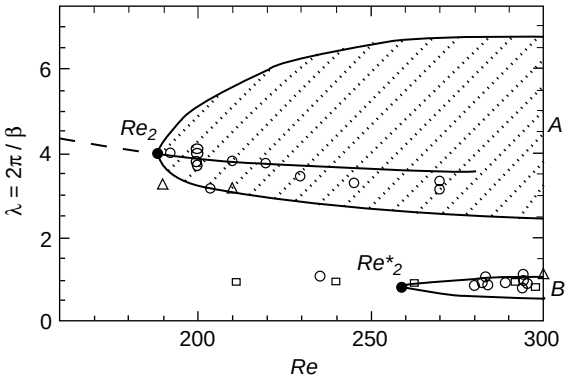

Fig. 37. Neutral loops of global Mode A and B instabilities in the wake of a circular cylinder [24].

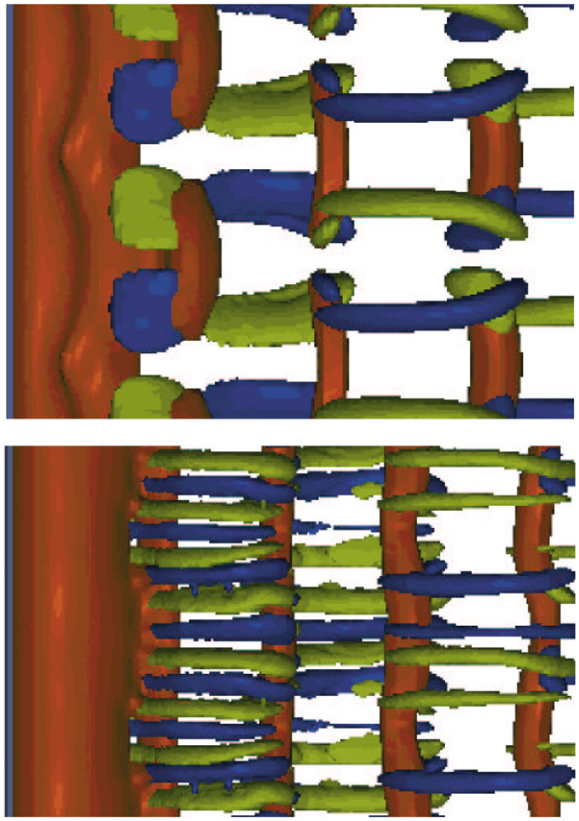

Fig. 38. Mode A (upper) and B (lower) instability in the wake of a circular cylinder [197].

4.10.2. Laminar flow past a rectangular corrugated cylinder

The envelope of bluff bodies the linear and nonlinear instability of which has recently been studied was enlarged by the DNS-based analyses of Darekar and Sherwin [171]. These authors considered a cylinder of rectangular cross-section of base-height D on the Oxy plane, the corrugation of which was determined by a wavelength L_z in the z-direction and a peak height of the waviness W_x. The essential generalisation that the specific geometry offers compared with that of the circular cylinder is the introduction of three-dimensionality, determined by the independent parameters W_x/L_z and L_z/D. The underlying experimental observation for this and analogous geometries has been that corrugated cylinders have distinct advantages over the circular cylinder geometry in terms of suppression of vortex shedding and drag reduction [172]. While experiments were performed at $Re = 4 \times 10^4$ a spectral/hp element methodology was used for computations at $Re \leqslant 150$,

based on cylinder-base height, after the corrugated geometry was mapped onto a rectangular cartesian grid. The Reynolds numbers chosen for the computations ensured full resolution of the numerical results obtained but at the same time revealed previously unknown BiGlobal instability mechanisms at different flow regimes.

At a constant L_z/D value these regimes are classified as I, II (A) and (B) and III (A) and (B). In regime I the principal effect of the corrugation is a weak three-dimensionalisation of the Kármán vortex street. An increase in the peak-waviness height leads to a regime II (A) where a drastic decrease in the lift and a milder one in the drag coefficient is observed. Simultaneous increase of the parameter L_z/D, leads to regime II (B) which is a combination between the previous two, the lift and drag coefficients saturating in a time-periodic state with a low-frequency modulation. Returning to the original value of the parameter L_z/D and increasing W_x/L_z further, regimes III (A) and (B) are reached, in the first of which the lift coefficient is reduced to zero and the drag coefficient attains its minimum value, while in regime III (B) a small nonzero lift is produced and the drag also increases by a few percent over that prevailing in regime III (A). The key qualitative characteristics of the wake in the three regimes are, respectively, two-dimensionality, transitional flow and complete suppression of vortex shedding. Perspective views of the different regimes in the wake behind the corrugated cylinder are shown in Fig. 39.

The DNS computations of [171] rather than covering the entire parameter space, a task practically impossible using DNS, serve as a challenge for a quasi-three-dimensional extension of BiGlobal linear instability theory. Progress could be made by exploiting analytical introduction of three-dimensionality, as done in the computations of [171]; on the other hand, the potential practical benefits from a detailed exploration of parameter space and the associated increase of the predictive capacity of methodologies aiming at drag-reduction of bluff-body configurations render such an extension of the BiGlobal linear instability theory highly desirable. Such an extension will also provide impetus to analyses of flows at substantially higher Reynolds numbers compared with those in [171], a task practically impossible by use of DNS.

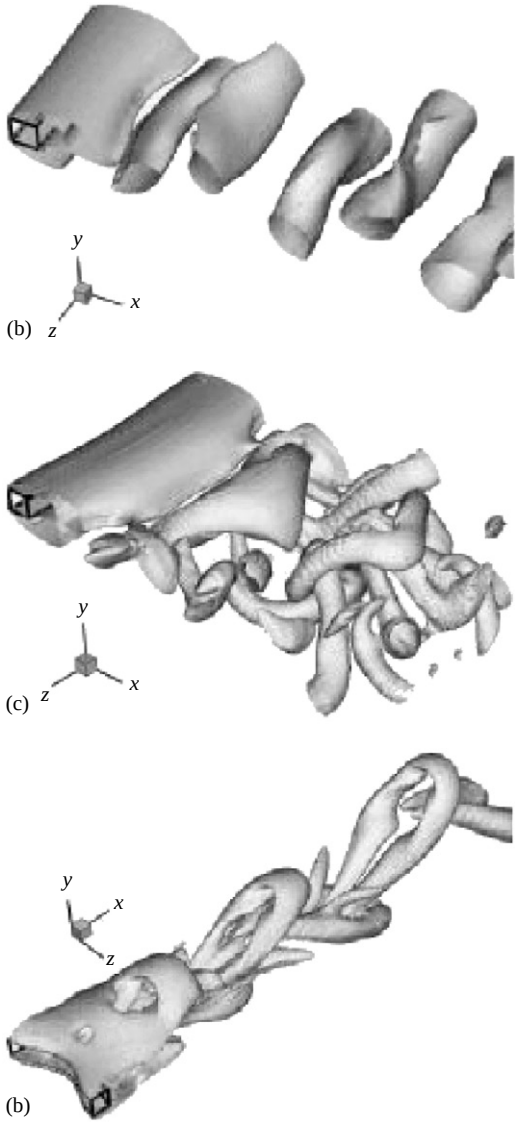

Fig. 39. Visualisation of régimes I (upper), II-B (middle) and III-B (lower) in the wake of a corrugated cylinder [171].

4.11. Turbulent flow in the wake of a circular cylinder and an aerofoil

The progression from laminar flow on the unswept circular or rectangular cylinder towards flight Reynolds numbers highlights one of the most commonly encountered problems of flow on aerofoils at these conditions, that of transitional or turbulent flow separation. Large-scale cellular structures are long known to be associated with this phenomenon [173] which has received a fair amount of attention and interpretations; a qualitative depiction is shown in the upper part of Fig. 40 [174]. Arguments have been put forward in the literature, that these cellular structures may be related with end-effects of the measurement section; such arguments can be dismissed on account of the repeatability of the phenomenon shown in Fig. 40 with varying spanwise extent of the measurement domain, both in the case of the cylinder and that of the aerofoil. One conjecture was put forward by Goelling [174] on the basis of his experimental results on the cylinder, namely that these structures point to a BiGlobal instability mechanism.

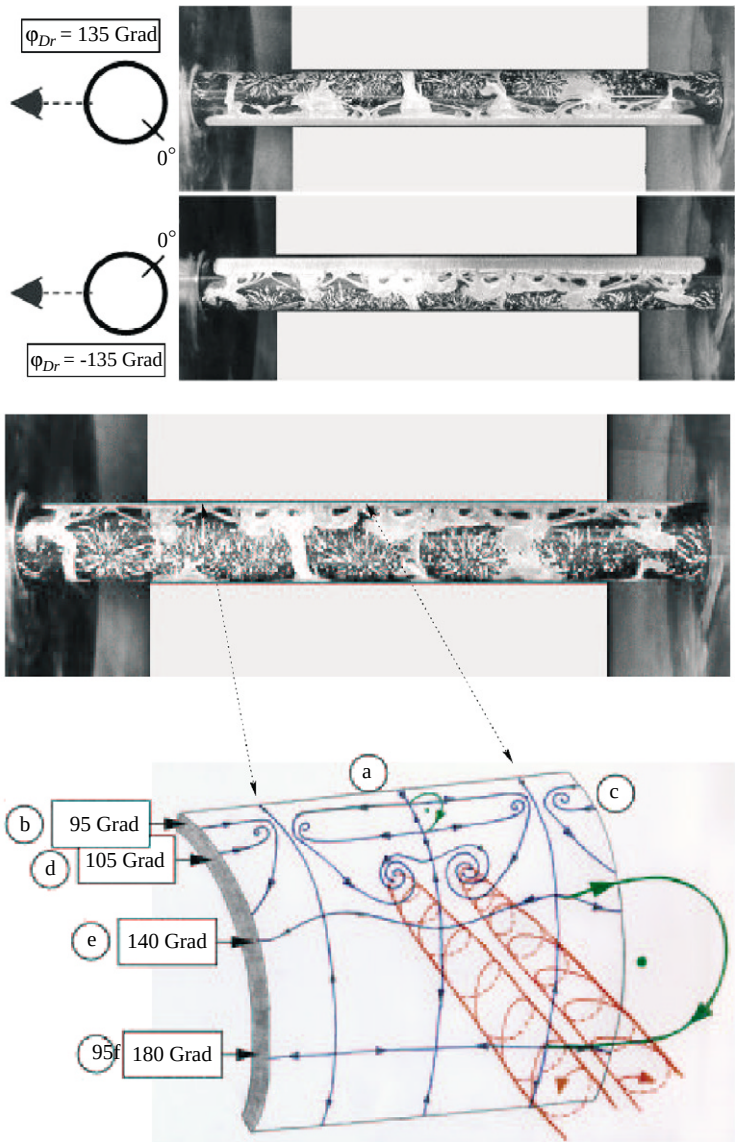

Fig. 40. Upper: symmetric cellular structures arising in transitional flow on a circular cylinder [174]. Lower: detailed view of one of the structures and sketch of its topological characteristics.

Experimental findings in support of this conjecture are the following. On a qualitative level, the two-dimensional closed separation bubble on the unswept cylinder first becomes spanwise unsteady with increasing *Re*; the related spanwise periodic vortical cellular structure appearing as a result is shown in the lower part of Fig. 40. Associated is the formation of Kármán-like vortices, having their axes parallel to the generator of the cylinder, while up to this point the same qualitative scenario is followed on the aerofoil. The topological description of one of the spanwise periodic cells at the upper side of the cylinder is shown in the lower part of Fig. 40; a pair of streamwise vortices separates from one of these cells, either from the cylinder or from the aerofoil at comparable flow parameters. On a quantitative level Humphreys [173] has argued that the spanwise periodicity length L_z of the structures on the circular cylinder scales with its diameter D. In flow visualisations he found $L_z/D \in [1.7, 2.4]$. In recent experiments Goelling [174] confirmed this bracket at corresponding *Re* values and showed that an increase of Reynolds number decreases the spanwise periodicity

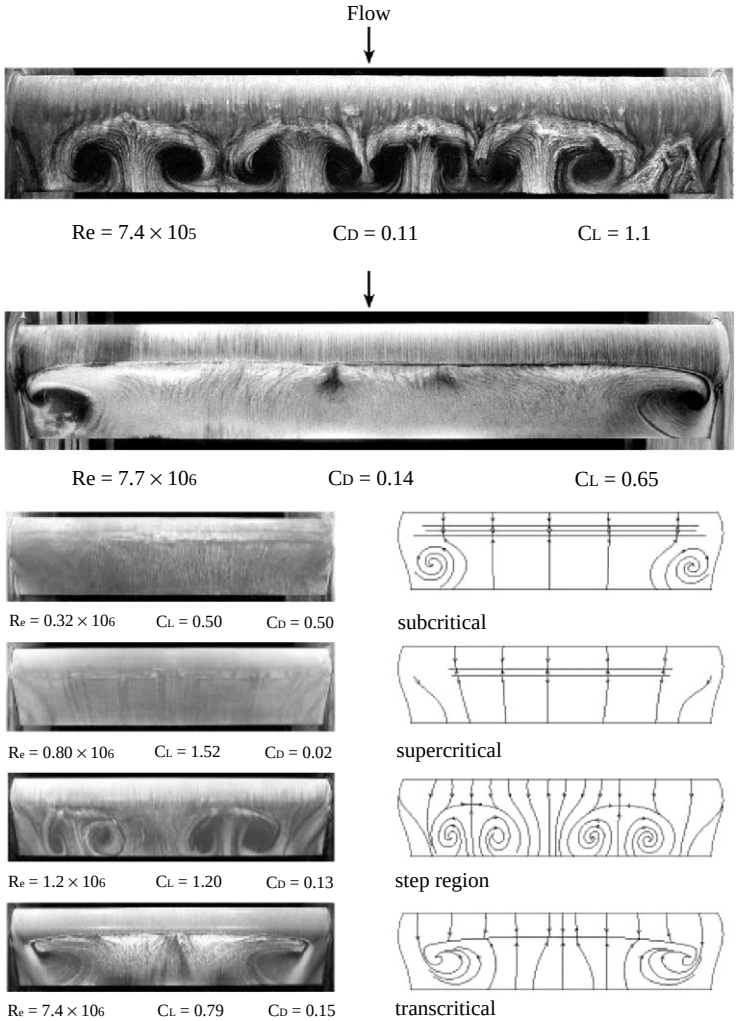

Fig. 41. Upper: asymmetric cellular structures in transitional flow over an aerofoil [180]. Lower: topological characteristics of the cell structures.

length to $L_z \approx D$. Interestingly, this progression is not continuous; this is interpreted as a hint of amplification of different BiGlobal eigenmodes as Re increases.

The link to the BiGlobal instability scenario discussed in Section 4.10.1 is provided by the shear-layer which engulfs the wake-region within which the unstable BiGlobal "B" mode develops and flow outside the cylinder wake [175]. With increasing Reynolds number the laminar shear-layer emanating from the cylinder surface becomes unstable and turbulent, whereby transition is associated with the appearance of small-scale streamwise-oriented turbulent vortices [176,177]. The transition point moves upstream as the Reynolds number increases above $Re\ 5 \times \sim 10^3$. It has been conjectured [174] that the interaction of the laminar boundary-layer at the cylinder surface with the unsteady flowfield in the near-wake is the reason for the appearance (through a BiGlobal instability mechanism) of the large-scale spanwise periodic structures on the cylinder surface itself. Such structures have also been observed by Schewe [178–180] on his generic aerofoil experiment, with periodicity lengths in the same range as on the cylinder at comparable conditions, as seen in Fig. 41. Whether this mechanism can be described in the framework of a BiGlobal linear instability of separated flow or bluff-body instability deserves further investigation. In case of the absence of a steady or time-periodic laminar two-dimensional basic state underlying a BiGlobal instability analysis in the problem at hand, one may employ the recently developed and successfully applied to one-dimensional instability problems triple-decomposition methodology of Reau and Tumin [181].

The connection of the topological features in the present flow with those in the BiGlobally unstable laminar separation bubble on an aerofoil, discussed earlier, including mechanisms for vortex shedding from cylinders and aerofoils also deserves investigation in the framework of the present theory.

4.12. On turbulent flow control

The scope of the discussion of the previous section can be naturally broadened to incorporate the broader field of turbulent separated flow control. The reader is referred to the recent milestone review of this problem by Greenblatt and Wygnanski [25] who highlighted the potential of *periodic excitation*, i.e. oscillatory momentum injection as effective and efficient means of flow control, irrespective of the latter being found in a laminar, transitional or turbulent state. Based on overwhelming amounts of experimental information Wygnanski and co-workers ([182–185,25] and references therein) arrived at the conclusion that periodic excitation can be more efficient for certain airfoil applications than classic boundary-layer control methodologies based on steady suction/injection and provided two key parameters to quantify excitation.

The amount of injected flow was referred to free-stream conditions to arrive at the momentum coefficient

$$C_\mu = \frac{\rho U_j^2 G}{\frac{1}{2}\rho_\infty U_\infty^2 L}, \tag{75}$$

where G denotes a characteristic length associated with the excitation, e.g. a slot width, U_j is the magnitude of the injected velocity and $L = O(1)$ is the length of the body in consideration, e.g. the length of the separation region, for simplicity taken to be the chord length of an aerofoil [182]. The actuation itself is characterised by a reduced frequency

$$F^+ = \frac{f_e X}{U_\infty}, \tag{76}$$

where X is a distance from the location on the body surface at which excitation is provided to the end of the body (or the natural reattachment point) in question and f_e is the excitation frequency. The underlying theme of the experimental work in this group is that efforts must be directed towards utilising the natural flow instability, enhanced by the periodic addition of momentum at the appropriate location, magnitude and frequency to interact with the large-scale coherent structures of the flow.

In the case of turbulent flow it is found that the most effective oscillation frequencies of the periodic forcing are widely disparate from those of turbulence; furthermore, it is proposed to monitor the dependence of the reduced frequency in conjunction with the momentum coefficient. Nishri and Wygnanski [186] proposed a generic deflected flap configuration as an example on which the controlling parameters could be isolated and discovered that practically independently of Reynolds number

$$F^+ \sim 1 \tag{77}$$

is the optimum reduced frequency for control of turbulent separated flow, independently of the level of free-stream turbulence [183,184]. This suggests that structures scaling with the separation bubble length itself, and not the order-of-magnitude smaller TS-wavelengths associated with shear-layer instability, are being modified by a reduced frequency (77) a result that may be pointing to the BiGlobal eigenmodes structure shown in Fig. 15. The result that $F^+ = O(1)$ has been corroborated in a multitude of turbulent separated flow control experiments [25] and its potential association with a generic BiGlobal instability mechanism is worthy of further investigation.

4.13. Analyses based on the linearised Navier–Stokes equations (LNSE)

Finally, as an exception to the main focus of the present paper on incompressible flows, a short discussion of the recent efforts of Collis and Lele [53] and Malik [54] in subsonic and hypersonic boundary layer flow stability, respectively, is provided. Both approaches use the (compressible) LNSE concept to study the problems of receptivity [62] and subsequent linear and nonlinear instability of boundary-layer (its instability per se being amenable to analysis based on the PSE) in a unified manner. One motivation provided by current practitioners of the LNSE approach is that while the nonlinear PSE provides a complete framework to study nonparallel and nonlinear phenomena in boundary-layer transition, question of receptivity, i.e. the accurate description of the process by which disturbances enter the boundary layer, cannot be tackled by PSE and even less so by OSE-based analyses; this problem is circumvented by use of the linearised Navier–Stokes equations.

A point in this case was the work of Collis and Lele [53] who considered the leading-edge region of a swept wing including an analytically described roughness element. Their work was placed within the framework of laminar-flow wings and receptivity of the flow to the introduced roughness was the main issue addressed. Technical details are omitted here and may be found in the original reference. Key results were provided by comparison of parallel-flow predictions and the LNSE; it was noted that nonparallel and curvature effects counteracted each other, but nonparallel effects dominated the configuration studied and strongly reduced the initial amplitude of the crossflow vortices developing on the wing surface compared with one-dimensional theory predictions. The implication is that, in the absence of the

LNSE predictions, a PSE-based analysis of crossflow vortices on the specific configuration would produce inaccurate results on account of wrong initialisation of the computations.

Malik [54], on the other hand, employed two-dimensional LNSE to study stability of a Mach 8 wedge flow. The domain considered was bounded by a solid wall with a suction slot, a shock on which appropriate conditions were imposed, an inflow boundary near but not at the wedge tip, at which appropriate inflow boundary conditions were imposed and a buffer-domain outflow boundary at which, in a manner analogous with spatial DNS, disturbances were artificially reduced to zero. Inside the domain thus defined the compressible analogon of the two-dimensional limit of (20)–(24) was solved, the key difference from solution of the two-dimensional ($\beta = 0$) BiGlobal EVP being the relaxation of the assumption of harmonic disturbances on time. Disturbances were introduced into the flow by localised wall suction/blowing. Key result of this work has been the generation of fast and slow acoustic modes and the subsequent dominance of second mode instability, in line with the predictions of one-dimensional linear theory and earlier spatial DNS of Mach 4.8 boundary layer flow of Eissler and Bestek [187]. The potential of LNSE instability analyses of essentially nonparallel basic flows and its potential synergy with the BiGlobal EVP have not been exploited yet.

5. Discussion and research frontiers

The present review has emerged as an attempt to summarise recent theoretical developments in the field of linear instability of essentially nonparallel flows of relevance to aeronautics. Both open and closed systems were considered, having the unifying characteristic of a basic state that is inhomogeneous in two and periodic in the third spatial direction. The scope has been narrowed by focussing mainly on solutions of the two-dimensional eigenvalue problem which describes linear instability of such nonparallel flows. Since the classic review of Huerre and Monkewitz [7] at the latest, the term 'global' flow instability has been used in a different context too. In this review, the term 'global' has been synonymous with instability of nonparallel basic flows; further, the more precise notion of 'BiGlobal' instability analysis has been introduced to denote the essential two-dimensionality of the corresponding basic state. This definition may encompass that of work in the vein of [7] in that 'absolute/global' instability in the latter methodology may be related, in principle, with instability of the two-dimensional ($\beta = 0$) global eigenmode in the present terminology in certain limiting cases. However, no work is known at present explicitly linking the two approaches although such a link may exist as evidenced by the qualitative consistency of the independently produced results of the two analysis approaches on the only problem on which they have been concurrently applied, that of global instability of a separation bubble, discussed herein.

The historical evolution of approaches for the formulation and numerical solution of the BiGlobal instability EVP has followed the rapid developments in computing hardware as well as those in efficient algorithms for the linear algebra of large matrices. Born in the late 1980s, the BiGlobal EVP initially focussed on the inviscid generalised Rayleigh equation applied to an analytic two-dimensional basic state, which from a numerical point of view requires the recovery of a single two-dimensional eigenfunction. The theory progressed into the viscous regime, where the generalised Orr–Sommerfeld and Squire coupled system was solved for the recovery of two-dimensional eigenfunctions. In the early work, the classic QZ algorithm has been used for the recovery of the eigenspectrum. Its limitations were quickly appreciated so that currently efficient Krylov subspace iteration methods are almost exclusively used. These permit addressing the incompressible/compressible two-dimensional EVP in primitive-variables formulation, requiring simultaneous solution of systems for the recovery of four/five two-dimensional eigenfunctions, respectively. A key observation in this evolutionary process of the methodologies for the numerical solution of the two-dimensional EVP has been the consistent failure of second-order accurate numerical methods to deliver reliable global instability results; for the problem at hand, in which resolution cannot be increased beyond hardware-limited bounds, a high-order method (spectral/finite element, spectral collocation, compact finite-difference) is in the author's view indispensable.

Alternative methodologies for the solution of the two-dimensional eigenvalue problem exist for the recovery of BiGlobal instability results. DNS may, in principle, be employed, though at a larger computing cost and, potentially, at the expense of information on members of the eigenspectrum other than the most unstable/least stable eigenmode going unnoticed. If applicable on physical grounds, a combination of Floquet analysis in a homogeneous spatial direction with one-dimensional EVPs in the second resolved inhomogeneous direction may be employed. If sufficient computing power is available but the overhead of DNS is deemed to be too high, developing and maintaining a Floquet/1D-EVP code may not be justified compared with a straightforward two-dimensional EVP in which the homogeneous spatial direction is treated by a discrete Fourier expansion. Yet another alternative for global instability analysis, that of LNSE, is slowly emerging in the literature.

The ability to address the numerical aspects of global instability analysis in an adequate manner does not necessarily imply that the results obtained are also adequate from a physical point of view. Consistent with the failure of the one-dimensional limit of linear theory on the corresponding problem, global linear analysis of wall-bounded Couette flow has not delivered unstable eigenmodes. This paradox is thus added to that of a duct of square cross-section and to the best-known failure of one-dimensional linear theory, Hagen–Poiseuille flow in a circular pipe. In other applications mixed success has been obtained: the discovery of new global eigenmodes in the swept attachment line boundary layer, or that in the rectangular duct, is not sufficient to explain the respective subcritical instability problems, although the BiGlobal eigenmodes of the first problem are essential building blocks of theoretical approaches which address the (nonlinear) physical problem successfully. On the other hand, BiGlobal linear instability analysis has also delivered spectacular successes in its own right. Instability in the wake of cylinders of circular or rectangular cross-section is one paradigm, as is flow in the long-standing numerical benchmark of the lid-driven cavity. Instability of separated flow is another example where application of global linear theory has delivered new physical insight into an old problem of external and internal aerodynamics.

For the most part, however, the field of potential applications of BiGlobal linear theory in aeronautics is wide open with an associated large potential for improvement of current understanding of flow physics. BiGlobal instability of vortical flows on lifting surfaces or the wake–vortex system has only started being examined by this general concept and already first successes have been reported (cf. crossflow vortices, Görtler vortices, streaks). The applicability of the concept on the entire aerofoil has commenced but much work needs to be done, not least from the point of view of algorithmic developments. In the latter respect, development of global flow methodologies on unstructured grids could come to bear both in the problem of an aerofoil and in that of blade configurations in turbomachinery. Open cavity instability research might profit from investigations into scenarios other than the empirical Rossiter mode, especially in view of the (far from idealised shear-layer) flowfield in three-dimensional cavities with/without stores. Corner flows, in which the issue of the basic flow itself is far from being settled, is another configuration in external aerodynamics, for which BiGlobal instability theory could prove beneficial and should be pursued further.

Progress in BiGlobal instability theory could be viewed as the advancing of knowledge stemming, firstly, from revisiting with the new methodology many of the idealised flows the linear instability of which has been addressed using one-dimensional analysis in the last century and, secondly, by solving problems of industrial significance, the instability of which cannot be addressed by classical means. BiGlobal instability analysis has been shown to encompass the results of classic linear theory either at appropriate limits (e.g. duct flows at $A \to \infty$) or as part of the two-dimensional eigenvalue problem solution (c.f. attachment-line boundary layer, corner flows and open cavity results discussed herein) such that linear theory in future work may in principle focus on the two-dimensional eigenvalue problem alone.

A different point of view on progress comes from the realisation of some essential problems in aeronautics. From a numerical point of view, most applications involve complex geometries for the resolution of which the tensor-product grids currently used by a BiGlobal analysis on canonical grids are either not optimal or entirely inappropriate. Efficient adaptive-grid algorithms are known in aeronautics for a long time; however, their accuracy properties may be inferior to those required by a global instability analysis (or, indeed, DNS); progress could result from designing flexible, efficient *and* accurate numerical algorithms for the two-dimensional EVP. Further progress from a physical point of view, on the other hand, could result from incorporation of inhomogeneity of the third spatial direction in the analysis. Specifically, an intrinsic difficulty of several applications in aeronautics is three-dimensionality of the underlying basic flowfields (e.g. vortical flows or the corner boundary layers discussed herein). These are approximated in current analyses (including some employing DNS) by an assumption equivalent to the parallel-flow approximation in boundary layers, although such an assumption is not permitted on physical grounds. One potentially interesting extension of global linear theory could enlarge the scope of current analysis based on the two-dimensional eigenvalue problem and address mild three-dimensionality in the third spatial direction by means more efficient than a DNS in which all three spatial directions are taken to be inhomogeneous, or the three-dimensional (TriGlobal) EVP.

Last but not least, the time may now be ripe to revisit the issue of 'coherent structures' of turbulent flow. This issue became popular in past decades before interest subsided in the absence of a convincing breakthrough delivered by approaches focussing on coherent structures compared with more traditional turbulent flow research methodologies. It should be stressed, however, that the structures discussed in the past were for the most part a result of post-dicting an existing flowfield. A key new element offered by global instability theory is the a priori knowledge of the global eigenmodes of a three-dimensional flowfield and its exploitation, for example in the framework of nonlinear global instability analyses, to advance understanding of their relation to turbulent flow structures. The potential benefit for

effective flow-control methodologies that such an understanding could deliver is, in the author's view, worthy of exploration.

Acknowledgements

This work was initiated by an Alexander von Humboldt Research Fellowship and partly supported by the European Office of Aerospace Research and Development under contracts monitored by C. Raffoul. His active interest as well as interactions with several colleagues over the last years, notably P.W. Duck (University of Manchester), U. Dallmann, W. Koch and S. Hein (DLR), S.J. Sherwin (Imperial College), E. Janke (BMW/Rolls-Royce), T. Colonius (Caltech), R.L. Kimmel and M. Stanek (Wright-Patterson AFB), are gratefully acknowledged.

Appendix A

With ever increasing computing hardware capabilities the list of flows of aeronautical interest whose global instability is addressed numerically increases steadily. In the cases studied so far, experience has shown that substantial discrepancies in the instability analysis results can occur on account of insufficient attention being paid to the issue of the basic flow. The set of algorithms which follow have been used for the recovery of basic flows relevant to external aerodynamics in closed and open systems, and shown to satisfy the key requirement of global instability analysis to deliver results of optimal quality on a modest number of discretisation points.

A.1. A spectral-collocation/finite-difference algorithm for the numerical solution of the nonsimilar boundary layer equations

In this case length, time and velocity scales may be built,

$$L=\beta_0/\beta_1,\quad T=1/\beta_1,\quad \text{and}\quad \beta_0, \tag{A.1}$$

respectively, defining a Reynolds number

$$Re=\frac{\beta_0 L}{\nu}. \tag{A.2}$$

The dimensional independent variables x and y may be transformed into dimensionless boundary-layer variables, ξ and η, according to

$$\xi=\frac{\beta_1}{\beta_0}x,\quad \text{and}\quad \eta=\frac{\beta_1}{\beta_0}\sqrt{\frac{Re}{2\xi}}y. \tag{A.3}$$

A streamfunction may be defined through

$$\psi_{\mathrm{H}}=\sqrt{2\beta_0\nu L\xi}f(\xi,\eta) \tag{A.4}$$

and the velocity components of the Howarth boundary layer flow, u_{H} and v_{H}, take the form

$$u_{\mathrm{H}}=\frac{\partial\psi_{\mathrm{H}}}{\partial y}=\beta_0\frac{\partial f}{\partial\eta}\quad\text{and}$$

$$v_{\mathrm{H}}=-\frac{\partial\psi_{\mathrm{H}}}{\partial x}=-\sqrt{\frac{\beta_1\nu}{2\xi}}\left[f+2\xi\frac{\partial f}{\partial\xi}-\eta\frac{\partial f}{\partial\eta}\right]. \tag{A.5}$$

The steady boundary layer equation

$$u_{\mathrm{H}}\frac{\partial u_{\mathrm{H}}}{\partial x}+v_{\mathrm{H}}\frac{\partial u_{\mathrm{H}}}{\partial y}=U_e\frac{\mathrm{d}U_e}{\mathrm{d}x}+\nu\frac{\partial^2 u_{\mathrm{H}}}{\partial y^2} \tag{A.6}$$

is then transformed into

$$\frac{\partial^3 f}{\partial\eta^3}+f\frac{\partial^2 f}{\partial\eta^2}+2\xi\left\{\frac{\partial f}{\partial\xi}\frac{\partial^2 f}{\partial\eta^2}-\frac{\partial f}{\partial\eta}\frac{\partial^2 f}{\partial\xi\partial\eta}\right\}=2\xi(1-\xi). \tag{A.7}$$

This nonsimilar boundary layer equation constitutes a parabolic problem which may be marched in ξ. The boundary conditions in η are no penetration and no-slip at the wall and (19) in the free-stream,

$$f(\eta=0)=0, \tag{A.8}$$

$$\frac{\partial f}{\partial\eta}(\eta=0)=0, \tag{A.9}$$

$$\frac{\partial f}{\partial\eta}(\eta\to\infty)=1-\xi. \tag{A.10}$$

The vorticity of the flow is given by

$$\zeta_{\mathrm{H}}=\nabla^2\psi_{\mathrm{H}}=\frac{\beta_1}{\sqrt{8\xi^3 Re}}\left\{-f+4\xi\frac{\partial f}{\partial\xi}+4\xi^2\frac{\partial^2 f}{\partial\xi^2}+2\eta\frac{\partial f}{\partial\eta}-4\xi\eta\frac{\partial^2 f}{\partial\xi\partial\eta}-\eta\frac{\partial f}{\partial\xi}+\eta^2\frac{\partial^2 f}{\partial\eta^2}+2\xi Re\frac{\partial^2 f}{\partial\eta^2}\right\}. \tag{A.11}$$

A numerical solution of (A.7) subject to boundary conditions (A.9) and (A.10) has been the subject of intense investigation in the past with respect to the appearance of the singularity in the solution and the determination of the abscissa for separation [136]. A simple modification of the boundary layer equations which takes the interactive nature of the boundary layer into account [138] succeeds in closely reproducing the results obtained by solution of the Navier–Stokes equations [137].

The nonsimilar boundary layer equations constitute a parabolic problem which may be solved by marching in the ξ direction. This is discretised by a grid of uniform spacing $\Delta\xi$. In the wall-normal η-direction the optimal resolution properties of a spectral expansion are exploited. Spectral methods have been applied to the solution of the boundary-layer equations by Streett et al. [188] who transformed the problem (A.7) using Görtler variables. Here, at each ξ-station we solve (A.7) by

Newton-Kantorowitz iteration, in boundary-layer variables, in a manner analogous to that used by Theofilis [52] for the generalised Hiemenz boundary layer. Specifically, we define

$$\tilde{u} = \frac{\partial f}{\partial \eta} \equiv \mathscr{D} f, \tag{A.12}$$

$$\tilde{v} = f, \tag{A.13}$$

which transforms (A.7) into the system

$$\mathscr{D}^2 \tilde{u} + \tilde{v}\mathscr{D}\tilde{u} + 2\xi\left[\mathscr{D}\tilde{u}\frac{\partial \tilde{v}}{\partial \xi} - \tilde{u}\frac{\partial \tilde{u}}{\partial \xi}\right] = 2\xi(1-\xi), \tag{A.14}$$

$$\tilde{u} - \mathscr{D}\tilde{v} = 0, \tag{A.15}$$

subject to the boundary conditions

$$\tilde{u}(0) = \tilde{v}(0) = 0, \quad \text{and} \quad \tilde{u}(\eta \to \infty) = 1 - \xi. \tag{A.16}$$

A standard Newton procedure follows, writing

$$\tilde{u}^{(n)} = \tilde{u}^{(o)} + \Delta\tilde{u}, \tag{A.17}$$

$$\tilde{v}^{(n)} = \tilde{v}^{(o)} + \Delta\tilde{v}, \tag{A.18}$$

while a second-order accurate backward-difference scheme discretisation in ξ results in the problem

$$\begin{aligned}
&\left\{\mathscr{D}^2 + \left[\tilde{v}^{(o)} + \frac{\xi}{\Delta\xi}(3\tilde{v}^{(o)} - 4\bar{v} + \bar{\bar{v}})\right]\mathscr{D}\right.\\
&\left. + \left[\frac{\xi}{\Delta\xi}(-6\tilde{u}^{(o)} + 4\bar{u} - \bar{\bar{u}})\right]\right\}\Delta\tilde{u}\\
&+ \left[\mathscr{D}\tilde{u}^{(o)} + 3\mathscr{D}\tilde{u}^{(o)}\frac{\xi}{\Delta\xi}\right]\Delta\tilde{v}\\
&= -\mathscr{D}^2\tilde{u}^{(o)} - \tilde{v}^{(o)}\mathscr{D}\tilde{u}^{(o)}\\
&\quad - \frac{\xi}{\Delta\xi}[\mathscr{D}\tilde{u}^{(o)}(3\tilde{v}^{(o)} - 4\bar{v} + \bar{\bar{v}})\\
&\quad + \tilde{u}^{(o)}(-3\tilde{u}^{(o)} + 4\bar{u} - \bar{\bar{u}})]\\
&\quad + 2\xi(1-\xi),
\end{aligned} \tag{A.19}$$

$$\Delta\tilde{u} - \mathscr{D}\Delta\tilde{v} = -\tilde{u}^{(o)} + \mathscr{D}\tilde{v}^{(o)} \tag{A.20}$$

to be solved at each station ξ for the Newton corrections, with $\bar{u}$ and $\bar{v}$ the converged solutions at $\xi - \Delta\xi$ and $\bar{\bar{u}}$ and $\bar{\bar{v}}$ those at $\xi - 2\Delta\xi$, respectively.

Once the boundary-layer solution at a downstream location on the plate has been obtained a variant of the EVD algorithm discussed may be used in a DNS context. System (16) and (17) is then closed by the following boundary conditions for separated boundary layer flow [137]

$$\text{At the inflow boundary}: \psi = \psi_H, \tag{A.21}$$

$$\zeta = \zeta_H, \tag{A.22}$$

$$\text{At the top boundary}: \partial\psi/\partial y = F(x), \tag{A.23}$$

$$\zeta = 0, \tag{A.24}$$

$$\text{At the outflow boundary}: \partial^2\psi/\partial x^2 = 0, \tag{A.25}$$

$$\partial^2\zeta/\partial x^2 = 0, \tag{A.26}$$

$$\text{At the wall}: \psi = 0, \tag{A.27}$$

$$\partial\psi/\partial y = 0, \tag{A.28}$$

where

$$F(x) = \begin{cases} \beta_0 - \beta_1 x, & x \leqslant x_0, \\ \beta_0 - \beta_1 x_0, & x > x_0. \end{cases} \tag{A.29}$$

A full discussion of these boundary conditions may be found in Briley [137]. In short, the boundary layer solution (A.4) and (A.11) is used at the inflow boundary $x = \beta_0\xi/\beta_1$; the flow is taken to be irrotational at the far-field boundary $y \to \infty$ where the free-stream velocity distribution (A.29) is imposed, x_0 being a free parameter which determines the size of the recirculation region. The outflow boundary conditions are satisfied to within $O(1/Re)$ by the quantities $\partial^2\psi/\partial x^2$ and $\nu\,\partial^2\zeta/\partial x^2$. Finally, (A.27) and (A.28) represent the physical boundary conditions of no penetration and no-slip at the solid wall. A subtle point worthy of mention here is that the boundary condition for ζ based on the Howarth boundary layer solution (A.11) is consistent with that derived from the full Navier–Stokes equations, $\zeta_w = \partial u/\partial y(y = 0)$; consequently no numerical instability is expected to be generated owing to a singularity in the boundary conditions at $(x = x_L, y = 0)$. This is significant, especially in the context of numerical solutions using spectral methods, since an incorrect specification of boundary conditions in conjunction with the absence of numerical dissipation may result in propagation of the error and global numerical instability.

Appendix B. An eigenvalue decomposition algorithm for direct numerical simulation

The principles of the algorithm discussed in what follows can be applied to recover three two-dimensional velocity components or indeed a three-dimensional flowfield [189]; however, for simplicity we confine the present discussion to solutions of system (16) and (17) which deliver a basic flowfield $\bar{\mathbf{q}} = (\bar{u}, \bar{v}, 0, \bar{p})^T$. It has been mentioned that the main advantage of the velocity–vorticity formulation is that the continuity equation is exactly satisfied. However, the problem of imposition of boundary conditions within the framework of an overall efficient numerical solution algorithm remains. This is compounded by the fact that the number of points discretising the two spatial directions in the subsequent analysis cannot be increased at will; while interpolation of a basic flow solution obtained on a very large number

of points onto a modest EVP grid is one possible option, it is more elegant to avoid the interpolation procedure altogether and seek an accurate basic flow solution on *the same* small number of discretisation points on which the subsequent global instability analysis is to be performed. This appears tailor-made for a spectral numerical solution approach [100]. Ehrenstein and Peyret [190] discussed one spectral algorithm for solving (16) and (17) using the influence-matrix approach [191]; in what follows we discuss a different solution based on an efficient real-space eigenvalue decomposition (EVD) algorithm. Regarding spatial discretisation, there is no restriction as to whether one or both spatial directions x and y may be treated as periodic in the basic flow problem; since aperiodic functions are wider in scope and in line with the spirit of the present two-dimensional linear instability analysis, we focus on such solutions only.

Chebyshev polynomials have almost exclusively been used in the past in the context of spectral simulations of the time-accurate Navier–Stokes and continuity equations, mainly due to the availability of fast transform algorithms necessary for efficient time-integration. However, for the present problems we have not restricted ourselves to this class of orthogonal polynomials. Considerable freedom exists in the choice of the expansion functions and the associated collocation grids by using Jacobi polynomials $P^{(q,r)}$ for the discretisation of both spatial directions; of course, $q=r=-0.5$ may be related to the Chebyshev—while $q=r=0$ are the Legendre polynomials. Collocation derivative matrices for both Jacobi–Gauss–Lobatto and equidistant grids can be constructed from first principles; if $(x_j,\ j=0,\ldots,n)$ is the collocation grid chosen, the entries d_{ij} of the $(0:n)\times(0:n)$ first-order derivative collocation matrix $\mathscr{D}$, derived analytically from the interpolating polynomial [192], are

$$d_{ij}=\frac{\prod_{k=0}^{n}(x_i-x_k)}{(x_i-x_j)\prod_{k=0}^{n}(x_j-x_k)},\quad i,j,k=0,\ldots,n,\ \ i\neq j\neq k, \tag{B.1}$$

$$d_{ii}=\frac{1}{\sum_{k=0}^{n}(x_i-x_k)},\quad i,k=0,\ldots,n,\ \ i\neq k. \tag{B.2}$$

These formulae result in the well-known ones if the analytically known Chebyshev–Gauss–Lobatto grid $(x_j=\cos j\pi/n,\ j=0,\ldots,n)$ is used [193]. Values of order m derivatives on the collocation grid x_j are obtained by $(\mathscr{D})^m$.

As far as temporal discretisation of (16) is concerned, the viscous nature of the problems in which we are interested introduces scales which dictate an implicit treatment of the linear term in this equation; the nonlinear term may be treated explicitly. Within the framework of solution methods which do not resort to splitting and introduction of intermediate fields but rather address the governing equations directly the combination of Crank–Nicholson (CN) with second-order Adams–Bashforth (AB2) or Runge–Kutta (RK) schemes has been extensively used for the time-integration of the viscous and the convective terms, respectively [100]. However, the family of compact schemes proposed by Spalart et al. [194] (SMR) presents more accurate and more stable alternatives to the CN-AB2 algorithm although it does not require additional computational effort to the latter scheme. The SMR algorithm may be written in compact form as

$$q'''=q''+\Delta t\{\mathscr{L}i(\kappa q''+\lambda q''')+\mu\mathscr{N}l(q'')+\nu\mathscr{N}l(q')\}, \tag{B.3}$$

where the superscript denotes fractional time-step, $\mathscr{L}i(q)$ and $\mathscr{N}l(q)$ are, respectively, the linear and nonlinear operators in the problem to be solved and Δt is the time-step. The rationale behind the derivation as well as sample values of the constants κ,λ,μ and ν of a self-starting SMR algorithm may be found in [194]. The time-discretisation of (16) using (B.3) delivers the following problem to be solved for (ζ,ψ) at each fractional time-step

$$\mathscr{M}_1\zeta'''=R, \tag{B.4}$$

$$\mathscr{M}_2\psi'''+\zeta'''=0, \tag{B.5}$$

where $\mathscr{M}_1=\partial^2/\partial x^2+\partial^2/\partial y^2-Re/(\lambda\Delta t)$ and $\mathscr{M}_2=\partial^2/\partial x^2+\partial^2/\partial y^2$, subject to the boundary conditions appropriate to the problem in consideration. R comprises the nonlinear and the terms arising from the discretisation at previous fractional time-steps,

$$\begin{aligned}R=&-(\kappa/\lambda)\left[\frac{\partial^2}{\partial x^2}+\frac{\partial^2}{\partial y^2}-Re/(\kappa\Delta t)\right]\zeta''\\&+(\mu Re/\lambda)(\psi''_y\zeta''_x-\psi''_x\zeta''_y)\\&+(\nu Re/\lambda)(\psi'_y\zeta'_x-\psi'_x\zeta'_y).\end{aligned} \tag{B.6}$$

The accuracy of the overall procedure clearly depends on the scheme utilised for calculation of the spatial derivatives. The spectral discretisation chosen introduces dense matrices and can only become competitive against other numerical approaches from the point of view of efficiency on account of the existence of a fast algorithm for the inversion of the implicit operators $\mathscr{M}_1$ in (B.4) and $\mathscr{M}_2$ in (B.5). While $\mathscr{M}_2$ is time-independent, the first implicit operator is a function of a CFL-controlled maximum permitted time-step Δt and needs to be inverted at every time-step. If one sacrifices the advantage of an adjustable time-step and keeps Δt fixed at a slightly lower than its optimal value, a powerful EVD algorithm may be constructed for the efficient solution of the incompressible two-dimensional Navier–Stokes and continuity equations in streamfunction-vorticity formulation.

Key papers on EVD algorithms are the work of Haidvogel and Zang [195] and that of Ku et al. [189]. The first authors discuss the solution of Poisson's equation subject to homogeneous Dirichlet boundary conditions in transform space while the second authors present an eigenvalue decomposition algorithm for the Poisson equation resulting from a time-splitting of the incompressible Navier–Stokes and continuity equations in primitive-variables formulation in the context of real-space spectral collocation using Neumann boundary data. Here we present a variant of the EVD algorithm for the solution of the equations of motion in real-space using the streamfunction-vorticity formulation. Using this formulation within a direct, as opposed to time-splitting or iterative, time-integration methodology one Poisson and one Helmholz problem are to be solved within each fractional time-step. This minimises the necessary computing effort and makes the present algorithm one viable candidate to obtain the desired basic states.

Physical boundary conditions can only be provided for the stream-function ψ itself and its derivatives on the domain boundary. For the sake of exposure of the idea in what follows the boundary conditions associated with the standard testbed lid-driven cavity problem are discussed. Further, we refrain from discussion of the Ku et al. algorithm, which we term EVD_2 for reasons which will become apparent in what follows, and concentrate on the EVD_4 extension of the algorithm in order to address problems in which both Dirichlet and Neumann boundary conditions are imposed on the stream-function while no boundary data are necessary for the vorticity. We take the square lid-driven cavity to be defined in the two-dimensional domain $(x_i \in [0,1],\ i=0,\ldots,m)\times(y_j\in[0,1],\ j=0,\ldots,n)$. The boundary conditions on ψ are

$$\psi_{in}=\psi_{0j}=\psi_{i0}=\psi_{mj}=0, \tag{B.7}$$

$$(\partial\psi/\partial y)_{in}=F(x_i), \tag{B.8}$$

$$(\partial\psi/\partial x)_{0j}=0, \tag{B.9}$$

$$(\partial\psi/\partial y)_{i0}=0, \tag{B.10}$$

$$(\partial\psi/\partial x)_{mj}=0, \tag{B.11}$$

where $f_{ij}\equiv f(x_i,y_j)$ represents either of ψ or ζ grid-values at a fractional time-step and $F(x)$ is a function used to distinguish between the classic singular lid-driven cavity in which $F(x)=1$ and a regularised [196] cavity in which $F(x)=16x^2(1-x^2)$. The numerical discretisation of (B.4) and (B.5) leads to a system of simultaneous equations of the type

$$\mathrm{M}f+f\mathrm{N}+c\mathrm{I}f=g, \tag{B.12}$$

where M represents the $(0:m)\times(0:m)$ discrete analogon of $\mathscr{D}_x^2$, N represents the transpose of the $(0:n)\times(0:n)$ discrete analogon of $\mathscr{D}_y^2$, I is the identity matrix, $c=-Re/(\lambda\Delta t)$ and $g=R$ if (B.4) is being solved, while $c=0, g=-\zeta$ in the case of (B.5). On account of the homogeneous boundary conditions (B.7) on ψ (B.5) becomes

$$\sum_{i=2}^{m-2}M_{ki}\psi_{il}+\sum_{j=2}^{n-2}N_{lj}\psi_{kj}=-\zeta_{kl}-M_{k1}\psi_{1l}-M_{km-1}\psi_{m-1l}-N_{l1}\psi_{k1}-N_{ln-1}\psi_{kn-1}. \tag{B.13}$$

The boundary conditions (B.8)–(B.11) may be expressed using the discrete analoga X and Y of the collocation derivative matrices $\mathscr{D}_x$ and $\mathscr{D}_y$, respectively, as given by (B.1) and (B.2). It follows that

$$\psi_{1l}=\sum_{i=2}^{m-2}\delta_{1i}\psi_{il},\quad \psi_{m-1l}=\sum_{i=2}^{m-2}\delta_{m-1i}\psi_{il}, \tag{B.14}$$

$$\psi_{k1}=\bar{\kappa}_k+\sum_{j=2}^{n-2}\varepsilon_{1j}\psi_{kj},\quad \psi_{kn-1}=\bar{\lambda}_k+\sum_{j=2}^{n-2}\varepsilon_{n-1j}\psi_{kj}, \tag{B.15}$$

where $\bar{\kappa}_k$ and $\bar{\lambda}_k$ are used to impose the boundary condition on the lid,

$$\bar{\kappa}_k=\frac{-F_kY_{0n-1}}{Y_{01}Y_{nn-1}-Y_{n1}Y_{0n-1}},\qquad \bar{\lambda}_k=\frac{F_kY_{01}}{Y_{01}Y_{nn-1}-Y_{n1}Y_{0n-1}} \tag{B.16}$$

and the vectors $\delta_{1i},\delta_{m-1i}$ and $\varepsilon_{1j},\varepsilon_{n-1j}$ are known functions of the entries of X and Y,

$$\delta_{1i}=\frac{X_{0m-1}X_{mi}-X_{mm-1}X_{0i}}{X_{01}X_{mm-1}-X_{m1}X_{0m-1}},\qquad \delta_{m-1i}=\frac{X_{m1}X_{0i}-X_{01}X_{mi}}{X_{01}X_{mm-1}-X_{m1}X_{0m-1}}, \tag{B.17}$$

$$\varepsilon_{1j}=\frac{Y_{0n-1}Y_{nj}-Y_{nn-1}Y_{0j}}{Y_{01}Y_{nn-1}-Y_{n1}Y_{0n-1}},\qquad \varepsilon_{n-1j}=\frac{Y_{n1}Y_{0j}-Y_{01}Y_{nj}}{Y_{01}Y_{nn-1}-Y_{n1}Y_{0n-1}}. \tag{B.18}$$

The essence of the EVD_4 algorithm is to diagonalise the $(0:m-4)^2$ matrix $\hat{M}$ and the $(0:n-4)^2$ matrix $\hat{N}$ whose entries are

$$\hat{M}_{ki}=M_{ki}+M_{k1}\delta_{1i}+M_{km-1}\delta_{m-1i},\quad k,i=0,\ldots,m-4, \tag{B.19}$$

$$\hat{N}_{lj}=N_{lj}+N_{l1}\varepsilon_{1j}+N_{ln-1}\varepsilon_{n-1j},\quad l,j=0,\ldots,n-4. \tag{B.20}$$

The Poisson problem (B.13) becomes

$$\hat{M}f_{kl}+f_{kl}\hat{N}=-\zeta_{kl}-\hat{N}_{l1}\bar{\kappa}_k-\hat{N}_{ln-1}\bar{\lambda}_k=r_{kl} \tag{B.21}$$

in which the nonsingular matrices $\hat{M}$ and $\hat{N}$ may be diagonalised using their eigenvalue decomposition

$$\hat{M}=(M^*)\mu^*(M^*)^{-1}\quad\text{and}\quad \hat{N}=(N^*)\nu^*(N^*)^{-1} \tag{B.22}$$

Table 6
An algorithm for the solution of the two-dimensional incompressible Navier–Stokes and continuity equations using the streamfunction-vorticity formulation and eigenvalue decomposition

1 Pre-processing Stage
- a. Set up the matrices $\hat{M}$ and $\hat{N}$, calculate their EVD and store the results
- b. Set up the matrices $\tilde{M}$ and ñ, calculate and store their EVD

2 Time-advancement
- I. First fractional time-step
  - a. Given an initial ψ'' calculate $\zeta'' = -\nabla^2\psi''$ or read-in (ψ'', ζ'') data generated at an earlier simulation
  - b. Calculate derivatives of ψ'' and ζ'' and form R
  - c. Use EVD_2 to solve $\nabla^2\zeta''' = R$
  - d. Use EVD_4 to solve $\nabla^2\psi''' = -\zeta'''$
  - e. Overwrite (ψ', ζ') by (ψ'', ζ'') and (ψ'', ζ'') by (ψ''', ζ''') respectively
- II. Second fractional time-step
  - a. Given ψ'', ζ'', ψ' and ζ' calculate their derivatives and form R
  - c. Use EVD_2 to solve $\nabla^2\zeta''' = R$
  - d. Use EVD_4 to solve $\nabla^2\psi''' = -\zeta'''$
  - e. Overwrite (ψ', ζ') by (ψ'', ζ'') and (ψ'', ζ'') by (ψ''', ζ'''), respectively
- III. Third fractional time-step
  - a.-e. Same as 2 II.
- IV. Check convergence in time and either Go To 2 I. or Exit

Table 7
Comparison of memory and runtime requirements for a single solution of a two-dimensional Poisson equation using direct inversion and the EVD_4 algorithm on one processor of a workstation and a supercomputer

Problem Size	SUN Sparc 10				NEC SX4			
	EVD		Direct inversion		EVD		Direct inversion	
	Size (Mb)	Time (sec)	Size (Mb)	Time (sec)	Size (Mb)	Time (sec)	Size (Mb)	Time (sec)
16×16	0.4	4.4	1.1	3.7	4.03	0.03	4.03	0.1
24×24	0.5	5.4	3.6	10.5	5.03	0.14	6.03	0.3
32×32	0.6	6.6	10.0	39.7	5.03	0.25	13.03	1.1
48×48	0.8	15.3	46.9	460.6	6.03	0.56	48.03	8.4
64×64	1.1	31.8	143.9	5203.5	6.03	1.08	140.03	40.7
96×96	1.8	143.3	(*)	(*)	8.03	2.48	680.03	417.4
128×128	2.8	523.1	(*)	(*)	8.03	4.41	(*)	(*)

Asterisks denote that the respective problem does not fit in the available memory on the workstation or that it cannot be solved within the existing batch queue time-limit on the supercomputer.

to yield

$$\mu^*(M^*)^{-1}f_{kl}(N^*) + v^*(M^*)^{-1}f_{kl}(N^*) = (M^*)^{-1}r_{kl}(N^*). \tag{B.23}$$

As a consequence, instead of having to solve the $(m-3)\times(n-3)$ system of simultaneous equations (B.21) one solves the $(m-3)\times(n-3)$ algebraic equations

$$f^* = r^*/(\mu^* + v^*) \tag{B.24}$$

for $f^* = (M^*)^{-1}f_{kl}(N^*)$, given $r^* = (M^*)^{-1}r_{kl}(N^*)$. The structure of the EVD_4 algorithm is summarised in Table 6. Clearly, the cost of this algorithm is a negligibly small fraction of the cost of a direct algorithm for the solution of the Poisson problem. This is documented in Table 7 where memory and runtime requirements are shown for solution of (16) and (17) in the lid-driven cavity problem.

References

[1] Tollmien W. Über die Entstehung der Turbulenz, Nach Ges Wiss Göttingen, 1929; 21–44.
[2] Drazin PG, Reid WH. Hydrodynamic stability. Cambridge: Cambridge University Press, 1981.

[3] Fasel H. Investigation of the stability of boundary layers by a finite-difference model of the Navier–Stokes equations. J Fluid Mech 1976;78:355–83.
[4] Kleiser L, Zang TA. Numerical simulation of transition in wall-bounded shear flows. Ann Rev Fluid Mech 1991;23:495.
[5] Herbert Th. Parabolized stability equations. Ann Rev Fluid Mech 1997;29:245–83.
[6] Briggs RJ. Electron-stream interaction with plasmas. Cambridge MA: MIT Press, 1964.
[7] Huerre P, Monkewitz PA. Local and global instabilities in spatially developing flows. Ann Rev Fluid Mech 1990;22:473–537.
[8] Bestek H, Gruber K, Fasel H. Self-excited unsteadiness of laminar separation bubbles caused by natural transition. In: Prediction and exploitation of separated flows. The Royal Aeronautical Society, 1989.
[9] Colonius T. An overview of simulation, modeling and active control of flow/acoustic resonance in open cavities. AIAA 2001;2001-0076:12.
[10] Pierrehumbert RT. A universal shortwave instability of two-dimensional eddies in an inviscid fluid. Phys Rev Lett 1986;57:2157–9.
[11] Jackson CP. A finite-element study of the onset of vortex shedding in flow past variously shaped bodies. J Fluid Mech 1987;182:23–45.
[12] Zebib A. Stability of viscous flow past a circular cylinder. J Eng Math 1987;21:155–65.
[13] Lee NY, Schultz WW, Boyd JP. Stability of fluid in a rectangular enclosure by spectral method. Int J Heat Mass Transfer 1989;32:513–20.
[14] Tatsumi T, Yoshimura T. Stability of the laminar flow in a rectangular duct. J Fluid Mech 1990;212:437–49.
[15] Wilkinson JH. The algebraic eigenvalue problem. Oxford: Clarendon, 1965.
[16] Ehrenstein U. On the linear stability of channel flows over riblets. Phys Fluids 1996;8:3194–6.
[17] Lin R-S, Malik MR. On the stability of attachment-line boundary layers. Part 2. the effect of leading-edge curvature. J Fluid Mech 1996;333:125–37.
[18] Theofilis V. On the verification and extension of the Görtler-Hämmerlin assumption in three-dimensional incompressible swept attachment-line boundary layer flow. Tech. Rep. IB 223-97 A 44, DLR, 1997.
[19] Saad Y. Variations of Arnoldi's method for computing eigenelements of large unsymmetric matrices. Lin Algebra Appl 1980;34:269–95.
[20] Braconnier T. The Arnoldi-Tchebycheff method for solving large complex non-Hermitian generalised eigenproblems. Tech. Rep. TR/PA/94/08, CERFACS, 1994.
[21] Kooper MN, van der Vorst HA, Poedts S, Goedbloed JP. Application of implicitly updated Arnoldi method with a complex shift-and-invert strategy in MHD. J Comput Phys 1995;118:320–8.
[22] Edwards WS, Tuckerman LS, Friesner RA, Sorensen DC. Krylov methods for the incompressible Navier–Stokes equations. J Comput Phys 1994;110:82–102.
[23] Henderson RD, Barkley D. Secondary instability in the wake of a circular cylinder. Phys Fluids 1996;8:1683–6.
[24] Barkley D, Henderson RD. Three-dimensional Floquet stability analysis of the wake of a circular cylinder. J Fluid Mech 1996;322:215–41.
[25] Greenblatt D, Wygnanski IJ. The control of flow separation by periodic excitation. Prog Aerosp Sci 2000;36:487–545.
[26] Stanewsky E. Adaptive wing and flow control technology. Prog Aerosp Sci 2001;37:583–667.
[27] Chomaz JM, Huerre P, Redekopp LG. Bifurcations to local and global modes in spatially developing flows. Phys Rev Lett 1988;60:25–8.
[28] Le Dizès S, Huerre P, Chomaz JM, Monkewitz PA. Linear global modes in spatially developing media. Philos Trans R Soc London A 1996;354:169–212.
[29] Cossu C, Chomaz JM. Global measures of global convective instabilities. Phys Rev Lett 1997;78:4387–90.
[30] Manneville P. Dissipative structures and weak turbulence. In: Garbaczewski P, Wolf M, Weron A, editors. Chaos: the interplay between stochastics, classics, and quanta, 1995. p. 257–72.
[31] Mack LM. Boundary layer linear stability theory. In: AGARD-R-709 Special course on stability and transition of laminar flow, 1984. p. 3.1–3.81.
[32] Lin CC. The theory of hydrodynamic stability. Cambridge: Cambridge University Press, 1955.
[33] Theofilis V. On the spatial structure of global linear instabilities and their experimental identification. Aerosp Sci Technol 2000;4:249–62.
[34] Bertolotti FP, Herbert Th, Spalart PR. Linear and nonlinear stability of the Blasius boundary layer. J Fluid Mech 1992;242:441–74.
[35] Theofilis V, Hein S, Dallmann UCh. On the origins of unsteadiness and three-dimensionality in a laminar separation bubble. Philos Trans R Soc London A 2000;358:3229–46.
[36] Dongarra JJ, Straughan B, Walker DW. Chebyshev tau-QZ algorithm methods for calculating spectra of hydrodynamic stability problems. J Appl Numer Math 1996;22:399–435.
[37] Theofilis V, Duck PW, Owen J. Global instability of flows in rectangular ducts. J Fluid Mech 2001, submitted.
[38] Hein S, Theofilis V, Dallmann UCh. Unsteadiness and three-dimensionality of steady two-dimensional laminar separation bubbles as result of linear nonlocal instability mechanisms. Tech. Rep. IB 223-98 A 39, DLR, 1998.
[39] Hawa T, Rusak Z. The dynamics of a viscous flow in a slightly asymmetric channel with a sudden expansion. AIAA 1999;99-3789:16.
[40] Theofilis V. Globally unstable basic flows in open cavities. AIAA 2000;2000-1965:12.
[41] Howarth L. On calculation of the steady flow in the boundary layer near the surface of a cylinder in a stream. A.R.C. Reports and Memoranda, vol. 1632, 1934.
[42] Vollmers H. Detection of vortices and quantitative evaluation of their main parameters from experimental velocity data. Meas Sci Technol 2001;12:1199–207.
[43] Stuff R. The relationship between the near- and far-field of vortex wakes from aircraft with high aspect ratio wings. In: Proceedings of AG-STAB Symposium, Braunschweig: Vieweg Verlag, 2000. p. 7.

[44] Crow SC. Stability theory for a pair of trailing vortices. AIAA J 1970;8:2172–9.
[45] de Bruin AC, Hegen GH, Rohne PB, Spalart PR. Flowfield survey in trailing vortex system behind a civil aircraft model at high lift. Tech. Rep. TP 96284, NLR, 1996.
[46] Crouch JD. Instability and transient growth of two trailing-vortex pairs. J Fluid Mech 1997;350:311–30.
[47] Fabre D, Jacquin L. Stability of a four-vortex aircraft wake model. Phys Fluids 2000;12:1–6.
[48] Kleiser L. Numerische Simulationen zum Laminar-Turbulenten Umschlagprozess der ebenen Poiseuille-Strömung. PhD thesis, Inst. Reaktorenentwicklung KFZ Karlsruhe, 1982.
[49] Orszag SA, Patera AT. Secondary instability of wall-bounded shear flows. J Fluid Mech 1983;128:347–85.
[50] Brachet ME, Orszag SA. Secondary instability of free shear flows. In: Tatsumi T, editor. IUTAM Turbulence and chaotic phenomena in fluids. Amsterdam: Elsevier, 1984. p. 27–9.
[51] Goldhirsh I, Orszag SA, Maulik BK. An efficient method for computing leading eigenvalues and eigenvectors of large asymmetric matrices. J Sci Comput 1987;2: 33–58.
[52] Theofilis V. On linear and nonlinear instability of the incompressible swept attachment-line boundary layer. J Fluid Mech 1998;355:193–227.
[53] Collis SS, Lele SK. Receptivity to surface roughness near a swept leading edge. J Fluid Mech 1999;380:141–68.
[54] Malik MR. Hypersonic boundary-layer receptivity and stability. In: Saric W, Fasel H, editors. Proceedings of the IUTAM Laminar–Turbulent Symposium V. Sedona, AZ, USA, 2000. p. 409–14.
[55] Herbert Th. Über endliche Amplituden periodischer Störungen der Grenzschicht an der ebenen Platte. Tech. Rep. FB 74-53, DLR, 1974 (Engl. Transl. ESA TT-169 (1975)).
[56] Herbert Th. Finite amplitude stability of plane parallel flows. AGARD 1977; CP-224: 3-1–3-10.
[57] Herbert Th. Secondary instability of plane channel flow to subharmonic 3D-disturbances. Phys Fluids 1983;26: 871–4.
[58] Gilbert N. Numerische Simulation der Transition von der laminaren in die tirbulente Kanalströmung. Tech. Rep. DFVLR-FB 88-55, DLR, 1988.
[59] Zang TA, Hussaini MY. Numerical experiments on subcritical transition mechanism. In: AIAA Paper 85-0296, 1985. p. 18.
[60] Henderson RD. Nonlinear dynamics and pattern formation in turbulent wake transition. J Fluid Mech 1997;352:65–112.
[61] Barkley D, Tuckerman LS, Golubitsky M. Bifurcation theory for three-dimensional flow in the wake of a circular cylinder. Phys Rev E 2000;61:5247–52.
[62] Morkovin MV. Bypass transition research: issues and philosophy. Tech. Rep. AFFDL-TR-68-149, Air Force Research Laboratory, Wright-Patterson Air Force Base, 1968.
[63] Herbert Th. Secondary instability of shear flows. In: GARD-R-709 Special Course on Stability and Transition of Laminar Flow, 1984. p. 7.1–7.13.
[64] Koch W, Bertolotti FP, Stolte A, Hein S. Nonlinear equilibrium solutions in a three-dimensional boundary layer and their secondary instability. J Fluid Mech 2000;406:131–74.
[65] Malik MR, Li F, Choudhari MM, Chang C-L. Secondary instability of crossflow vortices and swept-wing boundary layer transition. J Fluid Mech 1999;399:85–115.
[66] Henningson D. Stability of parallel inviscid shear flow with mean spanwise variation. Tech. Rep. FFA Report TN 1987-57, FFA, 1987.
[67] Hall P, Horseman NJ. The linear inviscid secondary instability of longitudinal vortex structures in boundary layers. J Fluid Mech 1991;232:357–75.
[68] Balachandar S, Malik MR. Inviscid instability of streamwise corner flow. J Fluid Mech 1995;282: 187–201.
[69] Otto SR, Denier JP. Numerical solution of a generalized elliptic partial differential eigenvalue problem. J Comput Phys 1999;156:352–9.
[70] Bridges TJ, Morris PJ. Differential eigenvalue problems in which the parameter appears nonlinearly. J Comput Phys 1984;55:437.
[71] Fasel H, Rist U, Konzelmann U. Numerical investigation of the three-dimensional development in boundary layer transition. AIAA J 1990;28(1):29–37.
[72] Parker SJ, Balachandar S. Viscous and inviscid instabilities of flow along a streamwise corner. Theoret Comput Fluid Dyn 1999;13:231–70.
[73] Lin R-S, Malik MR. On the stability of attachment-line boundary layers. Part 1. The incompressible swept Hiemenz flow. J Fluid Mech 1996;311:239–55.
[74] Heeg RS, Geurts BJ. Spatial instabilities of the incompressible attachment-line flow using sparse matrix Jacobi–Davidson techniques. Appl Sci Res 1998;59: 315–29.
[75] Härtel C, Carlsson F, Thunblom M. Analysis and direct numerical simulation of the flow at a gravity-current head. Part 2. the lobe-and-cleft instability. J Fluid Mech 2000;418:213–29.
[76] Härtel C, Meiburg E, Necker F. Analysis and direct numerical simulation of the flow at a gravity-current head. Part 1. flow topology and front speed for slip and no-slip boundaries. J Fluid Mech 2000;418: 189–212.
[77] Theofilis V. On steady-state flow solutions and their nonparallel global linear instability. In: Dopazo C, editor. Eighth European Turbulence Conference, June 27–30, 2000. Barcelona, Spain, 2000. p. 35–8.
[78] Em Karniadakis G, Sherwin SJ. Spectral/*hp* element methods for CFD. Oxford: Oxford University Press, 1999.
[79] Deville MO, Fischer PF, Mund EH. High-Order Methods for Incompressible Fluid Flow. Cambridge University Press, New York.
[80] Quartapelle L. Numerical solution of the incompressible Navier–Stokes equations. Basel: Birkhäuser, 1993.
[81] Ramanan N, Homsy GM. Linear stability of lid-driven cavity flow. Phys Fluids 1994;6:2690–701.
[82] Stüer H. Investigation of separation on a forward facing step. Tech. Rep. ISBN 3-906445-05-4, IHW-ETH Zürich, 1999.

[83] Kuhlmann HC, Wanschura M, Rath HJ. Flow in two-sided lid-driven cavities: non-uniqueness, instabilities and cellular structures. J Fluid Mech 1997;336:267–99.
[84] Ding Y, Kawahara M. Linear stability of incompressible flow using a mixed finite element method. J Comput Phys 1998;139:243–73.
[85] Morzyński M, Afanasiev K, Thiele F. Solution of the eigenvalue problems resulting from global non-parallel flow stability analysis. Comput Methods Appl Mech Eng 1999;169:161–76.
[86] Bayly BJ. Three-dimensional instability of elliptical flow. Phys Rev Lett 1986;57:2160–2.
[87] Theofilis V. Linear instability in two spatial dimensions. In: Papailiou K et al., editors. Proceedings of the European Computational Fluid Dynamics Conference ECCOMAS '98, Athens, Greece, 1998. p. 547–52.
[88] Theofilis V, Barkley D, Sherwin SJ. Spectral/*hp* technology for global flow instability. Aeronaut J 2002;106: 619–25.
[89] Zurmühl R. Matrizen und ihre technische Anwendungen. Berlin: Springer, 1961.
[90] Saad Y. Iterative methods for sparse linear systems. Boston, MA: PWS Publishing, 1996.
[91] Lehoucq R, Maschhoff K, Sorensen D, Yang C. ARPACK a collection of Fortran77 subroutines designed to solve large scale eigenvalue problems. 2001.
[92] Wintergerste T, Kleiser L. Secondary stability analysis of nonlinear crossflow vortices. In: Saric W, Fasel H, editors. Proceedings of the IUTAM Laminar-Turbulent Symposium V, Sedona, AZ, USA, 2000. p. 583–6.
[93] Jacquin L, Fabre D, Sipp D, Theofilis V, Vollmers H. Instability and unsteadiness of aircraft wake vortices. Aerosp Sci Technol 2002, to appear.
[94] Sleijpen G, van der Vorst H. A Jacobi–Davidson iteration method for linear eigenvalue problems. SIAM J Matrix Anal Appl 1996;17:401–25.
[95] Gourary MM, Rusakov SG, Ulyanov SL, Zharov MM, Gullapalli KK, Mulvaney BJ. Iterative solution of linear systems in harmonic-balance analysis. In: IEEE MTT-S International Microwave Symposium Dig., Denver, CO, 1997. p. 1507–10.
[96] Rizzoli V, Neri A, Mastri F, Lipparini A. A Krylov-subspace technique for the simulation of integrated RF/microwave subsystems driven by digitally modulated carriers. Int J RF Microwave 1999; 490–505.
[97] Rizzoli V, Mastri F, Sgallari F, Spalletta G. Harmonic-balance simulation of strongly nonlinear very large-size microwave circuits by inexact newton methods. In: MTT-S International Microwave Symposium Dig., San Francisco, CA, 1996. p. 1357–60.
[98] Nayar N, Ortega JM. Computation of selected eigenvalues of generalized eigenvalue problems. J Comput Phys 1993;108:8–14.
[99] Orszag SA. Accurate solution of the Orr–Sommerfeld stability equation. J Fluid Mech 1971;50:689–703.
[100] Canuto C, Hussaini MY, Quarteroni A, Zang TA. Spectral methods in fluid dynamics. Berlin: Springer, 1987.
[101] Hall P, Malik MR, Poll DIA. On the stability of an infinite swept attachment-line boundary layer. Proc R Soc London A 1984;395:229–45.
[102] Theofilis V, Dallmann U. On subcritical breakdown to turbulence in swept wing attachment line boundary layer flows. Notes Numer Fluid Mech 1996;60:351–8.
[103] Janke E, Balakumar P. On the secondary instability of three-dimensional boundary layers. Theoret Comput Fluid Dyn 2000;14:167–94.
[104] Hiemenz K. Die Grenzschicht an einem in den gleichförmigen Flüssigkeitsstrom eingetauchten geraden Kreiszylinder, Thesis, Göttingen. Dingl Polytechn J 1911;326:321–4.
[105] Poll DIA. Some aspects of the flow near a swept attachment line with particular reference to boundary layer transition. Tech. Rep. CoA Report 7805, Cranfield University, 1978.
[106] Hall P, Malik MR. On the instability of a three-dimensional attachment-line boundary layer: weakly nonlinear theory and a numerical approach. J Fluid Mech 1986;163:257–82.
[107] Spalart PR. Direct simulation of a turbulent boundary layer up to $R_\theta = 1410$. J Fluid Mech 1988;187:61–98.
[108] Jiménez J, Martel C, Agüí J, Zufiria J. Direct numerical simulation of transition in the incompressible leading edge boundary layer. No. MF-903, 1990.
[109] Joslin RD. Direct simulation of evolution and control of three-dimensional instabilities in attachment-line boundary layers. J Fluid Mech 1995;291:369–92.
[110] Görtler H. Dreidimensionale Instabilität der ebenen Staupunktströmung gegenüber wirbelartigen Störungen. In: Görtler H, Tollmien W, editors. 50 Jahre Grenzschichtforschung, Braunschweig: Vieweg und Sohn, 1955. p. 304–14.
[111] Hämerlin G. Zur Instabilitätstheorie der ebenen Staupunktströmung. In: Görtler H, Tollmien W, editors. 50 Jahre Grenzschichtforschung, Braunscheweig: Vieweg und Sohn, 1955. p. 315–27.
[112] Joslin RD. Simulation of three-dimensional symmetric and antisymmetric instabilities in attachment-line boundary layers. AIAA J 1996;34:2432–4.
[113] Theofilis V, Fedorov A, Obrist D, Dallmann UCh. An extended Görtler-Hämmerlin model for linear and nonlinear instability in the three-dimensional incompressible swept attachment-line boundary layer. J Fluid Mech 2002, submitted.
[114] Bertolotti FP. On the connection between cross-flow vortices and attachment-line instabilities. In: Saric W, Fasel H, editors. Proceedings of the IUTAM Laminar-Turbulent Symposium V, Sedona, AZ, USA, 2000. p. 625–30.
[115] Gregory N, Stuart JT, Walker W. On the stability of three-dimensional boundary layers with application to the flow due to a rotating disk. Philos Trans R Soc London A 1955;248:155–99.
[116] Reed H, Saric WS. Stability of three-dimensional boundary layers. Annu Rev Fluid Mech 1989;21: 235–84.
[117] Radeztsky RH, Reibert MS, Saric WS. Development of stationary crossflow vortices on a swept wing, AIAA 1994; 94-2373.
[118] Bippes H. Basic experiments on transition in three-dimensional boundary layers dominated by crossflow instability. Prog Aerosp Sci 1999;35:363–412.

[119] Fischer TM, Dallmann U. Primary and secondary instability analysis of a three-dimensional boundary layer flow. Phys Fluids 1991;3:2378–91.
[120] Fischer TM, Hein S, Dallmann U. A theoretical approach for describing secondary instability features in three-dimensional boundary-layer flows. In: AIAA Paper 93-0080, 1993.
[121] Haynes TS, Reed HL. Simulation of swept-wing vortices using nonlinear parabolised stability equations. J Fluid Mech 2000;405:325–49.
[122] Poll DIA. Some observations of the transition process on the windward face of a long yawed cylinder. J Fluid Mech 1985;150:85–115.
[123] Kohama Y, Saric WS, Hoos W. A high frequency, secondary instability of crossflow vortices. In: Proceedings of the Royal Aeronautical Society Conference on Boundary-layer and Control, 1991. p. 4-1–4-13.
[124] Reibert MS, Saric WS, Carillo RB, Chapman KL. Experiments in nonlinear saturation of stationary crossflow vortices in a swept wing boundary layer. AIAA 1996; 96-0184.
[125] Lerche T, Bippes H. Experimental investigation of crossflow instability under the influence of controlled disturbance excitation. In: Henkes RAWM, van Ingen JL, editors. Transitional boundary layers in aeronautics. Amsterdam, The Netherlands: North-Holland, 1996. p. 137–44.
[126] White EB. Secondary instability growth measurements in crossflow boundary layers. In: Wagner S, Kloker M, Rist U, editors. Euromech 423 Boundary Layer Transition in Aerodynamics, April 2–4. Germany: Stuttgart, 2001.
[127] Saric WS, Carillo RB, Reibert MS. Leading-edge roughness as a transition control mechanism, AIAA, 1998; 98-0781.
[128] Saric WS, Reed H. Supersonic laminar flow control on swept wings using distributed roughness. Paper No. AIAA-02-0147, 2002.
[129] Högberg M, Henningson D. Secondary instability of crossflow vortices in Falkner–Skan–Coke boundary layers. J Fluid Mech 1998;368:339–57.
[130] Wassermann P, Kloker M. Secondary instability of steady and unsteady crossflow vortices. J Fluid Mech 2002;456:49–84.
[131] Dovgal AV, Kozlov VV, Michalke A. Laminar boundary layer separation: instability and associated phenomena. Prog Aerosp Sci 1994;30:61–94.
[132] Dovgal AV, Sorokin AM. Instability of a laminar separation bubble to vortex shedding. Thermophys Aeromech 2001;8(2):189–97.
[133] Boiko AV, Grek GR, Dovgal AV, Kozlov VV. Origin of turbulence in near-wall flows. Berlin: Springer, 2002.
[134] Gaster M. Stability of velocity profiles with reverse flow. In: Hussaini MY, Streett CL, editors. Instability, transition and turbulence. Berlin: Springer, 1992. p. 212–5.
[135] Hammond DA, Redekopp LG. Local and global instability properties of separation bubbles. Eur J Mech B 1998;17:145–64.
[136] Rosenhead L. Laminar boundary layers. Oxford: Oxford University Press, 1963.
[137] Briley WR. A numerical study of laminar separation bubbles using the Navier–Stokes equations. J Fluid Mech 1971;47:713–36.
[138] Cebeci T, Stewartson K. On the calculation of separation bubbles. J Fluid Mech 1983;133:287–96.
[139] Theofilis V. Global linear instability in laminar separated boundary layer flow. In: Saric W, Fasel H, editors. Proceedings of the IUTAM Laminar-Turbulent Symposium V, Sedona, AZ, USA, 2000. p. 663–8.
[140] Hetsch T, Rist U. Instabilitäten in der Ablöseblase nach Briley. In: Heinemann HJ et al., editors. AG-Stab Bericht 2001: Strömungen mit Ablösung. 2001. p. 130–1.
[141] Dallmann UCh, Vollmers H, Shu W-H, Zhang H-Q. Flow topology and tomography for vortex identification in unsteady and in three-dimensional flows. In: Proceedings of the IUTAM Symposium on Simulation and Identification of Organised Structures in Flows, Lyngby, Denmark, 1997. p. 25–9.
[142] Theofilis V, Sherwin SJ. Global instabilities in trailing-edge laminar separated flow on a NACA 0012 aerofoil. In: Proceedings of the XV International Symposium on Airbreathing Engines ISABE 2001-1094, Bangalore, India, 2001.
[143] Barkley D, Gomes G, Henderson RD. Three-dimensional instability in flow over a backward facing step. J Fluid Mech 2002;473:167–90.
[144] Stüer H, Gyr A, Kinzelbach W, Laminar-turbulent transition of a separating flow on a forward facing step. In: Saric W, Fasel H, editors. Proceedings of the IUTAM Laminar-Turbulent Symposium V. Sedona, AZ, USA, 2000. p. 541–6.
[145] Becker S, Stoots CM, Condie KG, McEligot DM. Reynolds stress development in a transitioning boundary layer. In: APS Meeting, 2000.
[146] Colonius T, Basu AJ, Rowley CW. Numerical investigation of the flow past a cavity. AIAA Paper 99-1912, 1999.
[147] Jackson AP, Hillier R, Soltani S. Experimental and computational study of laminar cavity flows at hypersonic speeds. J Fluid Mech 2001;427:329–58.
[148] Gharib M, Roshko A. The effect of flow oscillations on cavity drag. J Fluid Mech 1987;177:501–30.
[149] Theofilis V, Colonius T, Rowley CW. Global instability of compressible flow in open cavities, 2000. unpublished.
[150] Ding Y, Kawahara M. Linear stability of incompressible flow in a cavity using finite element method. Int J Numer Methods Fluids 1998;27:139–57.
[151] Ghia U, Ghia KN, Shin CT. High-Re solutions for incompressible flow using the Navier–Stokes equations and a multigrid method. J Comput Phys 1982;48: 387–411.
[152] Schreiber R, Keller HB. Driven cavity flows by efficient numerical techniques. J Comput Phys 1983;49: 310–33.
[153] Albensoeder S, Kuhlmann HC, Rath HJ. Multiplicity of steady two-dimensional flows in two-sided lid-driven cavities. Theoret Comput Fluid Dyn 2001;14: 223–41.
[154] Burggraf O. Analytical and numerical studies of the structure of steady separated flows. J Fluid Mech 1966;24:113–51.

[155] Benson JD, Aidun CK. Transition to unsteady nonperiodic state in a through-flow lid-driven cavity. Phys Fluids A 1992;4:2316–9.
[156] Pan F, Acrivos A. Steady flows in rectangular cavities. J Fluid Mech 1967;28:643–55.
[157] Kerswell RR, Davey AL. On the linear instability of elliptic pipe flow. J Fluid Mech 1996;316:307–24.
[158] Carrier G. The boundary layer in a corner. Q Appl Math 1947;4:367–70.
[159] Dhanak MR, Duck PW. The effects of freestream pressure gradient on a corner boundary layer. Proc R Soc London A 1997;453:1793–815.
[160] Duck PW, Stow SR, Dhanak MR. Non-similar solutions to the corner boundary layer equations (and the effects of wall-transpiration). J Fluid Mech 1999;400:125–62.
[161] Kao TW, Park C. Experimental investigations of the stability of channel flows. Part 1. Flow of a single liquid in a rectangular channel. J Fluid Mech 1970;43: 145–64.
[162] Zamir M. Similarity and stability of the boundary layer in a streamwise corner. Proc R Soc London A 1981;377: 269–88.
[163] Brandt L, Andersson P, Henningson DS. Secondary instability of streaks in boundary layers. In: Dopazo C, editor. Eigth European Turbulence Conference, June 27–30, Barcelona, Spain, 2000. p. 141–5.
[164] Jiménez J. Stability of a pair of co-rotating vortices. Phys Fluids 1975;18:1580.
[165] Rennich SC, Lele SK. A method for accelerating the destruction of aircraft wake vortices. J Aircr 1999;36:398.
[166] Reddy SC, Henningson DS. Energy growth in viscous channel flows. J Fluid Mech 1993;252:209–38.
[167] Reddy SC, Schmid PJ, Baggett JS, Henningson DS. On the stability of streamwise streaks and transition thresholds in plane channel flows. J Fluid Mech 1998;365: 269–303.
[168] Williamson CHK. Annu Rev Fluid Mech 1996;28:477.
[169] Em Karniadakis G, Triantafyllou GS. Three-dimensional dynamics and transition to turbulence in the wake of bluff bodies. J Fluid Mech 1992;238:1.
[170] Noack BR, Eckelmann H. A global stability analysis of the steady and periodic cylinder wake. J Fluid Mech 1994;270:297–330.
[171] Darekar R, Sherwin SJ. Flow past a bluff body with a wavy separation line. J Fluid Mech 2001;426:263–95.
[172] Bearman PW, Owen JC. Reduction of bluff-body drag and suppression of vortex shedding by the introduction of wavy separation line. J Fluids Struct 1998;12: 123–30.
[173] Humphreys JS. On a circular cylinder in a steady wind. J Fluid Mech 1960;9:603–12.
[174] Gölling B. Experimentelle Untersuchungen des laminaren-turbulenten überganges der Zylindergrenzschichtströmung. Tech. Rep. Forschungsbericht 2001-14, DLR Institut für Aerodynamik und Strömungstechnik, 2001.
[175] Bloor MG, Gerrard JH. Measurement on turbulent vortices in a cylinder wake. Proc R Soc London A 1966;294:319–42.
[176] Schiller L, Linke W. Druck- und Reibungswiderstand des Zylinders bei Reynoldszahlen 5000 bis 40000. Z Flugtechnik Motorluft 1933;24:193–8.
[177] Zdravkovich MM. Flow around circular cylinder, vol. I. Oxford: Oxford University Press, 1997.
[178] Schewe G. On the force fluctuations acting on a circular cylinder in cross flow from subcritical up to transcritical Reynolds numbers. J Fluid Mech 1983;133:265.
[179] Schewe G. Sensitivity of transition phenomena to small perturbations in flow round a circular cylinder. J Fluid Mech 1986;172:33–46.
[180] Schewe G. Reynolds-number effects in flow around more-or-less bluff bodies. J Wind Eng Ind Aerodyn 2001;8:1267–89.
[181] Reau N, Tumin A. On harmonic perturbations in turbulent shear flows. In: Advances in turbulence VIII, Eighth European Turbulence Conference, June 27–30, Barcelona, Spain, 2000. p. 209–12.
[182] Seifert A, Bachar T, Koss D, Shepshelovich M, Wygnanski I. Oscillatory blowing: a tool to delay boundary-layer separation. AIAA J 1993;31:2052–60.
[183] Seifert A, Darabi A, Wygnanski I. Delay of airfoil stall by periodic excitation. J Aircraft 1996;33:691–8.
[184] Nishri B, Seifert A, Wygnanski I. Active control of a transitional separation bubble at low Reynolds number and elevated free-stream turbulence. In: La Graff JE, editor. Proceedings of the Minnowbrook III Workshop on Boundary Layer Transition and Unsteady Aspects in Turbomachinery Flows. Blue Mountain, Adirondracks, NY, 2000. p. 6.
[185] Darabi A, Lourenco L, Wygnanski I. On flow reattachment by periodic excitation. In: Advances in turbulence VIII, Eighth European Turbulence Conference, June 27–30, Barcelona, Spain, 2000. p. 201–4.
[186] Nishri B, Wygnanski I. Effects of periodic excitation on turbulent separation from a flap 1998;36(4):547–56.
[187] Eißler W, Bestek H. Spatial numerical simulation of nonlinear transition phenomena in supersonic boundary layers. In: Kral L, Zang TA, editors. ASNE FED-151, 1993. p. 69–76.
[188] Streett CL, Zang TA, Hussaini MY. Spectral methods for solution of the boundary layer equations. In: AIAA Paper 84-0170, 1984.
[189] Ku HC, Hirsh RS, Taylor TD. A pseudospectral method for solution of the three-dimensional Navier–Stokes equations. J Comput Phys 1987;70:439–62.
[190] Ehrenstein U, Peyret R. A Chebyshev collocation method for the Navier–Stokes equations with application to double-diffusive convection. Int J Numer Methods Fluids 1989;9:427–52.
[191] Kleiser L, Schumann U. Treatment of incompressibility and boundary conditions in 3-d numerical simulations of plane channel flows. In: Hirschel EH, editor. Proceedings, Third GAMM-Conference on Numerical Methods in Fluid Dynamics. Braunschweig, 1980. p. 165–73.
[192] Abramowitz M, Stegun I. Handbook of mathematical functions. New York: Dover, 1970.
[193] Boyd JP. Chebyshev and Fourier spectral methods. Berlin: Springer, 1989.
[194] Spalart PR, Moser RD, Rogers MM. Spectral methods for the Navier–Stokes equations with one infinite and two periodic directions. J Comput Phys 1991;96: 297–324.

[195] Haidvogel DB, Zang T. The accurate solution of Poisson's equation by expansion in Chebyshev polynomials. J Comput Phys 1979;39:167–80.
[196] Bourcier M, François C. Intégration numérique des équations de Navier–Stokes dans un domaine carré. La Rech. Aér 1969;131:23–33.
[197] Thompson MC, Hourigan K, Sheridan J. Three-dimensional mode development in low Reynolds number flow over a cylinder. In: Australasian Fluid Mechanics Conference, Sydney, Australia, 1995. p. 7.